



Title	Studies on X-Ray Absorption Fine Structure for Divalent and Trivalent First Transition Metal Complexes
Author(s)	Sakane, Hideto
Citation	大阪大学, 1991, 博士論文
Version Type	VoR
URL	<a href="https://doi.org/10.11501/2964357">https://doi.org/10.11501/2964357</a>
rights	
Note	

*The University of Osaka Institutional Knowledge Archive : OUKA*

<https://ir.library.osaka-u.ac.jp/>

The University of Osaka

Studies on X-Ray Absorption Fine Structure for  
Divalent and Trivalent First Transition Metal Complexes

by

Hideto SAKANE

Department of Chemistry  
Faculty of Science  
Osaka University

1991

Studies on X-Ray Absorption Fine Structure for  
Divalent and Trivalent First Transition Metal Complexes

by

Hideto SAKANE

Department of Chemistry

Faculty of Science

Osaka University

1991

## Contents

Chapter 1	General introduction.....	1
	References.....	7
Chapter 2	Experimental.....	10
2.1	Apparatus of beamlines for XAFS measurement at Photon Factory.....	10
2.2	X-ray absorption measurement cell.....	13
Chapter 3	Theoretical background of EXAFS.....	14
3.1	Derivation of EXAFS formula.....	14
3.2	Debye-Waller factor.....	21
3.3	Reference.....	25
Chapter 4	Data analysis.....	26
4.1	Extraction of EXAFS.....	27
4.2	Fourier transform.....	29
4.3	Fourier filtering.....	29
4.4	Curve-fitting.....	30
4.5	The phase shift and the back-scattering amplitude.....	31
4.6	XANES normalization.....	33
4.7	References.....	34
Chapter 5	XAFS of simple six- and four-coordinate first transition metal complexes.....	35
5.1	Introduction.....	35
5.2	Experimental.....	36
5.3	Results and discussion.....	40
5.3.1	XANES spectra.....	40

5.3.2	Fourier transforms .....	46
5.3.3	Curve-fitting results.....	52
5.3.4	Interatomic distances.....	59
5.3.5	Scale factors and Debye-Waller factors.....	64
5.3.6	Absorption edge shifts.....	71
5.3.7	Comparison of metal edge and Br edge of bromo complexes .....	76
5.3.8	Calculation of characteristic value of EXAFS parameters.....	78
5.4	References.....	83
Chapter 6	Solvent effect and counterion effect on XAFS of carboxylato chelate complexes.....	87
6.1	Introduction.....	87
6.2	Experimental.....	87
6.3	Results and discussion.....	89
6.3.1	Co(III) EDTA complexes.....	89
6.3.2	Oxalato and malonato complexes .....	98
6.4	References.....	109
Chapter 7	Structures of Fe(III) complexes with EDTA and analogous ligands in aqueous solutions revealed by XAFS.....	111
7.1	Introduction.....	111
7.2	Experimental.....	112
7.3	Results and discussion.....	113
7.4	References.....	124
	Concluding remarks.....	126
	Acknowledgements.....	128
	Papers relevant to the present study.....	129

## Chapter 1. General introduction

The absorption coefficient of a certain material in X-ray region generally decreases monotonously as the energy of the photon is increased. When the energy reaches a certain critical value, the absorption coefficient increases abruptly. This discontinuity corresponds to the threshold of the ejection of a core electron from an atom in the material and is called the absorption edge. In addition, the absorption coefficient often exhibits oscillations extending to as much as 1000 eV above the absorption edge. This variation is named X-ray absorption fine structure, XAFS. In general, XAFS is separated in two regions. The near edge part, up to about 50 eV above the absorption edge, is called X-ray absorption near-edge structure, XANES, and the other from about 50 to 1000 eV extended X-ray absorption fine structure, EXAFS. XAFS have been widely used as a tool of structural analysis, because the X-ray absorption spectrum can be measured irrespective of the state of the sample material, *e.g.* gas, liquid, solution, etc..

EXAFS reflects a final state interference involving scattering of the outgoing photoelectron at the neighboring atoms. The probability of absorption of an X-ray photon by a core electron depends on both the initial and the final state of the electron. The electron of the initial state stays at the localized core level corresponding to the absorption edge. Its final state consists of an ejected photoelectron. It can be represented as an outgoing spherical wave originating from the X-ray absorbing atom. If the

atom is surrounded by other atoms, the outgoing photoelectron wave will be back-scattered by the neighboring atoms, thereby producing an incoming wave. The final state is then affected by the interference between the outgoing and the incoming waves that gives rise to the sinusoidal variation of absorption coefficient versus X-ray energy known as EXAFS. The frequency of the EXAFS depends on the distance between the absorbing atom and the neighboring atom, while the amplitude of the EXAFS depends on the number and the back-scattering power of the neighboring atom. Therefore, the analysis of the EXAFS gives the distance and the number of atoms surrounding the absorber.

Near or below the edge, or over the XANES region, generally appear absorption peaks due to excitation of core electrons to some bound states (for example, 1s to nd, (n+1)s, or (n+1)p for K-edge, or for L-edges 2s for L<sub>I</sub> and 2p for L<sub>II</sub> and L<sub>III</sub> to the same set of vacant orbitals). This pre-edge region contains valuable information such as the energies of virtual orbitals, the electronic configuration, or the site symmetry. It arises from the effects such as many-body interaction, multiple scattering, distortion of the excited state wave function by Coulomb field, band structure, etc..

Although the XAFS phenomena have been known for a long time (since Fricke and Hertz in 1920<sup>1)</sup>), its significance concerning the structural content was not fully recognized until the work of Stern, Lytle, and Sayers.<sup>2)</sup> They pointed out that a Fourier transform of EXAFS with respect to the photoelectron wavenumber should peak at distances corresponding to nearest-neighbor coordination shells of atoms. Their conclusion was based on the

short-range order theory with an electron mean free path expression of Sawada et al.<sup>3)</sup> and a Debye-Waller type factor to account for the thermal disorder introduced by Shmidt.<sup>4)</sup> In addition, the availability of synchrotron radiation has resulted in the establishment of XAFS as a tool of structural analysis particularly through the work of Eisenberger and Kincaid.<sup>5)</sup> Since synchrotron sources typically have X-ray intensities three or more orders of magnitude greater in the continuum energies than do the standard X-ray tube sources, the time required for measuring a spectrum of concentrated samples fell from the order of a week to the order of minutes. At the same time these sources expanded possibilities to make the measurement of dilute samples that could not be realized before.

XAFS is useful in inorganic chemistry, especially when single crystals are not available or when structural information in solution is sought. Many instances of XAFS application to solution chemistry have been presented; the first,<sup>6-10)</sup> second,<sup>11-13)</sup> and third<sup>14)</sup> transition metal complexes of halogeno,<sup>7-9,11)</sup> pseudohalogeno,<sup>14)</sup> etc.<sup>6,7,10,12,13)</sup> in aqueous solutions<sup>6-8,11,12)</sup> and in other various solvents.<sup>7,9,10,13,14)</sup> As an applied analytical technique, Okamoto et al.<sup>15)</sup> successfully employed XAFS for the structural analysis of an anti-friction additive in used engine oils to which no other structural analytical technique could be applied. Typical example where single crystals are barely available is biochemical metal complexes *e.g.* metalloprotein.<sup>16)</sup> Unstable compounds,<sup>17)</sup> complexes that exhibit thermally induced transition such as spin-crossovers,<sup>18)</sup> or liquid-crystalline coordination compounds<sup>19)</sup> are also suitable for the XAFS study. XAFS has also been applied to

electrochemistry<sup>20)</sup> in *in situ* structural studies of electroactive species in solution or on electrode surface and deposited layers on electrode or electrode surface itself.

Several methods are suggested of analyzing the EXAFS interference.<sup>21)</sup> A common approach to the analysis of single-shell EXAFS data and only approach if more than one shell at a time must be analyzed is the use of numerical fitting procedures using the EXAFS parameterization function for fitting routine. The form of the EXAFS equation requires that nonlinear fitting algorithms be used. The problems of curve-fitting methods include: multi-dimensional parameter spaces which can be very time-consuming; and correlations among various parameters. The latter problem is more important for the accuracy of EXAFS results. In fact, each EXAFS wave contains two sets, concerning to amplitude and phase, of highly correlated variables. Significant correlations can occur both within and between these two set of variables as well as between different scattering terms. These problems are more acute for the minor components of a multi-distance system since the least-square refinement is dominated by the major component.

The interatomic distance and the coordination number from the result of EXAFS analysis are the only parameters used by chemists so far and all the other parameters obtained are discarded while these parameters have their theoretical background. The purpose of this work is to experimentally elucidate the chemical implications of EXAFS parameters which have been given less attention by chemists for the first transition metal complexes. This thesis consists of the following chapters.

Chapter 2 presents the apparatus of XAFS beamlines of Photon

Factory of the National Laboratory for High Energy Physics and the measurement cell for X-ray absorption.

In chapter 3, the theoretical background of EXAFS formula is described based on to Ishii's derivation.<sup>22)</sup> He gives a general rule for obtaining a matrix element of any multiple scattering in the lowest-order approximation and the correction terms to the basic EXAFS formula.

Chapter 4 describes the analysis processes of EXAFS used in this work. Detailed expressions are presented. XANES normalization process for comparison of the spectra with each other is also described.

Chapter 5 studies the XAFS for a series of simple six- and four-coordinate first transition metal complexes. It is found that the peak intensities in the EXAFS Fourier transforms for aqua complexes correlate with those for ammine complexes and chloro complexes correlate with bromo complexes. Curve-fitting calculations are performed for these and other many complexes and attempts are made to characterize these results and to reveal their chemical implications. A comparison of the EXAFS metal K-edge and Br K-edge of bromo complexes is also made. The last section attempts to make quantitative analysis of EXAFS parameters so that the parameter values can be estimated for a certain combination of a central metal ion and a ligand.

Chapter 6 studies the XAFS for Co(III) EDTA complexes in solids and solutions. The Co K-edge XANES of  $[\text{Co}(\text{edta})]^-$  complex varies with the kind of counter cations in the crystalline state and it also varies with the kind of solvents in the solution state. The amplitude of the oscillation in its EXAFS, or the peak height

in its Fourier transform, also varies as much as threefold depending on the kind of counter cations or solvents. The most plausible cause for the variations is the difference in the thermal disorder of the bonds which is enhanced by the formation of hydrogen bonding between carboxylato groups in the complex and the water molecules in crystal or the solvent molecules in solution. For more detailed study on the solvent effects, XAFS of some carboxylato complexes in various solvents are analyzed. The solvent effects are observed in Cr(III) and Co(III) trisoxalato complexes. Curve-fitting analysis indicates that the metal-ligand atom distances of Co(III) trisoxalato complex shows a linear relationship with the acceptor number of the solvents.

Chapter 7 studies the solution structure of Fe(III)-EDTA and analogous complexes. The Fe K-edge X-ray absorption spectra of Fe(III) complexes with EDTA and EDDDA in weakly acidic or neutral aqueous solutions are measured. The spectra of powdered crystalline samples of these complexes are also measured as the reference materials. The comparisons of the XANES spectra, including their pre-edge peak, and the EXAFS Fourier transforms conclude that in aqueous solution seven-coordinate structure is predominant for Fe(III)-EDTA complex and six-coordinate for Fe(III)-EDDDA complex.

## References

1. H. Fricke, *Phys. Rev.*, 16, 202 (1920); G. Hertz, *Z. Phys.*, 3, 19 (1920).
2. F. W. Lytle, *Adv. X-Ray Anal.*, 9, 398 (1966); D. E. Sayers, F. W. Lytle, and E. A. Stern, *ibid.*, 13, 248 (1970); D. E. Sayers, E. A. Stern, and F. W. Lytle, *Phys. Rev. Lett.*, 27, 1204 (1971).
3. M. Sawada, K. Tsutsumi, T. Shiraiwa, T. Ishimura, and M. Obashi, *Ann. Rep. Sci. Works, Faculty Sci., Osaka Univ.*, 7, 1 (1959); T. Shiraiwa, T. Ishimura, and M. Sawada, *J. Phys. Soc. Jpn.*, 13, 847 (1958).
4. V. V. Shmidt, *Bull. Acad. Sci. USSR, Phys. Ser.*, 25, 998 (1961); 27, 392 (1963).
5. P. Eisenberger and B. M. Kincaid, *Chem. Phys. Lett.*, 36, 134 (1975); B. M. Kincaid and P. Eisenberger, *Phys. Rev. Lett.*, 34, 1361 (1975).
6. M. Nomura and T. Yamaguchi, *J. Phys. Chem.*, 92, 6157 (1988); J. Garcia, M. Benfatto, C. R. Natoli, A. Bianconi, A. Fontaine, and H. Tolentino, *Chem. Phys.*, 132, 295 (1989); G. Onori, A. Santucci, A. Scafati, M. Belli, S. Della Longa, A. Bianconi, and L. Palladino, *Chem. Phys. Lett.*, 149, 289 (1988); K. Ozutsumi, T. Yamaguchi, H. Ohtaki, K. Tohji, and Y. Udagawa, *Bull. Chem. Soc, Jpn.*, 58, 2786 (1985).
7. Y. Tajiri and H. Wakita, *Bull. Chem. Soc. Jpn.*, 59, 2285 (1986).
8. K. F. Ludwig, Jr., W. K. Warburton, and A. Fontaine, *J. Chem. Phys.*, 87, 620 (1987).
9. M. Sano, T. Maruo, Y. Masuda, and H. Yamatera, *J. Sol. Chem.*, 15, 803 (1986); M. Sano, T. Maruo, and H. Yamatera, *J. Chem. Phys.*,

- 89, 1185 (1988).
10. N. Binsted, J. Evans, G. N. Greaves, and R. J. Price, *J. Chem. Soc., Chem. Commun.*, 1330 (1987); M. Miyake, O. Kaji, S. Nagahara, and T. Suzuki, *J. Chem. Soc., Faraday Trans. 2*, 82, 687 (1986); M. Miyake, N. Nakagawa, H. Ohyanagi, and T. Suzuki, *Inorg. Chem.*, 25, 700 (1986).
  11. M. I. de Barros Marques and P. Lagarde, *J. Phys., Condens. Matter*, 2, 231 (1990).
  12. T. Yamaguchi, M. Nomura, H. Wakita, and H. Ohtaki, *J. Chem. Phys.*, 89, 5153 (1988); T. K. Sham, *Phys. Rev. B*, 40, 6045 (1989).
  13. T. Yamaguchi, H. Wakita, and M. Nomura, *J. Chem. Soc., Chem. Commun.*, 433 (1988).
  14. S. Ahrland, K. Nilsson, I. Persson, A. Yuchi, and J. E. Penner-Hahn, *Inorg. Chem.*, 28, 1833 (1989).
  15. T. Okamoto, K. Fujita, and M. Kawamura, *Nippon Kagaku Kaishi*, 916 (1988).
  16. S. P. Cramer, "X-Ray Absorption," ed by D. C. Koningsberger and R. Prins, John Wiley & Sons, New York, 1988, p.257.
  17. O. Fussa, S. Kauzlarich, J. L. Dye, and B. K. Teo, *J. Am. Chem. Soc.*, 107, 3727 (1985); O. Fussa-Rydel, J. L. Dye, and B. K. Teo, *ibid.*, 110, 2445 (1988).
  18. J. Zarembowitch, P. Thuéry, A. Dworkin, and A. Michalowicz, *J. Chem. Res. (S)*, 146 (1987); P. Thuéry, J. Zarembowitch, A. Michalowicz, and O. Kahn, *Inorg. Chem.*, 26, 851 (1987).
  19. G. Albertini, A. Guido, G. Mancini, S. Stizza, M. Ghedini, and R. Bartolino, *Europhys. Lett.*, 12, 629 (1990).
  20. G. J. Hansen and W. E. O'Grady, *Rev. Sci. Instrum.*, 61, 2127 (1990); L. R. Sharpe, W. R. Heineman, and R. C. Elder, *Chem. Rev.*,

90, 705 (1990).

21. B. K. Teo, "EXAFS: Basic Principles and Data Analysis," Springer-Verlag, Berlin, 1985.
22. T. Ishii, *Bussei Kenkyu*, 41, 204 (1983); T. Ishii, *Prog. Theor. Phys.*, 72, 412 (1984); T. Ishii, "Principles of the Theory of EXAFS - EXAFS Formulae," Aioi, Japan, 1989, p.24, unpublished; T. Ishii, "Principles of the Theory of EXAFS - Debye Waller Type of Factors," Okayama, Japan, 1988, p.1, unpublished.

## Chapter 2. Experimental

X-Ray absorption spectra measurements were performed at Photon Factory of the National Laboratory for High Energy Physics. Sample preparations will be described in each chapter.

### 2.1 Apparatus of beamlines for XAFS measurement at Photon Factory

The beamlines of BL-10B, BL-7C, and BL-6B in Photon Factory were used for XAFS measurements. A schematic diagram of the XAFS measurement instruments on BL-7C and BL-6B is shown in Fig. 2.1. The monochromators of BL-7C and BL-6B are equipped with a Si(111) double crystal, while that of BL-10B with a Si(311) channel-cut crystal or a Si(111) double crystal. The height of the monochromatized synchrotron radiation beam in BL-7C and BL-6B is kept nearly constant, therefore the stage used for mounting the sample and ionization chambers need not be moved during an energy scan. However, since the beam height in BL-10B moves with scanning of the monochromator angle, the stage position must be controlled in order to track the beam height. In using the Si(111) double crystal monochromator, the planes of the two crystals are slightly detuned from parallel to reduce harmonics. The ionization chambers are filled with a pure gas or a mixture of either Ar, N<sub>2</sub>, or He under atmospheric pressure. The Cu electrodes of the ionization chambers have a spacing of 10 mm and a width of 60 mm. The light-path length for the chamber can be selected from three different lengths of 5.5 cm, 17 cm, and 31 cm.

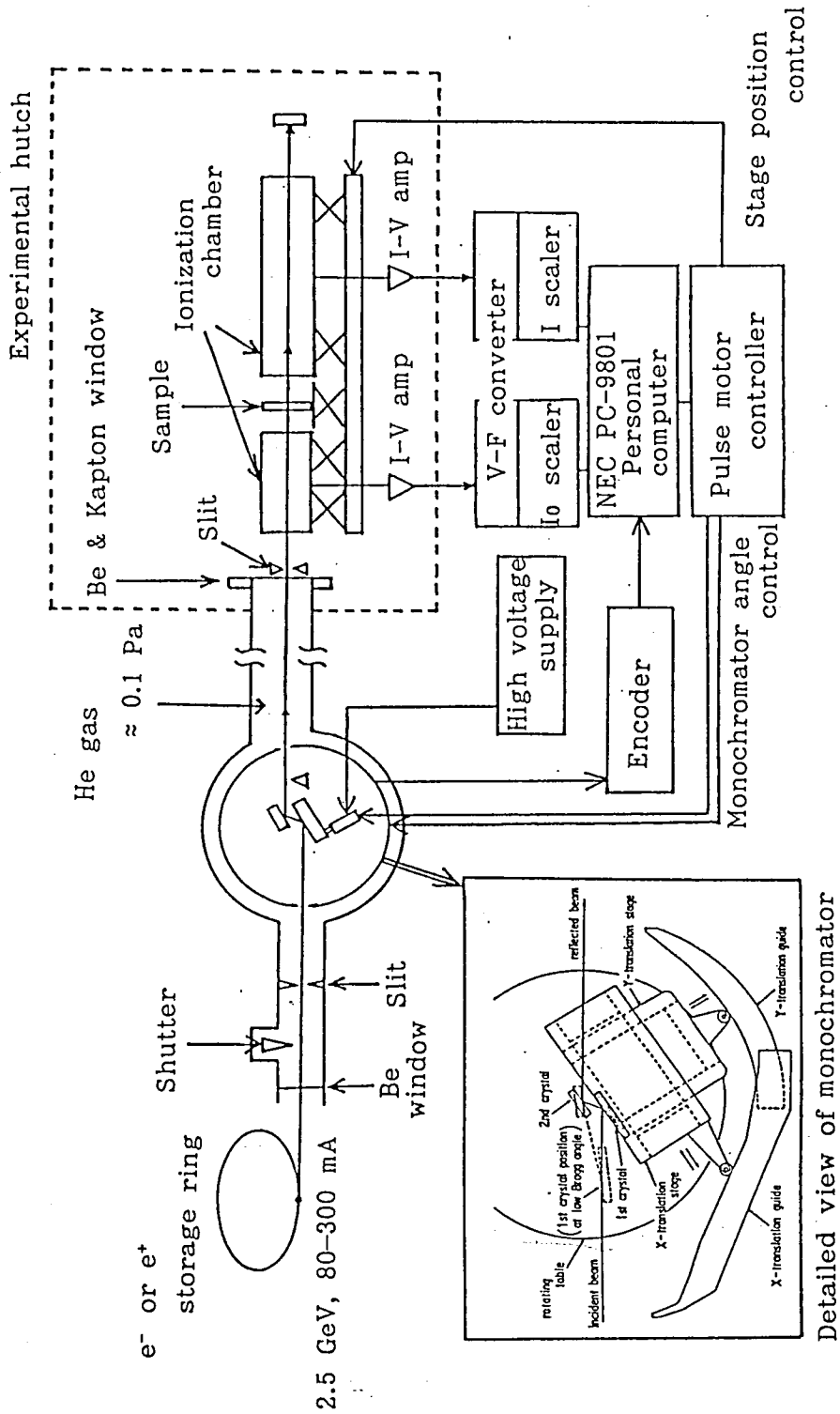


Figure 2.1. Experimental apparatus of BL-7C and BL-6B in Photon Factory.

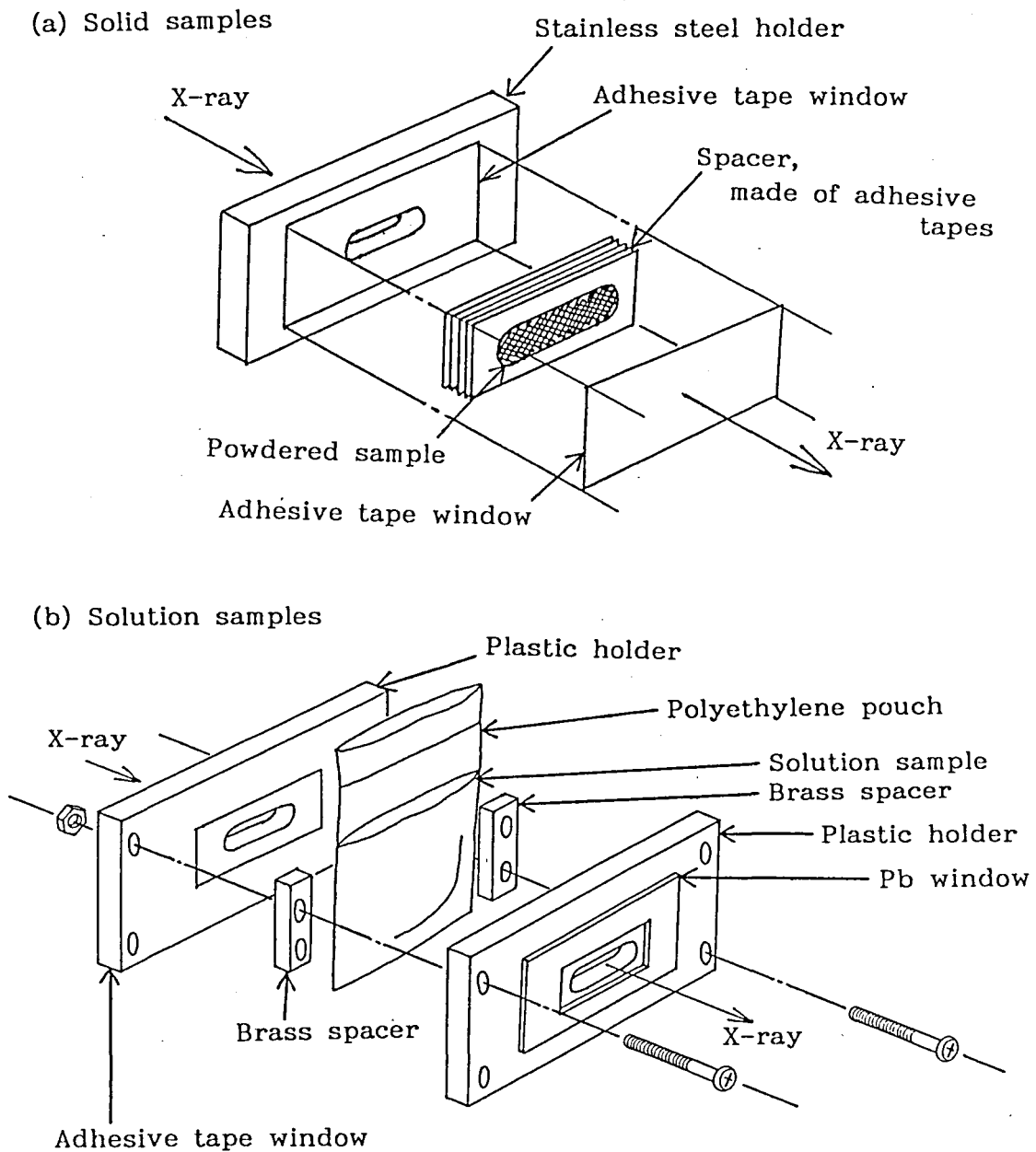


Figure 2.2. Sample cells and holders for X-ray absorption measurements.

Kapton films are used as windows of the chambers. Selection of the detector gas and the path length depends on the X-ray energy range of the measurement. The outputs from the ionization chambers are amplified, digitized, and fed to a personal computer. The absorption data are stored on a floppy disk for further treatments.

## 2.2 X-ray absorption measurement cell

Powder samples were mixed with BN powder and held between two sheets of adhesive tape (as shown in Fig. 2.2 (a)). For the ordinary stable solution samples, a polyethylene pouch and plastic holders were used as the measurement cell as shown in Fig. 2.2 (b). The X-ray absorbing path was adjusted by changing the Brass spacers. The thickness of the sample was so adjusted that the edge-jump of the absorption spectrum becomes between 0.5 and 2.0.

## Chapter 3. Theoretical background of EXAFS

### 3.1 Derivation of EXAFS formula

The basic EXAFS formula has been derived in the literature by several authors. The form accepted widely now was first derived by Sayers, Stern, and Lytle.<sup>1)</sup> Lee described<sup>2)</sup> the physics in the EXAFS more clearly. He has shown that the basic EXAFS formula consists of two elementary processes; interferences between the direct photoelectron wave from the absorbing atom and the wave scattered by the neighboring atom, and the wave back-scattered to the absorbing atom by the neighboring atom. The phase shift comes from the interference between the direct wave and the wave double-scattered successively by the neighboring and the absorbing atoms.

Derivation of the basic EXAFS formula requires several assumptions listed as follows:

(1) One-photon absorption.

The vector potential  $A$  of the photon is assumed to be so small, that only the first order of  $A$  is considered. The transition probability  $W$  depends on the first order perturbation of the wave function.

(2) Dipole transition approximation.

The size of the initial state wave function of the core electron is small enough compared to the wavelength of the photon.

(3) One-electron transition.

Only one electron is excited at the photo-absorption.

(4) Single electron scattering approximation.

The scattering of the ejected core electron at the neighboring atom occurs without any interaction with the other electrons of the atom.

(5) Muffin-tin potential approximation.

The potential of the scattering atom has spherical symmetry, and the potential range of an atom is far shorter than the distance  $r_{AB}$  between the absorbing, A, and the scattering atoms, B. This approximation makes it possible to assume the photoelectron wave as an plane wave. The scattering atom is not affected by other atom.

(6) Single scattering approximation.

If the energy of the photoelectron is high enough, the multiple scattering processes by the neighboring atoms can be neglected.

The following derivation of EXAFS formula is according to Ishii's method.<sup>3)</sup> This method is based on Lee's scheme.<sup>2)</sup> A general rule for describing matrix elements for any multiple scattering path is found in the lowest-order approximation. Here, the single-scattering lowest-order terms by neighboring atoms of the Ishii's method are picked out.

### Transition probability of electron by photo-excitation

Treating the electromagnetic field with classical model and the electronic system with quantum mechanics, the Hamiltonian  $H$  of an atom that is irradiated with weak light is

$$H = \frac{1}{2m} \left( p - \frac{e}{c} A \right)^2, \quad (3.1)$$

where  $p$ ,  $m$ ,  $e$ , and  $c$  are the momentum operator, the mass, and the charge of an electron, and the velocity of light, respectively. Taking the first order of  $A$  (Assumptions 1 and 3) and considering  $p = -i\hbar \nabla$ ,  $\nabla \cdot A = 0$  (because light propagates in the form of transverse waves), Eq. (3.1) becomes

$$H = H_0 + H_1 \quad (3.2)$$

$$H_0 = -\frac{\hbar^2}{2m} \nabla^2 + V(r) \quad (3.3)$$

$$H_1 = -\frac{e}{mc} A \cdot p \quad (3.4)$$

where  $V(r)$  is the total potential seen by the final-state photoelectron.  $H_0$  is the unperturbed term and  $H_1$  is the perturbation term. Now, let the  $A$  be  $\epsilon_q \exp(iq \cdot r)$  ( $q$  is the wavenumber vector of the photon and  $\epsilon_q$  is the unit vector of the polarization direction of the photon), then the probability  $W$  of the transition of the electron from  $E_i$  energy level to  $E_k + E_b$  is

$$W \propto |\langle f | \exp(iq \cdot r) \cdot \epsilon_q p | i \rangle|^2, \quad (3.5)$$

where  $|f\rangle$  and  $|i\rangle$  mean the final and the initial state wave function, respectively.

#### Dipole transition

Because the size of the core state wave function is nearly equal to  $n^2 a_B / Z$  (the  $n$  is the principal quantum number, the  $a_B$  ( $\approx 0.529 \text{ \AA}$ ) is Bohr radius, and the  $Z$  is the atomic number),

$$qr \approx \frac{n^2 E}{3.7Z} \quad (3.6)$$

is obtained for the photon energy of  $E$  keV. Therefore, if  $Z \gg 1$ , then  $qr \ll 1$  and  $\exp(iq \cdot r)$  can be replaced by unity in Eq. (3.5)

(Assumption 2). Eq. (3.5) can be rewritten as (omitting  $g$ )

$$W \propto |\langle f | \mathbf{\epsilon} \cdot \mathbf{r} | i \rangle|^2. \quad (3.7)$$

### Scattering by atom

With Assumption 4, the final state wave function can be given by

$$| f \rangle = | k \rangle + G_0^- T | k \rangle \quad (3.8)$$

$$T = \sum_i \hat{t}_i + \sum_{h \neq i} \hat{t}_i G_0 \hat{t}_h + \sum_{\substack{h \neq i \\ n \neq h}} \hat{t}_i G_0 \hat{t}_h G_0 \hat{t}_n + \dots, \quad (3.9)$$

where  $| k \rangle$  is free-space limit electron wave function.  $G_0$  is the free space propagating operator (Green's function) and  $T$  is the scattering matrix. The first term of Eq. (3.8) is the unperturbed term and the second one denotes the scattered waves. The superscript  $-$  of  $G_0$  and  $T$  denotes the direction in which the operators act, *i.e.* incoming to the absorber.  $\hat{t}_i$  is the elementary scattering operator for the potential of the  $i$ -th atom. The Green's function for an electron propagating from  $r$  to  $r'$  is defined as follows;

$$\frac{1}{2m} (P_r^2 - \hbar^2 k^2) G_0(r, r') = \delta(r - r') \quad (3.10)$$

$$P_r = i\hbar \nabla_r,$$

where  $\delta(r)$  is a Dirac delta function and  $k$  is the photoelectron wave vector.

### Scattering matrix element

Because the first two terms of Eq. (3.9) give the single scattering phenomena by the neighboring atom, the right-hand side of Eq. (3.7) becomes

$$\langle f | \boldsymbol{\varepsilon} \cdot \mathbf{r} | i \rangle = \langle k | \boldsymbol{\varepsilon} \cdot \mathbf{r} | i \rangle + I_a + I_b \quad (3.11)$$

$$I_a = \langle k | t_B G \boldsymbol{\varepsilon} \cdot \mathbf{r} | i \rangle \quad (3.12)$$

$$I_b = \langle k | t_A G t_B G \boldsymbol{\varepsilon} \cdot \mathbf{r} | i \rangle. \quad (3.13)$$

The subscripts A and B denote the absorbing and the back-scattering atom, respectively. The first matrix element on the right-hand side of Eq. (3.11) is responsible for the usual unperturbed photoelectric effect. Let us consider the K-shell excitation ( $s$  initial state), and the element is given by

$$\langle k | \boldsymbol{\varepsilon} \cdot \mathbf{r} | i \rangle = (\boldsymbol{\varepsilon} \cdot \hat{\mathbf{k}}) M, \quad (3.14)$$

where  $\hat{\mathbf{k}}$  means the unit vector for vector  $k$ .  $M$ , the dipole matrix element, is related to the atomic absorption coefficient  $\mu_0$  by

$$\mu_0 \propto |M|^2. \quad (3.15)$$

$I_a$  is the process of single scattering by the scattering atom at  $r$ .  $I_b$  is that of double scattering by the scattering and the absorbing atom. In using atomic units ( $\hbar = 1$ ,  $m = 1$ ,  $e = 1$ ,  $c = 137.036$ ), the elementary scattering operator is given by

$$- \frac{t^+(n', n'')}{2\pi} = f_i(n', n''), \quad (3.16)$$

where  $f(r', r'')$  is the scattering amplitude. If  $kr_{AB}$  is enough large and the potential range is much smaller than  $r_{AB}$  (Assumptions 5 and 6),  $I_a$  and  $I_b$  can be approximate as

$$I_a = \frac{M}{r_B} (\boldsymbol{\varepsilon}, \mathbf{r}_B) \exp(ikr_B - ik_B \cdot \mathbf{r}) f_B(k, k_{AB}), \quad (3.17)$$

$$I_b = \frac{M}{r_B^2} (\epsilon, \mathbf{r}_B) \exp[ik(r_B + r_B)] f_A(k, -k_{AB}) f_B(-k_{AB}, k_{AB}), \quad (3.18)$$

where the position of A (the absorbing atom) is taken to be the origin.

### Basic EXAFS formulae

From eq. (3.7) and (3.11), the transition probability is

$$W = cM^2 |K + I_a' + I_b'|^2 \quad (3.19)$$

$$K = (\epsilon, \mathbf{k}), \quad MI_a' = I_a, \quad MI_b' = I_b,$$

where  $c$  is the proportional constant. Expansion of Eq. (3.19) consists of six terms. Because the terms  $I_a'^* I_b'$  and  $|I_b'|^2$  are higher order than  $1/(kr_B)^2$ , these two terms will not be considered.

The excited electron is ejected and scattered by atoms A and B (the neighboring atom) in many directions. In order to compute the average absorption cross section of such a macroscopic system, it is necessary to average over all such directions  $\mathbf{k}$  in Eq. (3.19). Taking to the order of  $1/r_B^2$  and signifying the average operation as « », the averages of terms of Eq. (3.19) are;

$$\langle K^2 \rangle = \frac{1}{3}, \quad (3.20)$$

$$\text{Re} \langle 2KI_a' \rangle = (\epsilon, \mathbf{r}_B)^2 \text{Re} \frac{i}{kr_B^2} [f_B(k, \pi) \exp(i2kr_B) + f_B(k, 0)], \quad (3.21)$$

$$\langle I_a'^* I_a' \rangle = (\epsilon, \mathbf{r}_B)^2 \text{Re} \frac{-i}{kr_B^2} f_B(k, 0), \quad (3.22)$$

$$\text{Re} \langle 2KI_b' \rangle = (\epsilon, \mathbf{r}_B)^2 \text{Re} \frac{i}{kr_B^2} f_B(k, \pi) \exp(i2kr_B) [\exp(i2\phi_A) - 1], \quad (3.23)$$

where  $f(k, \theta)$  means  $f(k', k)$ ,  $|k| = |k'| = k$ , and  $\theta$  is the angle between  $k$  and  $k'$ . As in Lee's derivation,<sup>2)</sup> the forward-scattering term

$f_B(k,0)$  in one of the cross terms is offset by with Eq. (3.22). Then the polarized basic formula for EXAFS  $\chi$  is obtained.

$$\begin{aligned}\chi(k, \varepsilon) &= \sum_B \frac{\langle\langle |K + I_a' + I_b'|^2 \rangle\rangle - \langle\langle K^2 \rangle\rangle}{\langle\langle K^2 \rangle\rangle} \\ &= \sum_B (\varepsilon \cdot r_B)^2 \cdot \text{Im} \left[ \frac{-3}{kr_B^2} f_B(k, \pi) \cdot \exp(i2kr_B + i2\phi_A) \right],\end{aligned}\quad (3.24)$$

where  $\phi_A$  is the phase shift due to the scattering by the absorbing atom. For measurement of a single crystal sample with polarized X-ray source, one should use Eq. (3.24) with consideration for the directions of photon  $\varepsilon$  and the sample orientation.

Meanwhile, an average of Eq. (3.24) over all possible polarization directions must be computed in the following cases:

- (i) X-Ray is randomly polarized.
- (ii) Powdered crystalline samples are measured.
- (iii) Samples are in disorder systems such as liquid, gas, etc..

The average result is

$$\chi(k) = \sum_B \text{Im} \left[ \frac{-1}{kr_B^2} f_B(k, \pi) \cdot \exp(i2kr_B + i2\phi_A) \right].\quad (3.25)$$

$f_B(k, \pi)$  can be separated into the amplitude term and the phase term as follows:

$$\begin{aligned}f_B(k, \pi) &= F_B(k) \cdot \exp(i\phi_B), \\ F_B(k) &= |f_B(k, \pi)|, \quad i\phi_B = \tan^{-1} \left( \frac{\text{Im} f_B(k, \pi)}{\text{Re} f_B(k, \pi)} \right).\end{aligned}\quad (3.26)$$

where  $F_B(k)$  and  $\phi_B$  are the back-scattering amplitude and phase functions, respectively. In general, three extra terms are added to Eq. (3.25) to account for inelastic scattering processes (losses)

the photoelectron experiences as it travels between the absorbing atom and the neighboring atom and small disorders of  $r_B$ . The first is due to multiple excitations of the other passive electrons within the absorbing atom. This is approximated by an amplitude reduction factor  $s_0(k)^2$  which depends only on the type of the central atom involved. The second is the inelastic losses due to excitation of neighboring environment, including the neighboring atoms and the intervening medium. This factor is usually approximated by an exponential damping term  $\exp(-2r_B/\lambda_B(k))$  where  $\lambda_B(k)$  is the inelastic electron mean free path.<sup>4)</sup> The last is due to the displacements of atoms relative to a mean coordination distance that will cause a smearing of the interference function and reduction in the net scattering amplitude. As long as the relative displacements are sufficiently small, this effect is described by a Debye-Waller factor,  $\exp(-2\sigma_B^2 k^2)$ , where  $\sigma_B$  is the root-mean-square displacement of  $r_B$ .

Finally, the ordinary basic EXAFS formula is obtained with the coordination number  $N_B$ :

$$\chi(k) = \sum_B \frac{s_0^2 N_B}{k r_B^2} F_B(k) \cdot \exp\left(\frac{-2r_B}{\lambda_B(k)}\right) \cdot \exp(-2\sigma_B^2 k^2) \cdot \sin(2kr_B + 2\phi_A + \phi_B). \quad (3.27)$$

### 3.2 Debye-Waller factor

The Debye-Waller factor  $\sigma$  plays an important role in EXAFS spectroscopy. It contains important structural and chemical informations. It is important to note that the  $\sigma$  that enters into EXAFS is not the same as that which enters the Debye-Waller term in diffraction. In diffraction the mean square deviation that enters is one about the lattice site for each atom, while for EXAFS

the deviation is a relative one between the absorbing and back-scattering atoms. Generally speaking, the Debye-Waller factor  $\sigma$  has two components,  $\sigma_{\text{stat}}$  and  $\sigma_{\text{vib}}$  due to static disorder and thermal vibrations, respectively. Photoelectrons having typical energy in EXAFS region travel between the absorbing-scattering atom pair for a short time such as  $10^{-16}$  s. On the other hand, one period of the thermal vibrational motions is longer than  $10^{-13}$  s. Then, the neighboring atoms be regarded as standing during each elementary scattering process. These two factors can only be separated by a temperature dependent study of  $\sigma$ . However, if  $\sigma_{\text{vib}}$  can be estimated from vibrational spectroscopies or if  $\sigma_{\text{stat}}$  is known from other studies, the other term can be calculated from experimentally determined  $\sigma$ . Assuming small disorders with a symmetric pair distribution function for static disorder and harmonic vibration for thermal disorder, the Debye-Waller factor  $\sigma$  is given by

$$\sigma^2 = \sigma_{\text{stat}}^2 + \sigma_{\text{vib}}^2. \quad (3.28)$$

### Static disorder

For continuous symmetric Gaussian pair distribution function of distance  $r$

$$g(r) = \frac{1}{\sqrt{(2\pi)\sigma_{\text{stat}}^2}} \exp\left(-\frac{(r-r_0)^2}{2\sigma_{\text{stat}}^2}\right). \quad (3.29)$$

$\sigma_{\text{stat}}$  is just the root-mean-square displacement from the mean distance  $r_0$ . For discrete bonds,  $\sigma_{\text{stat}}$  is related to the root-mean-square standard deviation;

$$\sigma_{\text{stat}} \approx \sqrt{\left(\frac{\sum_B^N (r_B - r_0)^2}{N}\right)}. \quad (3.30)$$

Integration of the EXAFS contribution over all distances can derive that a symmetric Gaussian distribution of distances gives rise to an exponential damping  $\exp(-2\sigma_{\text{stat}}^2 k^2)$  in the EXAFS in  $k$  space. If other factors in Eq. (3.27) can be assumed as identical, they can be taken out of the integral. For small disorder,  $r \approx r_0$  such that the  $1/r^2$  factor can be also be taken out of the integral. Then the integral of interest is;

$$\begin{aligned} & \int_0^{\infty} g(r) \sin[2kr + \phi(k)] dr \\ &= \frac{1}{\sqrt{(2\pi)\sigma_{\text{stat}}^2}} \int_0^{\infty} \exp\left(-\frac{u^2}{2\sigma_{\text{stat}}^2}\right) \sin[2kr + \phi(k)] du, \end{aligned} \quad (3.31)$$

where  $u=r-r_0$  and  $\phi(k)=2\phi_A+\phi_B$ . This integration becomes

$$\begin{aligned} & \frac{1}{\sqrt{(2\pi)\sigma_{\text{stat}}^2}} \int_{-\infty}^{\infty} \exp\left(-\frac{u^2}{2\sigma_{\text{stat}}^2}\right) (\sin[2kr_0 + \phi(k)] \cos(2ku) \\ & \quad + \cos[2kr_0 + \phi(k)] \sin(2ku)) du \\ &= \frac{1}{\sqrt{(2\pi)\sigma_{\text{stat}}^2}} \sin[2kr_0 + \phi(k)] \int_{-\infty}^{\infty} \exp\left(-\frac{u^2}{2\sigma_{\text{stat}}^2}\right) \cos(2ku) du \\ &= \frac{1}{\sqrt{(2\pi)\sigma_{\text{stat}}^2}} \sin[2kr_0 + \phi(k)] \cdot \sqrt{(2\pi)\sigma_{\text{stat}}^2} \exp(-2\sigma_{\text{stat}}^2 k^2) \\ &= \exp(-2\sigma_{\text{stat}}^2 k^2) \cdot \sin[2kr_0 + \phi(k)]. \end{aligned} \quad (3.32)$$

### Thermal Disorder

For nearest neighbors, it is useful to assume the force-constant model as the Einstein model in which all of the relevant atom pairs vibrate independently at the same frequency. In this model, the distribution of distance owing to the vibrational contribution is also Gaussian function which has the root-mean-square deviation given by<sup>5)</sup>

$$\sigma_{\text{vib}}^2 = \frac{h}{8\pi^2\mu\nu} \coth\frac{h\nu}{2k_B T}, \quad (3.33)$$

where  $\nu$  is the vibrational frequency,  $\mu$  is the reduced mass,  $k_B$  is the Boltzmann constant, and  $T$  is the temperature. Therefore, the EXAFS contribution of  $\sigma_{\text{vib}}$  is given by the same procedure of  $\sigma_{\text{stat}}$  from Eqs. (3.29), (3.31), and (3.32).

### 3.3 References

1. D. E. Sayers, F. W. Lytle, and E. A. Stern, *Adv. X-Ray Anal.*, 13, 248 (1970); D. E. Sayers, E. A. Stern, and F. W. Lytle, *Phys. Rev. Lett.*, 27, 1204 (1971).
2. P. A. Lee, *Phys. Rev. B*, 13, 5261 (1976); P. A. Lee, P. H. Citrin, P. Eisenberger, and B. M. Kincaid, *Rev. Mod. Phys.*, 53, 769 (1981).
3. T. Ishii, *Bussei Kenkyu*, 41, 204 (1983); T. Ishii, *Prog. Theor. Phys.*, 72, 412 (1984); T. Ishii, "Principles of the Theory of EXAFS - EXAFS Formulae," Aioi, Japan, 1989, p.24, unpublished; T. Ishii, "Principles of the Theory of EXAFS - Debye Waller Type of Factors," Okayama, Japan, 1988, p.1, unpublished.
4. M. Sawada, K. Tsutsumi, T. Shiraiwa, T. Ishimura, and M. Obashi, *Ann. Rep. Sci. Works, Faculty Sci., Osaka Univ.*, 7, 1 (1959); T. Shiraiwa, T. Ishimura, and M. Sawada, *J. Phys. Soc. Jpn.*, 13, 847 (1958).
5. J. M. Tranquada, S. M. Heald, and A. R. Moodenbaugh, *Phys. Rev. B*, 36, 8401 (1987).

## Chapter 4. Data analysis

Several methods are suggested to analyze EXAFS interference.<sup>1,2)</sup> Fourier transform of the data expressed in  $k$  space is the earliest analysis. It gives a modified radial distribution function in  $r$  space. Problems of the Fourier transform technique include: side lobes or ripples due to the finite data range which can interfere with the weaker peaks; background peaks at or below a distance of *ca.* 1 Å due to residual background which may interfere not only with the short distances of interest but also with the longer distances because of the ripples due to the finite range of the transform. This technique has the advantage of providing a simple physical picture of the local structure around the absorber. Fourier transform is usually used as the intermediate step with following inverse transforming from  $r$  space data to  $k$  space to select the distance range of interest. The beat-node method may be used for systems with a large disparity (about larger than 0.1 Å) in distances. The sum of two sine waves at different frequencies,  $2kr_1$  and  $2kr_2$ , produces beating in the EXAFS amplitude with a period of  $2k(r_1-r_2)$ . Then  $r_1-r_2$  is observed from the first minimum in the EXAFS amplitude. The ratio technique determines Debye-Waller factors and coordination numbers in the single-shell system by plotting the log of the ratio of the amplitude of a sample and a model versus  $k^2$ . If the other factors are similar, the plot gives a straight line of slope  $-2(\sigma^2-\alpha_m^2)$  with an intercept of  $\ln(N_m/M)$ , where the subscript  $m$  denotes the value of the model.

A common alternative approach to the analysis of single-shell EXAFS data and the only approach if more than one shell at a time must be analyzed is the use of numerical fitting procedures, the curve-fitting calculation. It is obvious that the curve-fitting methods can provide higher resolution and more accurate results for systems with closely spaced interatomic distances. In the present study, EXAFS analyses are performed by Fourier transform comparison and curve-fitting calculations. The computations were performed with EPSON PC-286VS, NEC PC-9801VM21, or NEC PC-9801RA21 personal computers. All the analysis programs are written in Microsoft QuickBASIC for this study. This analytical package is interactive, graphical, and fast even on the personal computers. The analytical procedures are mainly based on Matsubayashi's method<sup>3)</sup> and some improvements are made.

#### 4.1 Extraction of EXAFS

In an X-ray absorption experiment, the spectrum is obtained as  $\mu(E)x$ , where  $\mu$  is the total absorption coefficient,  $E$  is the incident X-ray energy, and  $x$  is the sample thickness. Normalized EXAFS interference function,  $\chi(k)$ , is defined as

$$\chi(k) = \frac{\mu(k)x - \mu_s(k)x}{\mu_0(k)x} \quad (4.1)$$

$$k = \sqrt{\left[\frac{2m}{\hbar^2} (E - E_0)\right]} \quad (4.2)$$

$$\mu_s = \mu_0 + \mu_b. \quad (4.3)$$

$\mu_0$  is the absorption of the hypothetical isolated absorbing atom

and  $\mu_b$  is the background absorption due to lower-energy absorption edges, Compton scattering, and other processes that are not immediate interest.  $E_b$  is the energy threshold, *i.e.* the minimum energy required to free the electron. Since  $\mu_0$  affects EXAFS information very much and is hardly obtained by experiments, estimation of  $\mu_0$  is the most important part through the analysis procedure.

$\mu_b$  is calculated by least-square fitting of the pre-edge region with the Victoreen's formula,  $A\lambda^3 - B\lambda^4 + C$ , where  $\lambda$  is the X-ray wavelength. The original Victoreen's formula for true absorption<sup>4)</sup> does not include the constant term  $C$ . Although, experimentally observed  $\mu$  contains the differences of the responses of the detectors, amplifiers' gain, and so on, this constant term must be taken into the calculation. Because this fitting calculation is rather depending on the regression region, the calculations are done with monitoring the higher energy side in the absorption spectra and the difference of known Victoreen's constants,<sup>1,5)</sup>  $A_h - A_l$  and  $B_h - B_l$ , where the subscripts  $h$  and  $l$  denote the higher and the lower energy side of the absorption edge.

$\mu_0$  is estimated by the following two schemes. First, the temporary  $\mu_0$  (hereafter note as  $\mu_t$ ) is calculated by 3-6 order polynomial least-square fitting weighted with  $k$  to the power of 2-5. Then, the temporary  $\chi$  (hereafter note as  $\chi_t$ ) is defined as  $\chi_t = \mu - \mu_t$ . Next, second-order 11-15 points smoothing is applied for appropriate times to  $\chi_t \cdot k^3$ . And, two cubic spline interpolation curves for the maxima and the minima of the smoothed  $\chi_t \cdot k^3$  are calculated. The final  $\mu_0$  is obtained as the

sum of the average of the two splines and  $\mu_t$ .  $E_0$  is chosen for the energy of the midpoint of the edge jump.

## 4.2 Fourier transform

In this study, the Fourier transform calculations of EXAFS are performed according to the next way;

$$\rho(r) = \frac{1}{\sqrt{\pi}} \int W(k) \frac{k}{F(k)} \chi(k) \exp[-i(2kr + \phi(k))] dk \quad (4.4)$$

$W(k)$  is the Hamming window function which is used in order to reduce ripples in the Fourier transform due to the finite transform range.

$$W(k) = 0.54 + 0.46 \cos\left(\frac{2\pi[k - \frac{1}{2}(k_{\min} + k_{\max})]}{k_{\max} - k_{\min}}\right). \quad (4.5)$$

The phase shift  $\phi(k)$  and the back-scattering amplitude  $F(k)$  are used the theoretical values tabulated by Teo and Lee<sup>6)</sup> or McKale et al.<sup>7)</sup> with interpolating by a natural spline function.

## 4.3 Fourier filtering (Inverse Fourier transform)

Fourier filtering involves Fourier transforming the  $\chi(k)$  data into the  $r$  space (Fourier transform), selecting the  $r$  range of interest with a smooth window, and inverse transforming the data to  $k$  space. The smooth window used is

$$\begin{aligned} w(r) &= 0.54 + 0.46 \cos\left(\frac{2\pi[r - \frac{1}{2}(r_{\min}^s + r_{\max}^s)]}{r_{\min}^s - r_{\min}^s}\right) & r_{\min}^s \leq r \leq r_{\min}^s \\ &= 1 & r_{\min}^s \leq r \leq r_{\max}^s \\ &= 0.54 + 0.46 \cos\left(\frac{2\pi[r - \frac{1}{2}(r_{\max}^s + r_{\min}^s)]}{r_{\max}^s - r_{\min}^s}\right), & r_{\max}^s \leq r \leq r_{\max}^s \end{aligned} \quad (4.6)$$

where  $r_{\min}$  and  $r_{\max}$  are  $r$  space range for the transform.  $r_{\min}^e$  and  $r_{\max}^e$  are the  $r$  range of applying the square window.

The Fourier transform of EXAFS  $\rho(r)$  are back-transformed as

$$\chi(k) = \frac{F(k)}{k} \frac{2}{\sqrt{\pi}} \int w(r) \cdot \rho(r) \exp[-i(2kr + \phi(k))] dr. \quad (4.7)$$

$\phi(k)$  and  $F(k)$  are the same as those of Fourier transform.

#### 4.6 Curve-fitting

The curve-fitting technique attempts to best fit the  $k^n \chi(k)$  spectra in  $k$  space with some phenomenological EXAFS models. The refinement procedure can be based on least-squares. In this study, the Fourier-filtered experimental EXAFS spectrum  $k^3 \chi(k)$  were fitted with the following model:

$$k^3 \chi_{\text{calc}} = k^3 \sum_j \frac{B_j}{k_j r_j^2} F_j(k_j) \cdot \exp(-2\sigma_j^2 k_j^2) \sin[2k_j r_j + \phi_j(k_j) + \phi_{0j}], \quad (4.8)$$

$$k_j = \sqrt{[k^2 - \frac{2m}{\hbar^2} \Delta E_{0j}]}, \quad (4.9)$$

where subscript  $j$  indicates the coordination shell.  $\phi_0$  is a corrective parameter for phase shift depending on the oxidation state of the absorbing atom and corrects the error of  $\phi(k)$  which has been pointed out by Ishii.<sup>8)</sup> In EXAFS curve-fitting calculation the coordination shells are distinguished from their scattering atom, interatomic distance  $r$ , amplitude factor  $B$ , Debye-Waller factor  $\sigma$ ,  $\phi_0$ , or edge shift  $\Delta E_0$ . Since  $r$ ,  $\phi_0$ , and  $\Delta E_0$  for a certain shell are highly correlated in the non-linear least-square refinements with each other, only one or two parameters of them are allowed to move in the calculation.  $B$  is related to Eq. (3.27)

as follows:

$$B = SN \quad (4.10)$$

$$S = s_0^2 \exp\left(\frac{-2r}{\lambda}\right), \quad (4.11)$$

where  $S$  is the scale factor and  $s_0^2$  and  $\lambda$  are assumed as independent to  $k$ .  $\Delta E_0$  is a corrective parameter for the difference between experimentally determined  $E_0$  and theoretical one. The back-scattering amplitude  $F(k)$  and the phase shift  $\phi(k)$  are the same as those of Fourier transform.

The index for the fitness is a residual calculated by

$$R = \sqrt{\left[ \frac{\sum k^6 (\chi - \chi_{\text{cald}})^2}{\sum k^6 \chi^2} \right]}, \quad (4.12)$$

where the summations are taken for all data points in the fitting range.

#### 4.5 The phase shift and the back-scattering amplitude

If any appropriate model sample is available in EXAFS experiments, the phase shift and the back-scattering amplitude for an unknown system can be determined by parametrization for the model sample spectra with simple analytical forms. Typical functional forms for the phase shift are  $p_0 + p_1 k$ ,  $p_0 + p_1 k + p_2 k^2$ , or  $p_0 + p_1 k + p_2 k^2 + p_3 k^3$ , and those for back-scattering amplitude are Lorentzian or  $a k^{-b}$  ( $b > 0$ ). The primary advantage of using empirically derived parameters from model compounds is that if they are analyzed in the same fashion as the unknown sample then factors such as errors in the analytical procedures are automatically compensated for by the direct comparison of the

model compound and the unknown. However, this method has the disadvantage that the determination of the empirical parameters of the model compound may introduce errors that do not cancel in the analysis introducing systematic errors into the final results.

Since Teo and Lee calculated the amplitude and phase functions for EXAFS,<sup>6)</sup> it is usual that  $\Delta E_0$  is allowed to move in analyzing model sample spectra and fixed to the value in analyzing unknown systems. And, the corrections of the amplitude and the phase function are also made by their tabulated values. They calculated the functions using an electron-atom scattering theory introduced by Lee and Beni<sup>9)</sup> and two types of Hartree-Fock wave functions, Clementi-Roetti and Herman-Skillman. Recently, McKale et al.<sup>7)</sup> tabulated the back-scattering amplitude and the phase shift for scattering atoms calculated with a curved-wave formalism. They used Herman-Skillman-Hartree-Fock wave functions. Two interatomic distances were calculated, 2.5 Å and 4.0 Å. The advantage of theoretical parameters is that they can be calculated without reference to model compounds and be tabulated for use for all elements. The analysis based on the theoretical parameters, although, now is not a model free procedure. Model compounds are necessary to determine  $\Delta E_0$  and the scale factor  $S$  that may not be missed in obtaining the distances and the coordination numbers for unknown samples.

In this study, the phase shifts for absorbing atoms were the value<sup>6)</sup> of Teo and Lee's for Herman-Skillman wave functions and the phase shifts and the back-scattering amplitudes for scattering atoms were of McKale et al.<sup>7)</sup> at  $r=2.5$  Å unless otherwise noted in the experimental section of each chapter. For the curve-fitting

calculation of model compound data, the constant term,  $\phi_0$ , of the phase shift is refined to correct inconsistency depending on the oxidation state of the absorbing atom and the error of the phase shift. The  $\phi_0$  fixed constant to the value obtained by the model in the calculation for the unknown. In the analysis without model  $\phi_0$  are fixed to 0.

#### 4.6 XANES normalization

XANES spectra must be normalized in order to compare them with each other. The normalization process is made up of two parts: The first is background absorption subtraction.  $\mu_b$  of Eq. (4.3) is used as the background absorption function. The second is absorption strength normalization. It is convenient to normalize in respect to the edge-jump absorption magnitude in comparing between XANES of different edges rather than general expressions for absorbance, *e.g.* molar absorption coefficient. The absorption edge-jump value is determined to be the twice of the absorption at  $E=E_0$ . Then, the normalized X-ray absorption spectra  $\mu_N$  for XANES is obtained as follows:

$$\mu_N(E) = \frac{\mu(E) - \mu_b(E)}{2[\mu(E=E_0) - \mu_b(E=E_0)]}. \quad (4.13)$$

#### 4.7 References

1. B. K. Teo, "EXAFS: Basic Principles and Data Analysis," Springer-Verlag, Berlin, 1985.
2. D. E. Sayers and B. A. Bunker, "X-Ray Absorption," ed by D. C. Koningsberger and R. Prins, John Wiley & Sons, New York, 1988, p.211.
3. N. Matsubayashi, Doctoral Thesis, Osaka University, Osaka, Japan, 1986.
4. J. A. Victoreen, *J. Appl. Phys.*, 14, 95 (1943); 19, 855 (1948); 20, 1141 (1949).
5. "International Table for X-Ray Crystallography," ed by K. Lonsdale, Kynoch, Birmingham, 1968, Vol. III, Section 3.2.
6. B. K. Teo and P. A. Lee, *J. Am. Chem. Soc.*, 101, 2815 (1979).
7. A. G. McKale, B. W. Veal, A. P. Paulikas, S. K. Chan, and G. S. Knapp, *J. Am. Chem. Soc.*, 110, 3763 (1988).
8. T. Ishii, *Prog. Theor. Phys.*, 72, 412 (1984).
9. P. A. Lee and G. Beni, *Phys. Rev. B*, 15, 2862 (1977).

## Chapter 5. XAFS of simple six- and four-coordinate first transition metal complexes

### 5.1 Introduction

EXAFS method gives the interatomic distances of coordination atoms from the central metal ion in a complex and the number of coordination atoms. However, in some cases, it is hard to determine coordination number  $N$ , since the  $N$  and the disorder in bond distance  $\sigma$  (Debye-Waller factor) are highly correlated. The absorption edge shift  $\Delta E_0$  is also correlated with the interatomic distance. Then, in general, structure analysis by EXAFS method needs any model compound, because the optimum values of these parameters on the analysis or the corrections may be determined only by using the model compound's data.

In many cases in which the EXAFS are used as a structural tool,  $\sigma$ ,  $\Delta E_0$ , and other parameters that are difficult to understand their chemical implications are treated as merely adapting parameters. But, the chemical implications of these EXAFS parameters have become clear. Sham pointed out<sup>1)</sup> that the ligand exchange rate in solution should be closely related to the strength of metal-ligand bond and hence the bond length and  $\sigma$ . Miyanaga<sup>2)</sup> showed the linear correlation of EXAFS Fourier transform intensity of aqua complexes with the logarithm of the water exchange rate constant.

In this chapter, X-ray absorption spectra of many simple six- and four-coordinate divalent and trivalent first transition metal complexes in solids and in aqueous solutions are measured. If a

typical value of the  $\sigma$  and other parameters contributing to the EXAFS intensity for a pair of atoms are known, the  $N$  might be estimated more reliably. EXAFS for a series of the complexes are analyzed in order to study how the parameter vary with the kind of central metal ions and ligands and the relations of their values with the chemical properties of the complexes.

## 5.2 Experimental

**Sample preparations.** Most of the powdered samples were prepared according to the literature references, and some of them are purest reagents commercially purchased. Table 5.1 lists the measured solid samples and their references.  $\text{Fe}(\text{ClO}_4)_2 \cdot 6\text{H}_2\text{O}$  was synthesized by evaporation of a solution of metallic Fe in  $0.4 \text{ mol dm}^{-3}$   $\text{HClO}_4$  aqueous solution. All the preparations were performed under nitrogen atmosphere. The isothiocyanato complexes of Mn(II) and Fe(III) are represented by the thiocyanato complexes (S-bonded) in Ref. 4. But it was reported<sup>7)</sup> that the vibrational spectra of the Mn(II) and Fe(III) hexathiocyanato complexes showed the N-bonded  $\text{SCN}^-$  groups.  $[(\text{C}_2\text{H}_5)_4\text{N}]_2[\text{ZnX}_4]$  ( $\text{X} = \text{Cl}, \text{Br}, \text{I}$ ) were synthesized by the same method as that for  $[(\text{CH}_3)_4\text{N}]_2[\text{ZnCl}_4]$ .<sup>4)</sup> V(III) aqueous solution was prepared by mixing an equal mole amount of V(II) and V(IV) sulfate solutions. The solution samples of Ti(III), Cr(II), and Fe(II) aqua complexes were prepared by the electrolytic reductions of sulfate or perchlorate solutions. Other aqueous solutions were prepared by dissolution of appropriate solid samples, to which adequate acid or ligands were added if needed. Table 5.2 lists the concentrations of the solution samples. Since some of low valence state ions are

Table 5.1. Solid Samples for X-ray Absorption Measurements.

## (a) Six-coordinate samples

Compound	Ref.
$\text{Ti}_2(\text{SO}_4)_3 \cdot 8\text{H}_2\text{O}$	(N)
$\text{Na}_3[\text{V}(\text{NCS})_6] \cdot 12\text{H}_2\text{O}$	(3)
$\text{CrSO}_4 \cdot 5\text{H}_2\text{O}$	(4)
$\text{Cr}_2(\text{SO}_4)_3 \cdot 18\text{H}_2\text{O}$	(N)
$\text{Cr}(\text{ClO}_4)_3 \cdot 6\text{H}_2\text{O}$	(4)
$[\text{Cr}(\text{NH}_3)_6]\text{Cl}_3$	(4)
$\text{K}_3[\text{Cr}(\text{NCS})_6] \cdot 4\text{H}_2\text{O}$	(4)
$\text{MnSO}_4 \cdot 5\text{H}_2\text{O}$	(N)
$\text{Mn}(\text{ClO}_4)_2 \cdot 6\text{H}_2\text{O}$	(K)
$\text{K}_4[\text{Mn}(\text{NCS})_6] \cdot 3-4\text{H}_2\text{O}$	(4)
$\text{FeSO}_4 \cdot 7\text{H}_2\text{O}$	(N)
$\text{Fe}(\text{ClO}_4)_2 \cdot 6\text{H}_2\text{O}$	see text
$\text{K}_4[\text{Fe}(\text{CN})_6] \cdot 3\text{H}_2\text{O}$	(N)
$\text{Fe}(\text{ClO}_4)_3 \cdot 6\text{H}_2\text{O}$	(N)
$\text{K}_3[\text{Fe}(\text{NCS})_6] \cdot 4\text{H}_2\text{O}$	(4)
$\text{K}_3[\text{Fe}(\text{CN})_6]$	(W)
$\text{CoSO}_4 \cdot 7\text{H}_2\text{O}$	(N)
$\text{Co}(\text{NO}_3)_2 \cdot 6\text{H}_2\text{O}$	(N)
$\text{Co}(\text{ClO}_4)_2 \cdot 6\text{H}_2\text{O}$	(K)
$[\text{Co}(\text{NH}_3)_6]\text{Cl}_2$	(4)
$[\text{Co}(\text{NH}_3)_6]\text{Cl}_3$	(N)
$\text{Na}_3[\text{Co}(\text{NO}_2)_6]$	(W)
$\text{K}_3[\text{Co}(\text{CN})_6]$	(N)
$\text{NiSO}_4 \cdot 6\text{H}_2\text{O}$	(W)
$\text{Ni}(\text{NO}_3)_2 \cdot 6\text{H}_2\text{O}$	(N)
$[\text{Ni}(\text{NH}_3)_6]\text{Cl}_2$	(4)
$\text{BaK}_2[\text{Ni}(\text{NO}_2)_6]$	(4)
$\text{CuSO}_4 \cdot 5\text{H}_2\text{O}$	(W)
$\text{Cu}(\text{ClO}_4)_2 \cdot 6\text{H}_2\text{O}$	(4)
$[\text{Cu}(\text{NH}_3)_6]\text{Cl}_2$	(5)
$\text{CaK}_2[\text{Cu}(\text{NO}_2)_6]$	(6)
$\text{ZnSO}_4 \cdot 7\text{H}_2\text{O}$	(W)
$\text{Zn}(\text{NO}_3)_2 \cdot 6\text{H}_2\text{O}$	(N)
$\text{Zn}(\text{ClO}_4)_2 \cdot 6\text{H}_2\text{O}$	(4)

(b) Four-coordinate samples

Compound	Ref.
$[(C_2H_5)_4N]_2[MX_4]$ M(II)=Mn, Fe, Co, Ni, Cu, Zn X(-I)=Cl, Br	(4)
$[(C_2H_5)_4N]_2[MI_4]$ M(II)=Mn, Co, Zn	(4)
$[(C_2H_5)_4N][FeCl_4]$	(4)

(W), (N), and (K) were purchased from  
(W): Wako Pure Chemical Industries, Ltd.,  
(N): Nakarai Chemicals, Ltd.,  
(K): Kishida Chemicals, Ltd.,  
respectively.

Table 5.2. Aqueous Solution Samples  
for X-ray Absorption Measurements.

Complex	Concn M	Notes
$[\text{Ti}^{\text{III}}(\text{H}_2\text{O})_6]^{3+}$	0.75	4M $\text{H}_2\text{SO}_4$ aq sln
$[\text{V}^{\text{III}}(\text{H}_2\text{O})_6]^{3+}$	0.5	0.5M $\text{H}_2\text{SO}_4$ aq sln
$[\text{Cr}^{\text{II}}(\text{H}_2\text{O})_6]^{2+}$	0.5	2M $\text{H}_2\text{SO}_4$ aq sln
$[\text{Cr}^{\text{III}}(\text{H}_2\text{O})_6]^{3+}$	(1) 1	perchlorate sln
	(2) 0.5	sulfate sln
	(3) 0.1	perchlorate sln, 0.5M $\text{HClO}_4$
$[\text{Cr}^{\text{III}}(\text{NH}_3)_6]^{3+}$	0.4	1M $\text{NH}_3$ aq sln
$[\text{Mn}^{\text{II}}(\text{H}_2\text{O})_6]^{2+}$	(1) 1	
	(2) 0.1	0.1M $\text{HClO}_4$ aq sln
$[\text{Mn}^{\text{II}}(\text{NH}_3)_6]^{2+}$	0.4	$\text{MnCl}_2 \cdot 4\text{H}_2\text{O}$ in concd $\text{NH}_3$ aq
$[\text{Fe}^{\text{II}}(\text{H}_2\text{O})_6]^{2+}$	0.5	6M $\text{HClO}_4$ aq sln
$[\text{Fe}^{\text{II}}(\text{NH}_3)_6]^{2+}$	0.4	$\text{FeCl}_2 \cdot 4\text{H}_2\text{O}$ in concd $\text{NH}_3$ aq
$[\text{Fe}^{\text{III}}(\text{H}_2\text{O})_6]^{3+}$	(1) 0.5	6M $\text{HClO}_4$ aq sln
	(2) 0.1	1M $\text{HClO}_4$ aq sln
$[\text{Co}^{\text{II}}(\text{H}_2\text{O})_6]^{2+}$	(1) 1	
	(2) 0.1	0.1M $\text{HClO}_4$ aq sln
$[\text{Co}^{\text{III}}(\text{NH}_3)_6]^{3+}$	0.2	1M $\text{NH}_3$ aq sln
$[\text{Co}^{\text{III}}(\text{NO}_2)_6]^{3-}$	1	1M $\text{NaNO}_2$ aq sln
$[\text{Ni}^{\text{II}}(\text{H}_2\text{O})_6]^{2+}$	1	
$[\text{Ni}^{\text{II}}(\text{NH}_3)_6]^{2+}$	0.4	2M $\text{NH}_3$ aq sln
$[\text{Cu}^{\text{II}}(\text{H}_2\text{O})_6]^{2+}$	1	
$[\text{Zn}^{\text{II}}(\text{H}_2\text{O})_6]^{2+}$	(1) 1	
	(2) 0.5	

1 M = 1 mol/dm<sup>3</sup>

very sensitive to air and easily oxidized, all the procedures for these sample preparations were carried out under nitrogen atmosphere.

**Measurements and Calculations.** Central metal and Br K-edge X-ray absorption spectra were obtained at Photon Factory in the National Laboratory for High Energy Physics. EXAFS Fourier transformations were performed over  $k$  ranges of 2.7–12.5 Å<sup>-1</sup>, 2.7–14.3 Å<sup>-1</sup>, and 3.15–17.15 Å<sup>-1</sup> for aqua and ammine complexes, other six-coordinate ones, and four-coordinate ones, respectively. Curve-fitting calculations were carried out in the  $k$  ranges of 3.7–11.5 Å<sup>-1</sup> and 3.6–16 Å<sup>-1</sup> for six- and four-coordinate complexes, respectively.

### 5.3 Results and discussion

#### 5.3.1 XANES spectra

**Six-coordinate complexes.** XANES spectra for aqua and ammine complexes in solids and in aqueous solutions are shown in Fig. 5.1. There is a weak dipole-forbidden 1s→3d transition peak in the pre-edge region of every XANES spectrum except for Zn(II) complexes (filled 3d). The XANES spectra for divalent hexaaqua complexes have the ordinary shape for octahedral coordination sphere that has a large main peak immediately above the threshold. Ammine complexes of Mn(II), Fe(II), and Co(II) show similar XANES spectra to those for aqua complexes. It is interesting that for ammine complexes the small shoulders or peaks on the higher energy side of the main peak become clearer and stronger in the order of Mn < Fe < Co < Ni. This order is the

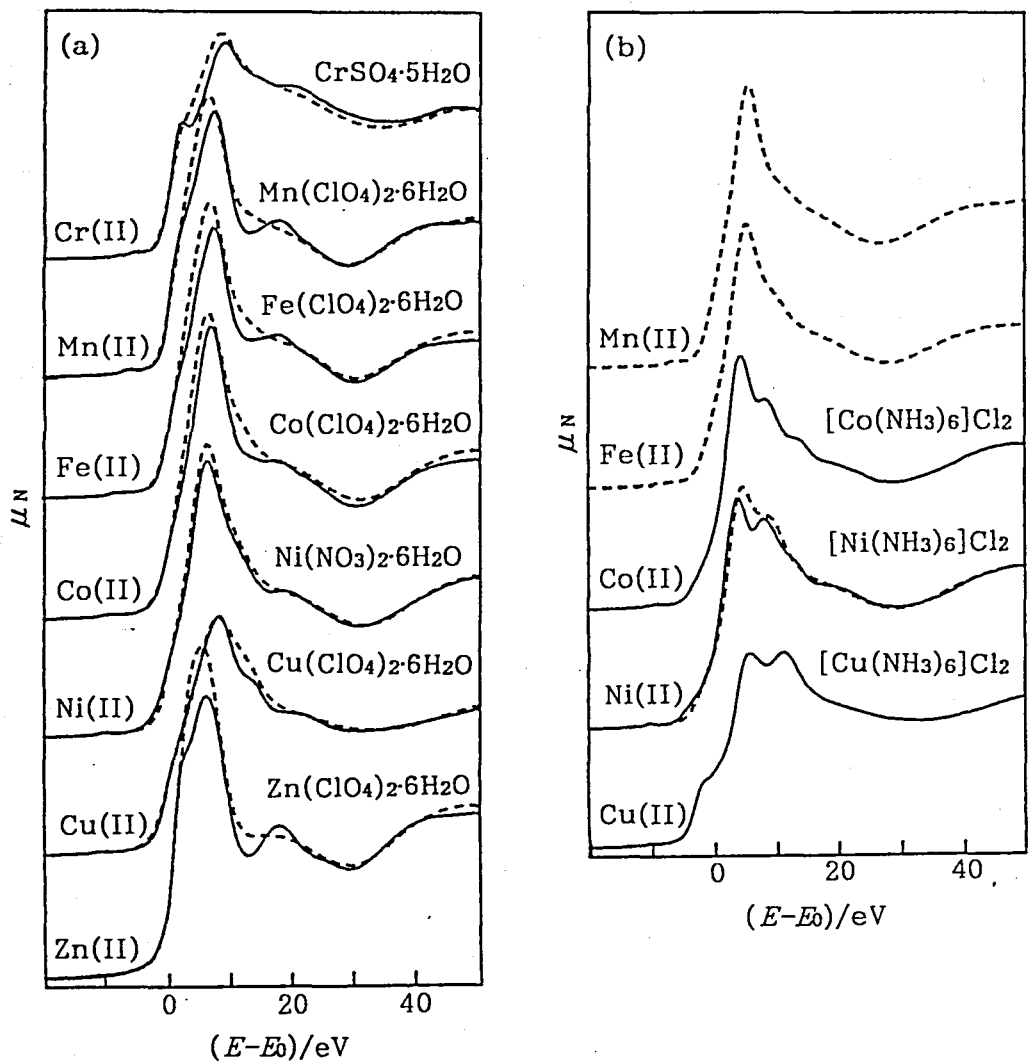


Figure 5.1. XANES spectra of metal K-edge for divalent (a) aqua and (b) ammine complexes. Solid and broken lines are for solid and for aqueous solution samples, respectively.

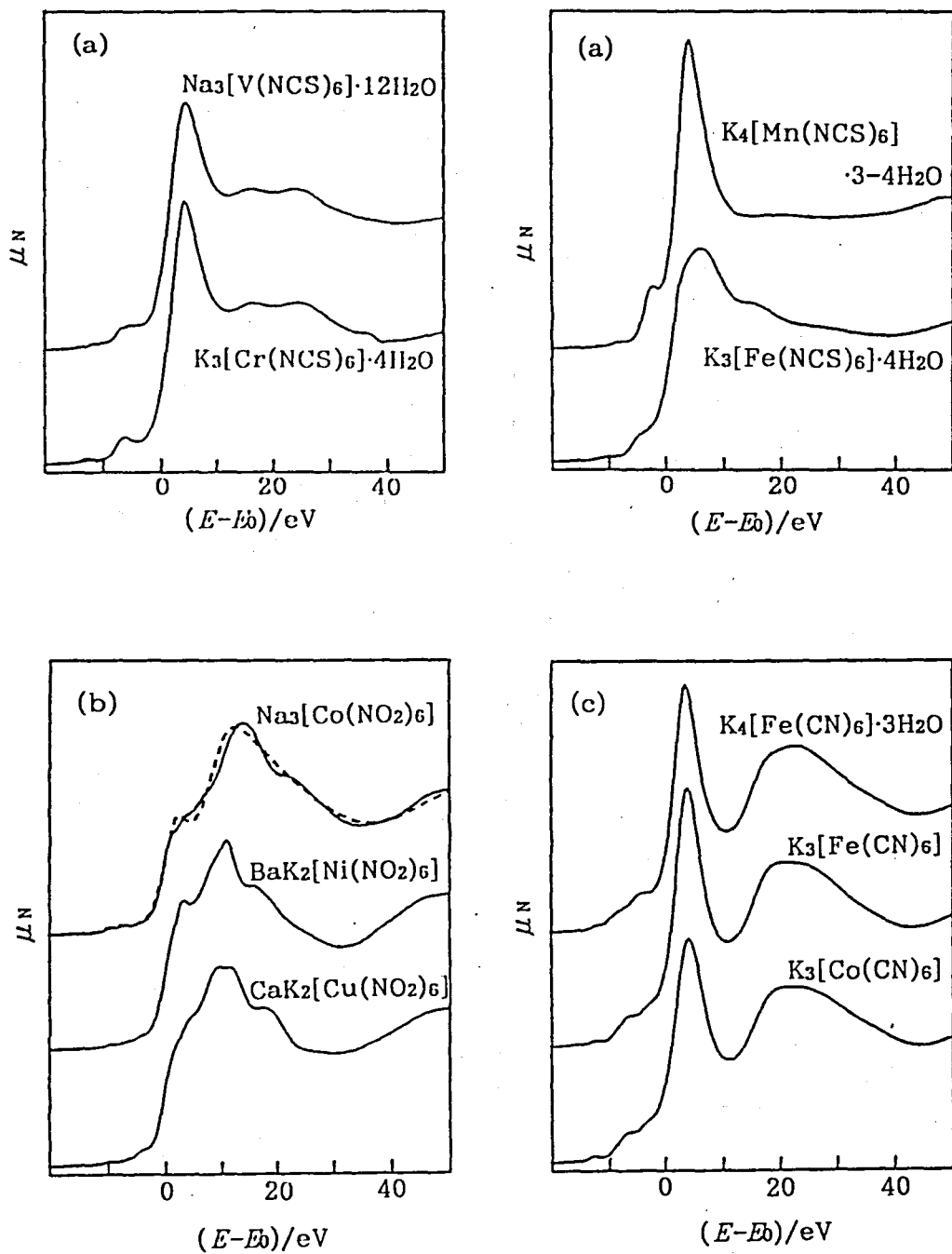


Figure 5.2. XANES spectra of metal K-edge for (a) isothiocyanato, (b) nitro, and (c) cyano complexes. Broken line in (b) are aqueous solution.

inverse of that for aqua complexes. These weak peaks would be caused by such multiple scattering effect of photoelectron as studied for Zn(II) aqua complexes.<sup>8)</sup>

Figure 5.2 shows XANES spectra for isothiocyanato, nitro, and cyano complexes. These spectra also have a large main peak. Among XANES spectra of the complexes having a common ligand resemblance is more distinct than among XANES spectra of the complexes of the same central metal ion.

Four-coordinate complexes. XANES spectra of central metal K-edge for divalent four-coordinate complexes are shown in Fig. 5.3. These spectra are very similar to each other except for Zn. The pre-edge  $1s \rightarrow 3d$  peak intensities decrease with the order of Mn to Cu, because of the number of 3d vacancies and the difference of resolution (the energy resolution at the Cu K-edge is about twice lower than that at the Mn K-edge). The main peaks (at the energy origin of the figures) are weaker than those for six-coordinate complexes. According to Bair and Goddard<sup>9)</sup> and Kosugi et al.,<sup>10)</sup> these main peaks can be assigned to the transition to 4p orbitals of the metals and the shoulder peaks between the pre-edge and the main peak are interpreted as the shake-down accompanying the  $1s \rightarrow 4p$  transition. The shake-down phenomenon appears also in XPS<sup>11)</sup> and arises from strong ligand-to-metal charge transfer (LMCT) from the highest-occupied ligand orbital (HOMO) to the unoccupied 3d of the metal. The energy level of HOMO of the initial state is lower than that of the 3d orbital and LMCT is observed in the UV-absorption spectrum. When the central metal absorbs X-ray and a core hole is produced, the vacant 3d orbital of the final state become lower in energy than

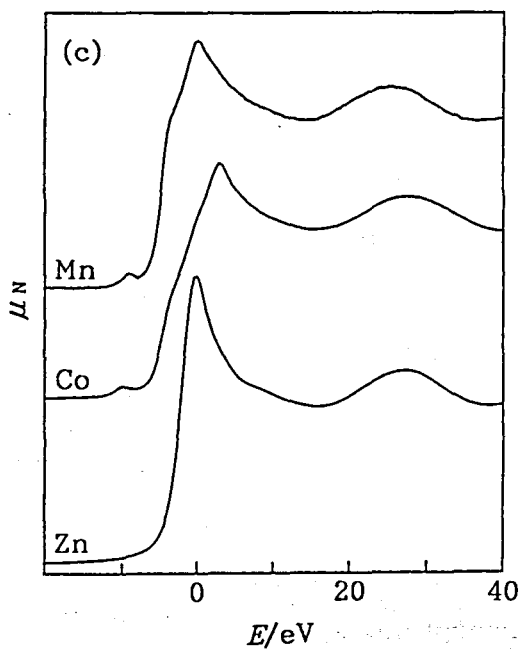
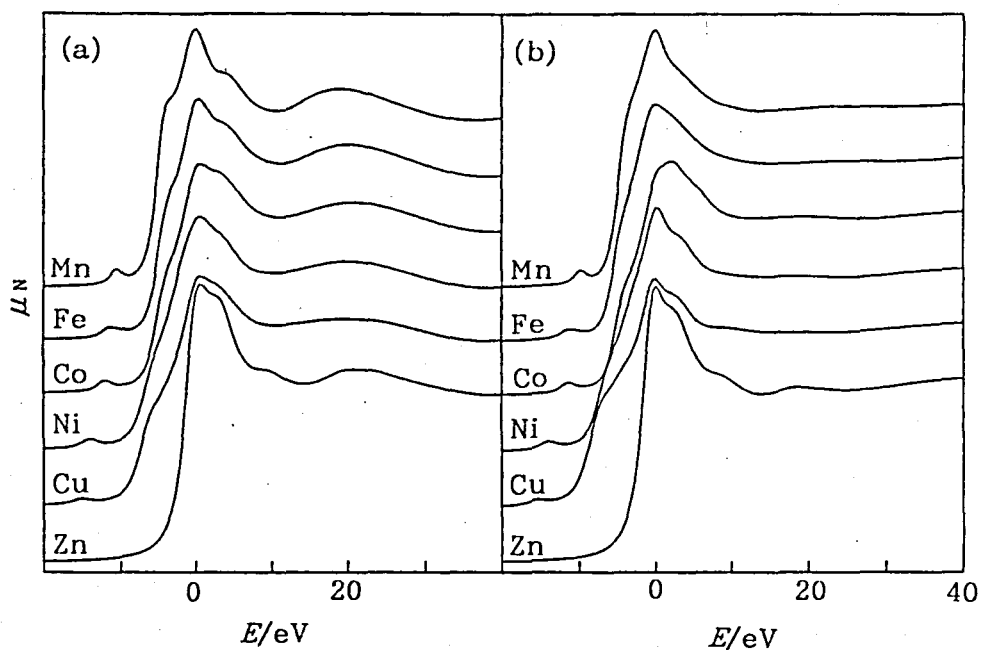


Figure 5.3. XANES spectra for metal K-edge for  $[(C_2H_5)_4N]_2[M^{II}X_4]$ . (a) Chloro complexes, (b) Bromo complexes, and (c) Iodo complexes. The Energy origin is set to the position for the main peak.

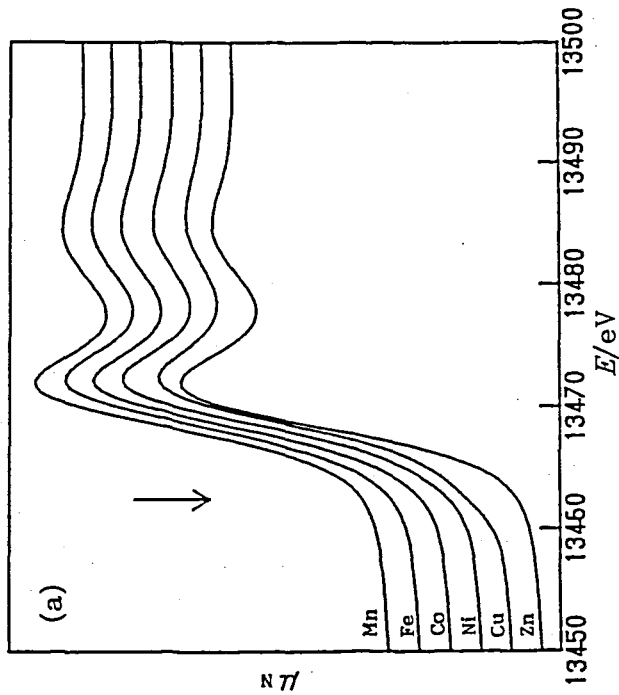
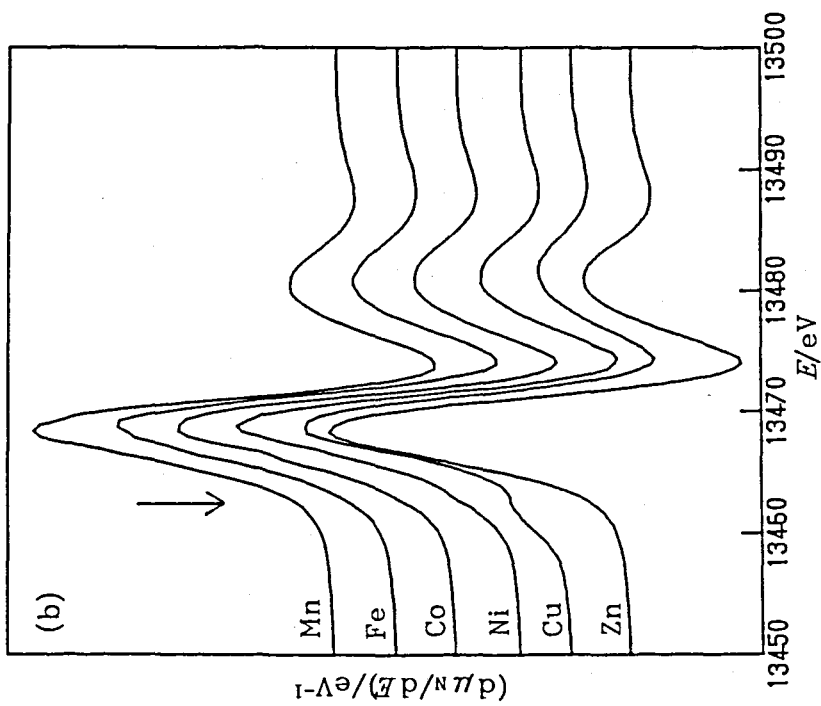


Figure 5.4. XANES spectra, (a), and their derivatives, (b), of Br K-edge for  $[(C_2H_5)_4N]_2[M^{II}Br_4]$ .

HOLO. The  $1s \rightarrow 4p$  peaks become weaker and lower in energy than those without shake-down transition. For the Zn(II) complexes, there are neither unoccupied 3d orbital nor LMCT. Therefore XANES for Zn(II) in Fig. 5.3 exhibit no shoulder peaks before their main peak and the main peaks are stronger than other metals. From Fig. 5.3 probabilities of the shake-down transition can not be made evident because estimation of absorption due to the transition to the continuum is difficult. However, it can be concluded that the energies of the LMCT of Ni and Cu are higher than those of Mn, Fe, and Co.

Figure 5.4 shows Br K-edge XANES spectra and their derivatives for bromo complexes. They are almost identical with each other but a little difference can be seen at the pre-edge (shown by the arrow in the figure). It is reported<sup>12)</sup> that Cl K-edge XANES for some Cu(II) chloro complexes have a clear pre-edge peak due to  $1s(\text{Cl}) \rightarrow 3d(\text{Cu})$  transition. The intensity of this pre-edge peak reflects the covalency of the coordination bond. Since the energy resolution is an order of magnitude lower than Cl K-edge, the pre-edge peaks for Br K-edge XANES are not so clear, though the pre-edge shoulders in the spectra were assigned to  $1s(\text{Br}) \rightarrow 3d(\text{metal})$  transition. The changes of the intensity of the shoulder show that the degree of covalency is as follows:  $\text{Mn} \approx \text{Fe} < \text{Co} < \text{Ni} < \text{Cu}$ .

### 5.3.2 Fourier transforms

Intensities of aqua, ammine, and halogeno complexes. If EXAFS Fourier transform is performed over the  $k$  range of  $0 \rightarrow \infty$  and  $\lambda(k)$  is independent to  $k$ ,  $r^2$  weighted peak intensity  $hr^2$ , where  $h$  is

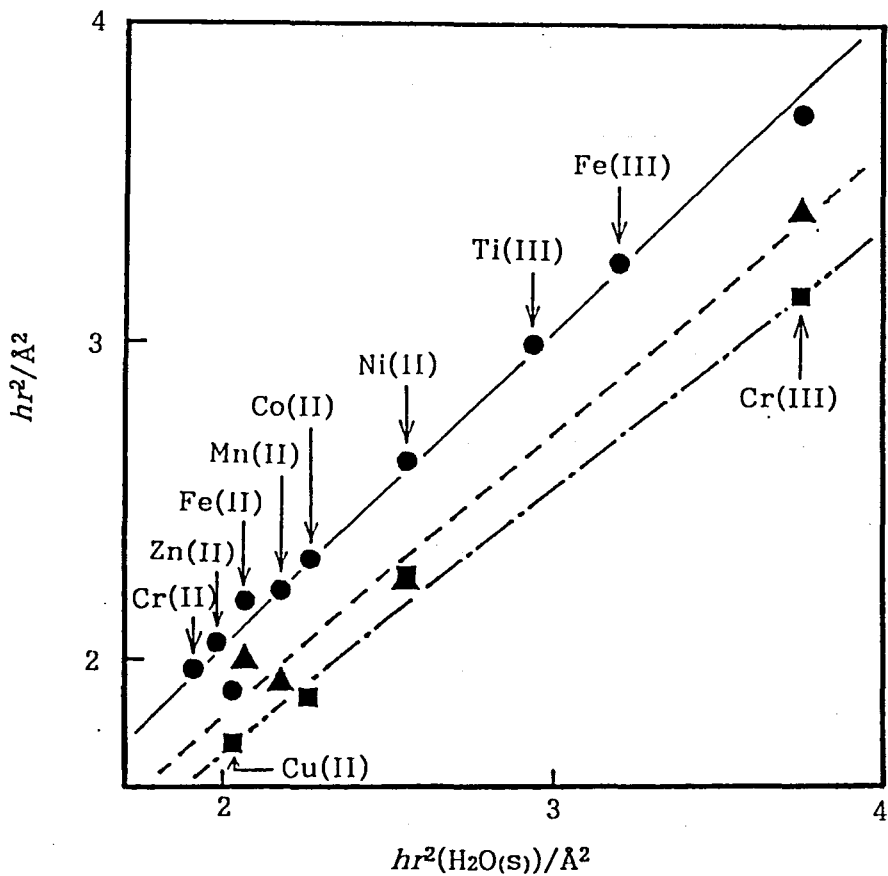


Figure 5.5. EXAFS peak intensities  $hr^2$  for six-coordinate first transition metal complexes. Aqua complexes in aqueous solutions (—●—), ammine complexes in aqueous solutions (—▲—), and in solids (—■—). The values for aqua complexes in solids,  $hr^2(\text{H}_2\text{O}(\text{s}))/\text{\AA}^2$ , are indicated on the abscissa.

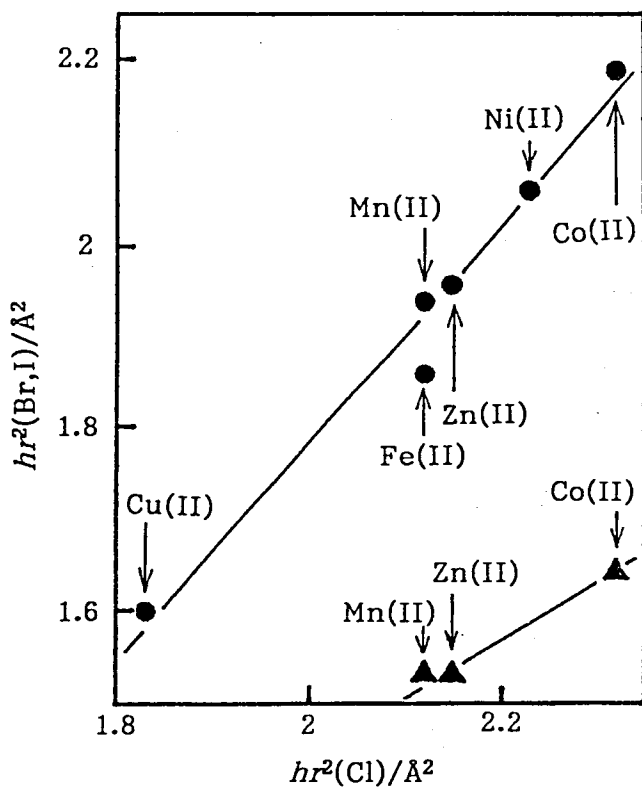


Figure 5.6. EXAFS peak intensities  $hr^2$  for four-coordinate first transition metal complexes. Bromo complexes (—●—) and iodo complexes (—▲—). The values for chloro complexes,  $hr^2(\text{Cl})/\text{\AA}^2$ , are indicated on the abscissa.

the peak height and  $r$  is the peak position, is derived from Eqs. (3.27), (4.4), (4.8), (4.10), and (4.11) as follows;

$$hr^2 \propto \frac{SN}{\sigma} = \frac{N}{\sigma} s_0^2 \exp\left(\frac{-2r}{\lambda}\right). \quad (5.1)$$

In Fig. 5.5, the  $hr^2$  values for aqua complexes in aqueous solutions and for ammine complexes in solids and in aqueous solutions are plotted against those for aqua complexes in solids. The values for bromo complexes against those for chloro complexes are also plotted in Fig. 5.6. There are linear correlations among these values. It was pointed out that the  $hr^2$  values of aqua complexes have correlation with the logarithm of the ligand exchange rate constants<sup>2)</sup> and reflect the character of the coordination bond. Here, the coordination number  $N$  is constantly 6 for Fig. 5.5 except for Cr(II) and Cu(II) that have the Jahn-Teller distortion or 4 for Fig. 5.6, and  $s_0^2$  and  $\lambda$  must be almost the same for all kinds of complexes. Furthermore, because  $\lambda$  is usually larger than 5 Å in inorganic materials,<sup>13)</sup> the differences in the exponential term of Eq. (5.1) among the complexes studied here must be less than about 10%. Thus, the result of Figs. 5.5 and 5.6 indicates that each metal ion has almost intrinsic  $\sigma$  value irrespective of its environments and ligands. It should be noted that the position of Cu(II) in Fig. 5.5 lies on the same line as other ions do, in spite of the fact that Cu(II) complexes have different degree of distortion among the aqua and the ammine complexes.

Isothiocyanato, nitro, and cyano complexes. Figure 5.7 shows EXAFS Fourier transforms for  $\text{Na}_3[\text{V}(\text{NCS})_6] \cdot 12\text{H}_2\text{O}$ ,  $\text{Na}_3[\text{Co}(\text{NO}_2)_6]$ , and  $\text{K}_3[\text{Co}(\text{CN})_6]$ . Two or three peaks are found in each of the transform. The first strong peak is corresponding to the direct

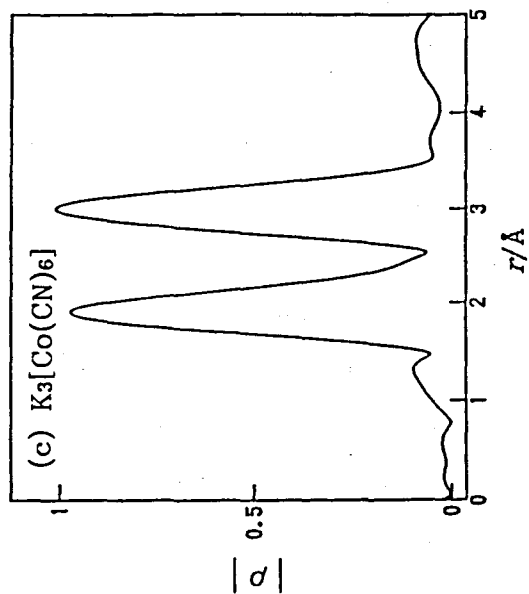
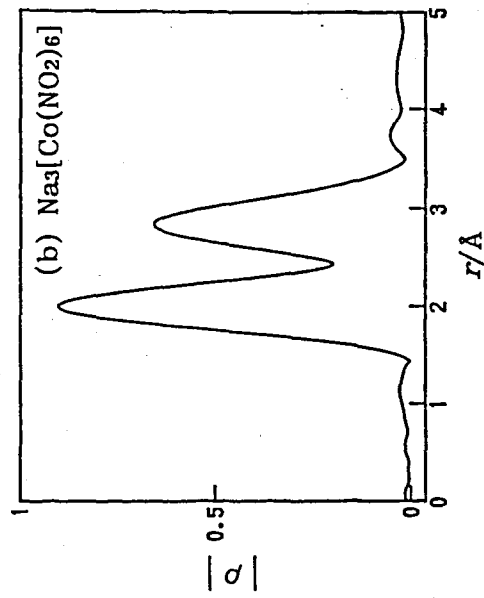
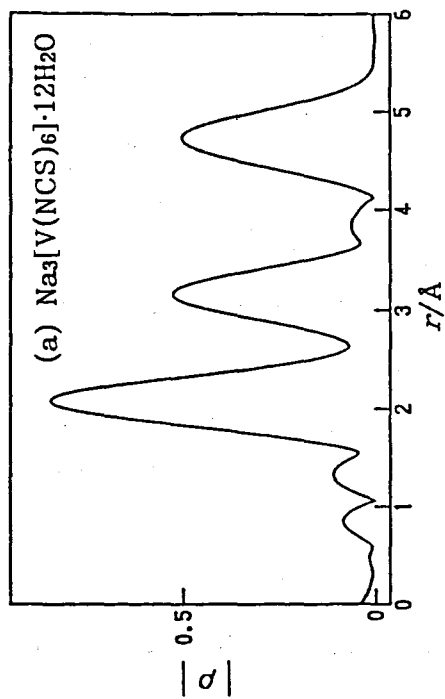


Figure 5.7. EXAFS Fourier transforms for (a)  $\text{Na}_3[\text{V}(\text{NCS})_6] \cdot 12\text{H}_2\text{O}$ , (b)  $\text{Na}_3[\text{Co}(\text{NO}_2)_6]$ , and (c)  $\text{K}_3[\text{Co}(\text{CN})_6]$ .

coordinating atoms. The second peak is the central carbon of  $\text{NCS}^-$ , oxygens of  $\text{NO}_2^-$ , or nitrogen of  $\text{CN}^-$  for isothiocyanato, nitro, or cyano complexes, respectively. The third peak of isothiocyanato complexes is sulfur. As can be seen from Eqs. (4.4) and (5.1), the peak heights in a certain Fourier transform of EXAFS reflect the following four factors; interatomic distance as  $\exp(-2r/\lambda)/r^2$ , coordination number  $N$ , Debye-Waller factor as  $1/\sigma$ , and the back-scattering amplitude  $F(k)$ . The longer the distance, the less the peak height not only by the factor of  $\exp(-2r/\lambda)/r^2$  but also by the factor of its larger Debye-Waller factor, because the more distant an atomic pair, usually the weaker the bond strength or more than one bonds from the absorbing to the scattering atom. For nitro complexes, because  $F(k)$  is almost the same for nitrogen and oxygen, that the second peak is intense relative respect to the first peak is due to their coordination number, *i.e.*  $N=6$  and  $12$  for nitrogen and oxygen, respectively.

On the other hand, the second peaks for isothiocyanato and cyano complexes and the second. These peaks have longer distance, the same coordination number, and similar scattering amplitude as those for the first peak, hence their peak height should be considerably reduced from that of the first peak. The third peaks for isothiocyanato complexes is also intense even though  $F(k)$  of sulfur is larger than that of carbon or nitrogen. This anomalous intensity is due to the forward-scattering of photoelectron wave by the intervening atoms. The scattering amplitude for the forward direction are much larger than unity. Therefore, when atoms including the absorbing atom and neighbors are arranged in a linear or nearly collinear fashion, the amplitude

is greatly enhanced and is commonly called "focusing" effect. This effect has been observed on copper metal,<sup>14)</sup> carbonyl complexes,<sup>15)</sup> and carboxylato complexes,<sup>16)</sup> etc.. Here, it is noted that the third peaks of isothiocyanato complexes contain "double focusing effect" by the two intervening atoms. The double focusing effect would be useful for detection of light elements lying more than 4 Å remote from an absorbing atom.

Sulfate salts of aqua complexes. Figure 5.8 shows the Fourier transforms of some sulfate salts. Crystallographic data show that  $\text{SO}_4^{2-}$  is coordinating to the central metal in Cr(II),<sup>17-19)</sup> Mn(II),<sup>20)</sup> and Cu(II)<sup>21)</sup> salts, whereas is not in Fe(II)<sup>22,23)</sup> and Ni(II)<sup>24,25)</sup> salts. The peak which is assigned to sulfur of  $\text{SO}_4^{2-}$  can be seen around 3.25 Å in the Fourier transform of Mn(II) sulfate. The peak at 3.1 Å in the transform of Ti(III) sulfate reveals the coordination of  $\text{SO}_4^{2-}$  to Ti, as can be presumed from its composition. The Fourier transforms of Fe(II), Co(II), and Ni(II) salts show no such peak. On the other hand, Cr(II) and Cu(II) sulfates do not show this peak though  $\text{SO}_4^{2-}$  is coordinating to the metal. In Cr(II) and Cu(II) salts the axial sulfate ions are more separated from the central atom than the equatorial ligands owing to the Jahn-Teller effect. These results show that the axial metal-oxygen bonds have a large Debye-Waller factor, *i.e.* a weak bond.

### 5.3.3 Curve-fitting results

Table 5.3 lists all the curve-fitting results and their  $r$  space filtering ranges. Some samples were measured and analyzed twice or more times in order to examine the reproducibility and errors

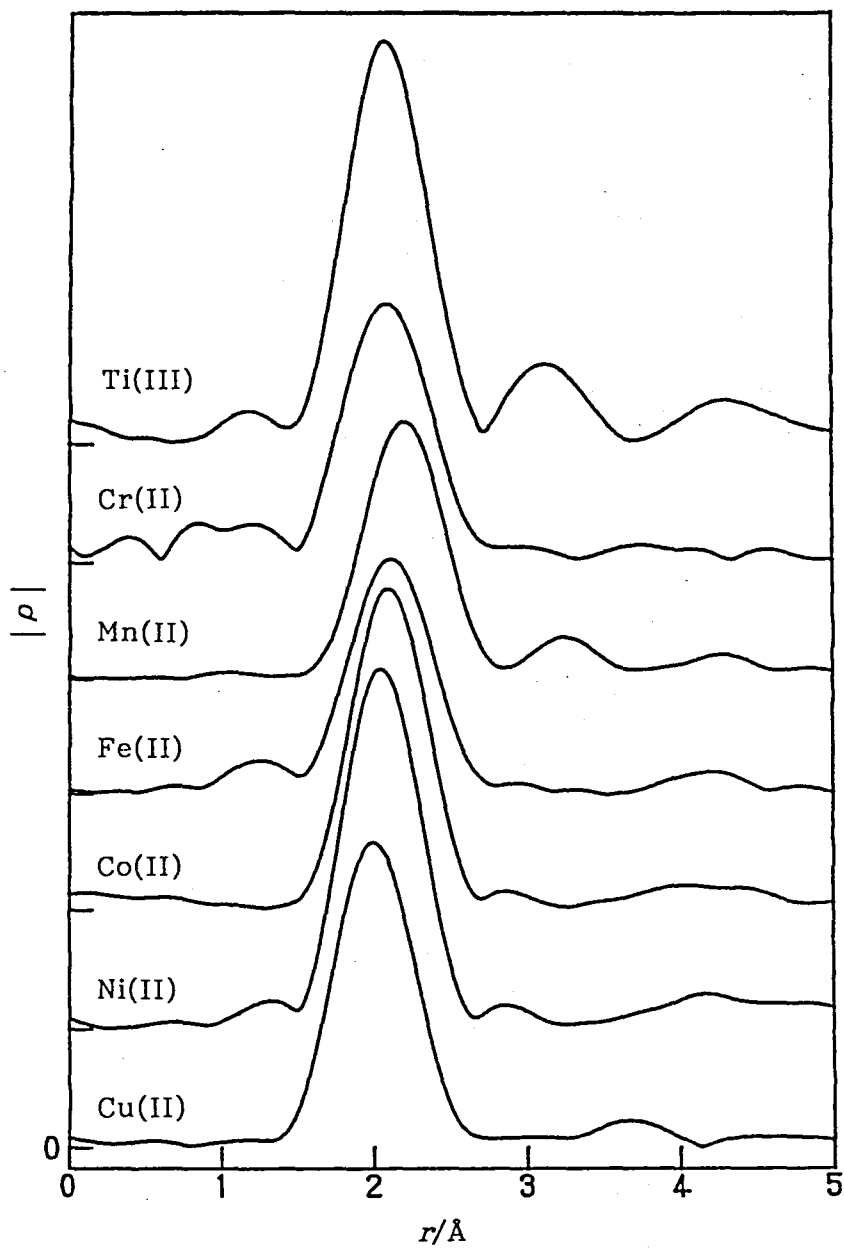


Figure 5.8. EXAFS Fourier transforms for some sulfate salts of first transition metals.

Table 5.3 (a). EXAFS Curve-fitting Results and  $r$  Space Filtering Range of Six-coordinate Samples.

Sample	EXAFS curve-fitting					$r$ range	
	$r/\text{\AA}$	$B$	$\sigma/10^{-2}\text{\AA}$	$\Delta E_0/\text{eV}$	R/%	$r_{\text{min}}/\text{\AA}$	$r_{\text{max}}/\text{\AA}$
Ti <sub>2</sub> (SO <sub>4</sub> ) <sub>3</sub> ·8H <sub>2</sub> O	2.041	2.4	5.3	9.2	8.7	1.39	2.79
	2.040	2.5	5.4	9.1	9.6	1.39	2.80
[Ti(H <sub>2</sub> O) <sub>6</sub> ] <sup>3+</sup> (aq)	2.067	2.7	6.2	9.6	5.3	1.42	2.83
[V(H <sub>2</sub> O) <sub>6</sub> ] <sup>3+</sup> (aq)	2.020	2.3	3.9	6.5	12.2	1.13	2.90
Na <sub>3</sub> [V(NCS) <sub>6</sub> ]·12H <sub>2</sub> O	2.061	2.4	3.5	7.0	10.2	1.48	2.73
	2.063	2.4	4.5	6.8	13.7	1.53	2.76
CrSO <sub>4</sub> ·5H <sub>2</sub> O	2.045	1.2	2.7	9.2	13.5	1.44	2.85
[Cr(H <sub>2</sub> O) <sub>6</sub> ] <sup>2+</sup> (aq)	2.059	1.4	4.1	7.8	10.7	1.25	2.88
Cr <sub>2</sub> (SO <sub>4</sub> ) <sub>3</sub> ·18H <sub>2</sub> O	1.980	2.5	2.8	5.4	7.0	1.32	2.75
Cr(ClO <sub>4</sub> ) <sub>3</sub> ·6H <sub>2</sub> O	1.980	2.6	2.9	5.5	8.1	1.33	2.77
	1.980	2.6	3.4	5.4	8.9	1.27	2.78
[Cr(H <sub>2</sub> O) <sub>6</sub> ] <sup>3+</sup> (aq) (1)	1.980	2.6	3.0	5.4	6.7	1.32	2.78
	1.980	2.6	3.3	5.6	8.4	1.27	2.76
(2)	1.982	2.6	3.3	5.6	7.1	1.29	2.78
(3)	1.981	2.7	3.7	5.5	8.4	1.23	2.77
	1.977	2.4	2.3	5.6	5.0	1.45	2.72
[Cr(NH <sub>3</sub> ) <sub>6</sub> ]Cl <sub>3</sub>	2.090	2.0	2.6	5.9	6.3	1.44	2.83
	2.088	2.2	2.4	5.8	8.1	1.37	2.84
[Cr(NH <sub>3</sub> ) <sub>6</sub> ] <sup>3+</sup> (aq)	2.093	2.3	3.1	5.8	7.9	1.41	2.84
	2.018	2.3	3.2	6.0	8.8	1.39	2.75
MnSO <sub>4</sub> ·5H <sub>2</sub> O	2.176	2.1	6.4	4.6	2.7	1.45	2.93
	2.165	2.4	7.4	3.9	3.6	1.42	2.96
	2.167	2.4	7.4	4.1	4.4	1.44	2.96
Mn(ClO <sub>4</sub> ) <sub>2</sub> ·6H <sub>2</sub> O	2.175	2.2	7.1	4.0	5.8	1.39	2.87
	2.171	2.3	6.7	3.5	2.5	1.51	2.90
	2.171	2.3	6.7	3.7	3.1	1.48	2.88
	2.174	2.3	7.4	4.2	3.3	1.51	2.92
[Mn(H <sub>2</sub> O) <sub>6</sub> ] <sup>2+</sup> (aq) (1)	2.171	2.5	7.3	3.2	1.8	1.50	2.87
	2.173	2.5	7.5	3.6	4.2	1.51	2.90
	2.166	2.6	7.7	2.7	4.2	1.47	2.89
	2.179	2.4	6.6	4.5	4.2	1.53	2.84
(2)	2.172	2.6	7.6	3.4	3.6	1.49	2.91
	2.180	2.5	7.2	4.5	2.4	1.44	2.93
[Mn(NH <sub>3</sub> ) <sub>6</sub> ] <sup>2+</sup> (aq)	2.270	2.3	7.3	4.4	4.8	1.60	2.91
K <sub>4</sub> [Mn(NCS) <sub>6</sub> ]·3-4H <sub>2</sub> O	2.207	2.3	7.4	2.4	9.6	1.62	2.83
	2.223	2.2	7.0	4.7	5.6	1.46	2.77

(aq) = aqueous solution

Table 5.3 (a). EXAFS Curve-fitting Results and  $r$  Space Filtering Range of Six-coordinate Samples (*continued*).

Sample	EXAFS curve-fitting					$r$ range	
	$r/\text{\AA}$	$B$	$\sigma/10^{-2}\text{\AA}$	$\Delta E_0/\text{eV}$	R/%	$r_{\text{min}}/\text{\AA}$	$r_{\text{max}}/\text{\AA}$
FeSO <sub>4</sub> ·7H <sub>2</sub> O	2.100	2.0	7.0	2.4	10.8	1.43	2.87
Fe(ClO <sub>4</sub> ) <sub>2</sub> ·6H <sub>2</sub> O	2.114	2.2	7.1	4.3	3.3	1.40	2.81
	2.116	2.4	6.8	3.9	2.7	1.46	2.80
	2.115	2.4	6.8	3.8	3.5	1.47	2.81
[Fe(H <sub>2</sub> O) <sub>6</sub> ] <sup>2+</sup> (aq)	2.116	2.5	7.3	3.6	6.2	1.41	2.82
	2.115	2.6	7.5	3.4	5.3	1.43	2.88
[Fe(NH <sub>3</sub> ) <sub>6</sub> ] <sup>2+</sup> (aq)	2.206	2.4	7.7	3.7	5.0	1.63	2.83
	2.208	2.4	7.8	3.7	4.4	1.59	2.84
K <sub>4</sub> [Fe(CN) <sub>6</sub> ]·3H <sub>2</sub> O	1.928	2.3	2.6	6.2	9.0	1.40	2.51
Fe(ClO <sub>4</sub> ) <sub>3</sub> ·6H <sub>2</sub> O	2.007	2.3	3.2	4.9	3.0	1.39	2.73
	2.005	2.5	4.0	4.5	5.5	1.32	2.74
[Fe(H <sub>2</sub> O) <sub>6</sub> ] <sup>3+</sup> (aq) (1)	2.011	2.8	5.2	5.4	8.4	1.33	2.73
	2.008	2.7	4.3	4.9	3.5	1.38	2.70
(2)	1.999	2.5	4.5	3.8	10.1	1.33	2.77
K <sub>3</sub> [Fe(NCS) <sub>6</sub> ]·4H <sub>2</sub> O	2.090	2.0	6.5	5.8	4.5	1.53	2.63
	2.091	2.0	6.6	5.9	4.6	1.55	2.62
K <sub>3</sub> [Fe(CN) <sub>6</sub> ]	1.952	2.3	2.3	6.1	7.1	1.42	2.57
CoSO <sub>4</sub> ·7H <sub>2</sub> O	2.081	2.4	6.2	3.5	3.8	1.38	2.77
Co(NO <sub>3</sub> ) <sub>2</sub> ·6H <sub>2</sub> O	2.078	2.2	6.5	3.1	9.5	1.57	2.82
Co(ClO <sub>4</sub> ) <sub>2</sub> ·6H <sub>2</sub> O	2.086	2.5	7.1	4.2	4.5	1.49	2.76
	2.088	2.3	6.5	4.0	6.5	1.44	2.75
	2.086	2.3	6.3	3.8	5.2	1.49	2.73
	2.084	2.4	6.7	3.7	4.0	1.44	2.76
[Co(H <sub>2</sub> O) <sub>6</sub> ] <sup>2+</sup> (aq) (1)	2.078	2.8	7.6	2.7	5.6	1.49	2.77
	2.086	2.6	7.0	2.9	4.5	1.44	2.73
	2.086	2.6	7.1	3.1	4.3	1.42	2.76
(2)	2.086	2.6	7.1	3.4	4.1	1.41	2.74
	2.086	2.6	7.0	3.3	4.6	1.39	2.76
[Co(NH <sub>3</sub> ) <sub>6</sub> ]Cl <sub>2</sub>	2.169	2.1	7.2	4.3	5.8	1.49	2.78
	2.175	2.1	7.2	5.3	6.6	1.53	2.79
	2.176	2.1	7.0	5.2	7.0	1.56	2.75
	2.173	2.1	7.0	4.8	6.1	1.50	2.76
[Co(NH <sub>3</sub> ) <sub>6</sub> ]Cl <sub>3</sub>	1.967	2.2	2.4	4.3	9.8	1.29	2.71
	1.968	2.2	2.1	4.4	9.2	1.35	2.74
[Co(NH <sub>3</sub> ) <sub>6</sub> ] <sup>3+</sup> (aq)	1.972	2.2	2.1	4.3	9.8	1.28	2.68
Na <sub>3</sub> [Co(NO <sub>2</sub> ) <sub>6</sub> ]	1.987	2.4	3.9	8.7	7.2	1.41	2.58
	1.984	2.4	3.9	8.3	6.9	1.39	2.55
[Co(NO <sub>2</sub> ) <sub>6</sub> ] <sup>3-</sup> (aq)	1.968	2.3	4.0	8.3	9.1	1.34	2.55
	1.972	2.5	4.1	8.0	6.9	1.40	2.53

(aq) = aqueous solution

Table 5.3 (a). EXAFS Curve-fitting Results and  $r$  Space Filtering Range of Six-coordinate Samples (*continued*).

Sample	EXAFS curve-fitting					$r$ range	
	$r/\text{\AA}$	$B$	$\sigma/10^{-2}\text{\AA}$	$\Delta E_0/\text{eV}$	R/%	$r_{\text{min}}/\text{\AA}$	$r_{\text{max}}/\text{\AA}$
K <sub>3</sub> [Co(CN) <sub>6</sub> ]	1.908	2.3	3.5	5.7	5.5	1.41	2.54
	1.903	2.4	3.2	4.8	8.4	1.30	2.55
NiSO <sub>4</sub> ·6H <sub>2</sub> O	2.039	2.4	5.3	2.1	9.7	1.43	2.72
Ni(NO <sub>3</sub> ) <sub>2</sub> ·6H <sub>2</sub> O	2.048	2.5	6.0	2.8	4.8	1.40	2.69
	2.046	2.5	5.9	3.0	7.1	1.45	2.69
[Ni(H <sub>2</sub> O) <sub>6</sub> ] <sup>2+</sup> (aq)	2.050	2.8	6.7	3.4	3.2	1.39	2.70
	2.051	2.8	6.7	3.4	3.8	1.37	2.69
[Ni(NH <sub>3</sub> ) <sub>6</sub> ]Cl <sub>2</sub>	2.121	2.3	6.4	3.2	4.2	1.53	2.73
	2.125	2.3	6.3	3.7	5.0	1.53	2.72
[Ni(NH <sub>3</sub> ) <sub>6</sub> ] <sup>2+</sup> (aq)	2.126	2.4	6.5	3.6	4.6	1.49	2.74
	2.127	2.3	6.4	3.8	5.7	1.53	2.75
BaK <sub>2</sub> [Ni(NO <sub>2</sub> ) <sub>6</sub> ]	2.101	2.2	5.4	8.9	6.5	1.58	2.70
CuSO <sub>4</sub> ·5H <sub>2</sub> O	1.968	1.5	4.2	8.4	9.9	1.23	2.81
	1.964	1.5	3.9	8.1	8.9	1.27	2.83
	1.965	1.5	4.0	8.3	7.7	1.29	2.81
	1.967	1.5	4.0	8.2	9.3	1.25	2.86
	1.968	1.4	3.6	8.7	8.7	1.31	2.82
Cu(ClO <sub>4</sub> ) <sub>2</sub> ·6H <sub>2</sub> O	1.964	1.5	4.6	6.9	7.4	1.30	2.75
[Cu(H <sub>2</sub> O) <sub>6</sub> ] <sup>2+</sup> (aq)	1.963	1.6	5.1	4.9	4.8	1.32	2.67
	1.965	1.6	5.0	5.7	7.7	1.30	2.65
	1.966	1.6	5.2	5.6	7.0	1.26	2.66
	1.960	1.6	5.3	5.2	5.7	1.15	2.66
[Cu(NH <sub>3</sub> ) <sub>6</sub> ]Cl <sub>2</sub>	2.033	1.4	5.2	5.9	7.1	1.41	2.65
	2.032	1.6	5.6	5.9	7.7	1.39	2.64
CaK <sub>2</sub> [Cu(NO <sub>2</sub> ) <sub>6</sub> ]	2.047	1.2	3.3	8.4	7.4	1.65	2.57
	2.035	1.2	4.3	6.6	4.0	1.58	2.60
ZnSO <sub>4</sub> ·7H <sub>2</sub> O	2.077	2.6	7.6	5.6	7.4	1.44	2.73
	2.077	2.4	7.2	5.0	9.5	1.39	2.70
Zn(NO <sub>3</sub> ) <sub>2</sub> ·6H <sub>2</sub> O	2.071	2.6	8.2	4.5	7.0	1.42	2.74
Zn(ClO <sub>4</sub> ) <sub>2</sub> ·6H <sub>2</sub> O	2.077	2.3	7.4	5.2	8.4	1.45	2.69
	2.077	2.4	8.8	4.4	4.9	1.31	2.76
	2.079	2.6	8.0	5.4	5.4	1.21	2.68
[Zn(H <sub>2</sub> O) <sub>6</sub> ] <sup>2+</sup> (aq) (1)	2.071	2.7	8.3	4.2	5.8	1.30	2.70
	(2) 2.075	2.7	8.2	5.5	6.5	1.37	2.75

(aq) = aqueous solution

Table 5.3 (b). EXAFS Curve-fitting Results and  $r$  Space Filtering Range of Metal K-edge of  $[(C_2H_5)_4N]_{4-n}[M^{n+}X^-]_n$ .

$M^{n+}$	$X^-$	EXAFS curve-fitting					$r$ range	
		$r/\text{\AA}$	$B$	$\sigma/10^{-2}\text{\AA}$	$\Delta E_b/\text{eV}$	R/%	$r_{\min}/\text{\AA}$	$r_{\max}/\text{\AA}$
Mn(II)	Cl	2.373	2.0	6.2	5.2	2.8	1.85	2.98
		2.374	2.1	6.4	5.2	3.3	1.80	2.99
Mn(II)	Br	2.519	2.2	6.8	3.3	1.6	1.91	3.12
		2.519	2.3	6.9	3.5	2.1	1.92	3.12
Mn(II)	I	2.711	1.6	6.5	2.7	12.9	2.24	3.27
		2.715	1.7	6.8	2.9	11.1	2.24	3.25
Fe(II)	Cl	2.320	2.1	6.3	5.0	2.4	1.77	2.86
		2.319	2.1	6.3	4.9	2.4	1.81	2.87
Fe(II)	Br	2.460	2.1	6.9	3.1	1.6	1.90	3.05
		2.462	2.2	7.0	3.6	1.9	1.91	3.05
Fe(III)	Cl	2.208	2.1	4.5	6.1	3.2	1.68	2.77
		2.207	2.1	4.6	6.0	4.4	1.72	2.77
Co(II)	Cl	2.288	2.1	6.0	4.7	2.4	1.78	2.83
		2.288	2.1	5.9	4.6	2.1	1.78	2.86
Co(II)	Br	2.420	2.2	6.2	1.9	2.7	1.91	2.99
		2.422	2.2	6.3	2.3	2.4	1.93	2.99
Co(II)	I	2.608	1.8	6.7	1.3	8.1	2.11	3.09
		2.610	1.7	6.3	1.6	6.6	2.10	3.11
Ni(II)	Cl	2.268	2.1	6.0	4.8	3.0	1.79	2.82
		2.269	2.1	6.2	5.1	3.1	1.79	2.82
Ni(II)	Br	2.405	2.2	6.5	3.6	1.7	1.89	2.92
		2.409	2.2	6.5	4.5	2.7	1.92	2.92
Cu(II)	Cl	2.247	2.1	7.0	4.9	9.2	1.72	2.82
		2.250	2.1	6.9	5.2	3.8	1.71	2.79
Cu(II)	Br	2.381	2.0	7.2	4.1	2.2	1.84	2.91
		2.381	1.9	7.1	3.9	2.4	1.87	2.93
Zn(II)	Cl	2.274	2.2	6.6	5.6	4.0	1.83	2.77
		2.278	2.2	6.6	5.8	2.8	1.79	2.80
Zn(II)	Br	2.409	2.2	6.8	2.4	2.6	1.94	2.96
		2.411	2.2	6.8	2.7	1.6	1.92	2.98
Zn(II)	I	2.614	1.9	7.2	2.8	4.5	2.08	3.23
		2.613	1.9	7.2	2.5	4.6	2.10	3.19

Table 5.3 (c). EXAFS Curve-fitting Results and  $r$  Space Filtering Range of Br K-edge of  $[(C_2H_5)_4N]_2[M^{II}Br_4]$ .

Metal	EXAFS curve-fitting					$r$ range	
	$r/\text{\AA}$	$B$	$\sigma/10^{-2}\text{\AA}$	$\Delta E_0/\text{eV}$	R/%	$r_{\min}/\text{\AA}$	$r_{\max}/\text{\AA}$
Mn	2.518	0.45	6.4	4.4	3.1	2.09	3.02
	2.517	0.45	6.5	3.9	2.7	2.07	3.05
Fe	2.467	0.46	6.7	4.6	5.6	1.99	3.00
	2.471	0.44	6.4	5.2	3.8	1.98	3.00
Co	2.420	0.51	6.2	4.0	2.6	1.93	2.98
	2.424	0.50	6.1	4.9	2.9	1.94	2.95
Ni	2.410	0.52	6.4	5.0	4.2	1.91	2.92
	2.405	0.50	6.2	3.9	1.5	1.92	2.94
Cu	2.380	0.49	7.1	6.8	4.2	1.89	2.97
	2.378	0.48	7.0	6.6	3.8	1.90	2.93
Zn	2.419	0.54	6.7	2.8	2.3	1.96	2.96
	2.422	0.53	6.6	3.1	1.5	1.93	2.92

of the measurements and data analysis. Variations of the interatomic distances  $r$  for a certain sample are smaller than those of  $B$  and  $\sigma$ , because a deviation from the best-fit value of the phase terms, *i.e.*  $r$  or  $\Delta E_0$ , will cause much larger increase of the sum of residual squared (R) than that of the amplitude terms,  $B$  and  $\sigma$ . The larger R values seems to lead to larger variations, but this is not necessarily the case. Although these variations are originally due to the noise or errors in measurements, the errors in the data analysis and the correlations among parameters in least-square calculations expand the influences of the measurement errors. The parameter correlations can be seen in Table 5.3. In most of the samples,  $r$  become longer as  $\Delta E_0$  become larger, and  $B$  become larger as  $\sigma$  become larger. Roughly speaking, increasing  $\Delta E_0$  by *ca.* 3 eV cause increase in  $r$  by *ca.* 0.01 Å and increasing  $B$  by *ca.* 10% cause increase in  $\sigma$  by *ca.* 20%. The errors and correlations should keep in mind through the discussions in the following sections.

#### 5.3.4 Interatomic distances

The interatomic distances  $r$  obtained from EXAFS curve-fitting and averages of corresponding bond distances  $r_{av}$  by X-ray diffraction studies are compared in Table 5.4. For Cr(II) and Cu(II) complexes, the bond lengths of the equatorial site are accounted in the calculation of  $r_{av}$ . Most of  $r$  agree with  $r_{av}$  within about 0.02 Å, especially excellent agreements are shown for aqueous solutions of aqua complexes. But some samples that have large residual R value show relatively large differences (*ca.* 0.05 Å) based on the measurements and the systematic errors of the

Table 5.4 (a). Comparison of Interatomic Distances  $r$  and  $\sigma^2$  by EXAFS with Average of Bond Distances  $r_{av}$  and  $\sigma_{stat}^2$  by X-ray Diffraction.

Compound	EXAFS		Diffraction		Ref.
	$r/\text{\AA}$	$\sigma^2/10^{-4}\text{\AA}^2$	$r_{av}/\text{\AA}$	$\sigma_{stat}^2/10^{-4}\text{\AA}^2$	
$\text{Na}_3[\text{V}(\text{NCS})_6] \cdot 12\text{H}_2\text{O}$	2.062	16	2.044	0.24	(3)
$\text{CrSO}_4 \cdot 5\text{H}_2\text{O}$	2.045	7.3	2.0472	0.91	(17)
			2.049	0.81	(18)
			2.0474	0.93	(19)
$[\text{Cr}(\text{NH}_3)_6]\text{Cl}_3$	2.089	6.2	2.07	0	(26)
$\text{MnSO}_4 \cdot 5\text{H}_2\text{O}$	2.169	50	2.170	3.3	(20)
$\text{FeSO}_4 \cdot 7\text{H}_2\text{O}$	2.100	49	2.14	7.4	(22)
			2.130	18	(23)
$\text{Fe}(\text{ClO}_4)_2 \cdot 6\text{H}_2\text{O}$	2.115	47	2.12	0	(27)
$\text{K}_3[\text{Fe}(\text{CN})_6]$	1.952	53	1.938	0.42	(28)
			1.944	0.057	(29)
$[\text{Co}(\text{NH}_3)_6]\text{Cl}_2$	2.173	50	2.114	—	(30)
$[\text{Co}(\text{NH}_3)_6]\text{Cl}_3$	1.967	5.0	1.966	0.71	(31)
$\text{Na}_3[\text{Co}(\text{NO}_2)_6]$	1.985	15	—	0	(32)
$\text{NiSO}_4 \cdot 6\text{H}_2\text{O}$	2.039	28	2.048	0.96	(24)
			2.048	1.0	(25)
$\text{Ni}(\text{NO}_3)_2 \cdot 6\text{H}_2\text{O}$	2.047	35	2.062	5.8	(33)
$\text{BaK}_2[\text{Ni}(\text{NO}_2)_6]$	2.101	29	2.0795	0	(34)
$[(\text{C}_2\text{H}_5)_4\text{N}]_2[\text{NiCl}_4]$	2.269	37	2.246	0	(35)
$\text{CuSO}_4 \cdot 5\text{H}_2\text{O}$	1.966	16	1.9571	2.2	(21)
$\text{Cu}(\text{ClO}_4)_2 \cdot 6\text{H}_2\text{O}$	1.964	21	2.13	14	(36)
$[\text{Cu}(\text{NH}_3)_6]\text{Cl}_2$	2.033	29	2.08	0	(5)
$\text{CaK}_2[\text{Cu}(\text{NO}_2)_6]$	2.041	15	2.0511	0.0072	(6)
$\text{Zn}(\text{NO}_3)_2 \cdot 6\text{H}_2\text{O}$	2.071	68	2.096	7.6	(37)
$\text{Zn}(\text{ClO}_4)_2 \cdot 6\text{H}_2\text{O}$	2.077	66	2.12	0	(38)

Table 5.4 (b). Comparison of Interatomic Distances  $r$  between EXAFS and X-ray Diffraction for Aqua Complexes in Aqueous Solution.

Metal	EXAFS $r/\text{\AA}$	Diffraction $r/\text{\AA}$	Ref.
Cr(III)	1.980	1.98	(39)
Mn(II)	2.173	2.20	(40)
Fe(II)	2.115	2.12	(40)
Fe(III)	2.006	2.005–2.010	(41)
Co(II)	2.084	2.08	(40)
Ni(II)	2.051	2.04	(40)
Cu(II)	1.964	1.94	(40)
Zn(II)	2.075	2.080–2.083	(40)

Table 5.5 (a). Interatomic Distances  $r/\text{\AA}$  obtained from EXAFS Curve-fitting for Six-coordinate Samples.

Metal	H <sub>2</sub> O(s)	H <sub>2</sub> O and SO <sub>4</sub> <sup>2-</sup> (s)	H <sub>2</sub> O(aq)	Ligand and State				
				NH <sub>3</sub> (s)	NH <sub>3</sub> (aq)	NCS <sup>-</sup> (s)	NO <sub>2</sub> <sup>-</sup> (s)	CN <sup>-</sup> (s)
Cr(II)		2.045	2.059					
Mn(II)	2.173	2.169	2.173		2.270	2.215		
Fe(II)	2.100S)		2.115		2.207			1.928
	2.115P)							
Co(II)	2.081S)		2.084	2.173				
	2.078N)							
	2.068P)							
Ni(II)	2.039S)		2.051	2.123	2.127		2.101	
	2.047N)							
Cu(II)	1.964	1.966	1.964	2.033			2.041	
Zn(II)	2.077S)		2.075					
	2.071N)							
	2.077P)							
Ti(III)		2.041	2.067					
V(III)			2.020			2.062		
			1.980	2.089	2.095	2.020		
Cr(III)	1.980P)							
	1.980S)							
Fe(III)	2.006		2.006			2.091		1.952
Co(III)				1.967	1.972		1.985	1.906

S) Sulfate, N) Nitrate, P) Perchlorate  
(s): solid, (aq): aqueous solution

Table 5.5 (b). Interatomic Distances  $r/\text{\AA}$  obtained from EXAFS Curve-fitting for Four-coordinate Samples.

Metal	Ligand			
	Cl <sup>-</sup>	Br <sup>-</sup>	I <sup>-</sup>	Br <sup>-</sup> (Br edge)
Mn(II)	2.374	2.519	2.713	2.518
Fe(II)	2.320	2.461		2.469
Co(II)	2.288	2.421	2.609	2.422
Ni(II)	2.269	2.407		2.407
Cu(II)	2.249	2.381		2.379
Zn(II)	2.276	2.410	2.614	2.421
Fe(III)	2.208			

analytical procedures. The inconsistency of  $r$  and  $r_{av}$  for  $\text{Cu}(\text{ClO}_4)_2 \cdot 6\text{H}_2\text{O}$  comes from the difference in the effect on the sensitivity of the dynamic Jahn-Teller distortion between the two methods.<sup>42)</sup> The differences are independent of the kind of the absorbing and the scattering atom or the counter ions. Therefore, the differences between  $r$  and  $r_{av}$  are mainly due to the errors of data analysis of EXAFS and the phase shift would be sufficiently corrected.

Table 5.5 summarizes the distances from Table 5.3. Among the central metal ions, the changes of  $r$  almost agree with those of the effective ionic radii<sup>43)</sup> except for six-coordinate Cr(II) and Cu(II). Differences between these changes are about within 0.02 Å. Taking the planar four-coordinate radius, the change for six-coordinate Cu(II) also agrees. The changes between the different kinds of the ligand are nearly constant except for  $\text{NO}_2^-$  and  $\text{CN}^-$ . For four-coordinate complexes, these changes agree with those of the effective ionic radii or covalent-bond radii<sup>44)</sup> of halide ions.

### 5.3.5 Scale factors and Debye-Waller factors

Scale factors. Scale factor  $S$  is calculated from  $B$  and coordination number  $N$  by Eq. (4.10). This factor is important in calculating the coordination numbers for unknown samples. Table 5.6 lists the scale factors calculated from Table 5.3. The coordination number  $N$  were assumed as four for six-coordinate Cr(II) and Cu(II) complexes because Debye-Waller factors must be very large at their axial sites and its contributions to EXAFS of the coordinate atoms of axial site are negligibly small. Owing to large analytical errors, the dependence of  $S$  values on the central metal ions and

Table 5.6 (a). Scale Factors *S* of EXAFS Curve-fitting for Six-coordinate Samples.

Metal	H <sub>2</sub> O(s)	H <sub>2</sub> O and SO <sub>4</sub> <sup>2-</sup> (s)	H <sub>2</sub> O(aq)	Ligand and State					
				NH <sub>3</sub> (s)	NH <sub>3</sub> (aq)	NCS <sup>-</sup> (s)	NO <sub>2</sub> <sup>-</sup> (s)	CN <sup>-</sup> (s)	
Cr(II)		0.31	0.35						
Mn(II)	0.38	0.38	0.42	0.38	0.37				
Fe(II)	0.34 <sup>s</sup> , 0.39 <sup>p</sup>		0.42	0.40				0.39	
Co(II)	0.41 <sup>s</sup> , 0.37 <sup>n</sup> 0.40 <sup>p</sup>		0.44	0.35					
Ni(II)	0.39 <sup>s</sup> , 0.41 <sup>n</sup>		0.46	0.38	0.39		0.37		
Cu(II)	0.39	0.36	0.40	0.38			0.30		
Zn(II)	0.41 <sup>s</sup> , 0.43 <sup>n</sup> 0.39 <sup>p</sup>		0.44						
Ti(III)		0.41	0.45						
V(III)			0.38			0.39			
Cr(III)	0.43 <sup>p</sup> , 0.42 <sup>s</sup>		0.43	0.35	0.38	0.38			
Fe(III)	0.40		0.44			0.33		0.39	
Co(III)				0.37	0.38		0.39	0.39	

s) Sulfate, <sup>n</sup> Nitrate, <sup>p</sup> Perchlorate  
(s): solid, (aq): aqueous solution

Table 5.6 (b). Scale Factors  $S$  of EXAFS Curve-fitting for Four-coordinate Samples.

Metal	Ligand			
	Cl <sup>-</sup>	Br <sup>-</sup>	I <sup>-</sup>	Br <sup>-</sup> (Br edge)
Mn(II)	0.52	0.56	0.42	0.45
Fe(II)	0.52	0.54		0.45
Co(II)	0.53	0.55	0.44	0.51
Ni(II)	0.52	0.54		0.51
Cu(II)	0.52	0.48		0.48
Zn(II)	0.56	0.56	0.47	0.54
Fe(III)	0.52			

Table 5.7 (a). Debye-Waller Factor  $\sigma^2/10^{-2}\text{\AA}$  obtained from EXAFS Curve-fitting for Six-coordinate Samples.

Metal	H <sub>2</sub> O and SO <sub>4</sub> <sup>2-</sup> (s)		Ligand and State					
	H <sub>2</sub> O(s)	H <sub>2</sub> O(aq)	H <sub>2</sub> O(aq)	NH <sub>3</sub> (s)	NH <sub>3</sub> (aq)	NCS <sup>-</sup> (s)	NO <sub>2</sub> <sup>-</sup> (s)	CN <sup>-</sup> (s)
Cr(II)		2.7	4.1					
Mn(II)	7.0	7.0	7.3	7.3	7.2			
Fe(II)	7.0 <sup>S</sup> , 6.9 <sup>P</sup>		7.4	7.7				2.6
Co(II)	6.2 <sup>S</sup> , 6.5 <sup>N</sup> 6.7 <sup>P</sup>		7.2	7.1				
Ni(II)	5.3 <sup>S</sup> , 5.9 <sup>N</sup>		6.7	6.4	6.5		5.4	
Cu(II)	4.6	4.0	5.1	5.4			3.8	
Zn(II)	7.4 <sup>S</sup> , 8.2 <sup>N</sup> 8.1 <sup>P</sup>		8.2					
Ti(III)		5.4	6.2					
V(III)			3.9			4.0		
Cr(III)	3.7 <sup>P</sup> , 2.8 <sup>S</sup>		3.1	2.5	2.9			
Fe(III)	3.6		4.7			6.5		2.3
Co(III)				2.2	2.1		3.9	3.4

S) Sulfate, N) Nitrate, P) Perchlorate  
(s): solid, (aq): aqueous solution

Table 5.7 (b). Debye-Waller Factors  $\sigma/10^{-2}\text{\AA}$  of EXAFS Curve-fitting for Four-coordinate Samples.

Metal	Ligand			
	Cl <sup>-</sup>	Br <sup>-</sup>	I <sup>-</sup>	Br <sup>-</sup> (Br edge)
Mn(II)	6.3	6.9	6.6	6.4
Fe(II)	6.3	7.0		6.5
Co(II)	5.9	6.3	6.5	6.1
Ni(II)	6.1	6.5		6.3
Cu(II)	6.9	7.1		7.1
Zn(II)	6.6	6.8	7.2	6.7
Fe(III)	4.6			

the ligands are not so clear. But, it seems that  $S$  of aqua complexes are larger than those of other complexes.

**Debye-Waller factors.** Debye-Waller factors  $\sigma$  are listed in Table 5.7. These values vary with the kind of central metal ions.  $\sigma$  for any trivalent ion is much smaller than that for the divalent ion of the same element or the same 3d-electronic configuration. This means that the metal-ligand bond of trivalent ion is much stronger than that of divalent one. For Mn to Zn six-coordinate divalent complexes, the order of  $\sigma$  is  $\text{Mn} \approx \text{Fe} > \text{Co} > \text{Ni} > \text{Cu} < \text{Zn}$ . This order is almost parallel to the inverse of the Irving-Williams series which indicates the order of stability of amine complexes of these ions in aqueous solution.

$\sigma$  can be calculated from other experiments. The static contributions  $\sigma_{\text{stat}}^2$  for some compounds obtained from the bond distances of X-ray diffraction studies and Eq. (3.30) are listed in Table 5.4 (a). This contribution is rather small compared to the EXAFS  $\sigma^2$ . It is expected that  $\sigma_{\text{stat}}$  manifest as the difference between  $\sigma$  of solids and that of solutions if other contributions are constant. However, Table 5.7 (a) shows no apparent difference for solids and solutions. This also shows that the static contribution of the solid samples are very small.

The thermal vibrational contribution  $\sigma_{\text{vib}}$  is related to the vibrational frequency  $\nu$  by Eq. (3.33). Table 5.8 lists some of  $\sigma_{\text{vib}}$  calculated by using the frequency of totally symmetric stretching vibration of the complex ions. The trends of the dependence on the kind of metal ions of  $\sigma$  in Table 5.7 (a) and  $\sigma_{\text{vib}}$  in Table 5.8 (a) show good qualitative agreement with each other but no quantitative agreement for six-coordinate complexes. In

Table 5.8. Calculated Debye-Waller Factors  $\sigma_{\text{vib}}$  by Using Vibrational Frequencies.

(a) six-coordinate

Compound	$\nu/\text{cm}^{-1}$	$\sigma_{\text{vib}}/10^{-2}\text{\AA}$
[Cr(H <sub>2</sub> O) <sub>6</sub> ]Cl <sub>3</sub>	490	5.8
[Mn(H <sub>2</sub> O) <sub>6</sub> ]SiF <sub>6</sub>	395	6.8
[Fe(H <sub>2</sub> O) <sub>6</sub> ]SiF <sub>6</sub>	389	6.9
[Ni(H <sub>2</sub> O) <sub>6</sub> ]SiF <sub>6</sub>	405	6.6
[Cu(H <sub>2</sub> O) <sub>4</sub> ]SO <sub>4</sub> ·H <sub>2</sub> O	440	6.2
[Zn(H <sub>2</sub> O) <sub>6</sub> ]SO <sub>4</sub> ·H <sub>2</sub> O	364	7.1
[Cr(NH <sub>3</sub> ) <sub>6</sub> ]Cl <sub>3</sub>	465	6.4
[Mn(NH <sub>3</sub> ) <sub>6</sub> ]Cl <sub>2</sub>	330	8.3
[Co(NH <sub>3</sub> ) <sub>6</sub> ]Cl <sub>2</sub>	357	7.7
[Co(NH <sub>3</sub> ) <sub>6</sub> ]Cl <sub>3</sub>	500	6.0
[Ni(NH <sub>3</sub> ) <sub>6</sub> ]Cl <sub>2</sub>	370	7.5

(b) four-coordinate [MX<sub>4</sub>]  $\sigma_{\text{vib}}/10^{-2}\text{\AA}$

Metal	Ligand		
	Cl <sup>-</sup>	Br <sup>-</sup>	I <sup>-</sup>
Mn(II)	7.5(256)	7.8(195)	12.6(108)
Fe(II)	7.2(266)	9.2(162)	
Co(II)	7.0(269)	8.9(166)	11.3(118)
Ni(II)	7.2(264)	—	
Zn(II)	6.8(276)	8.4(171)	10.9(118)
Fe(III)	6.0(330)		

$\nu/\text{cm}^{-1}$  are given in parentheses.

Vibrational frequencies  $\nu$  are taken from Ref. 45.

Table 5.8 (a), ammine complexes exhibits larger  $\sigma_{\text{vib}}$  than aqua complexes. However, such trends do not appear in Table 5.7 (a). For four-coordinate complexes, agreements of  $\sigma$  in Table 5.8 (b) with those in Table 5.7 (b) can not be significant in view of uncertainties in the present investigation. Though EXAFS  $\sigma$  include rather large errors, these discrepancies can not be explained by the errors only. It seems that the assumptions based on Eq. (3.33) is not proper. More exact expression is already established but the absolute intensity and peak profiles of Raman spectra are needed in calculation by the expression.<sup>46)</sup> Actually, it is almost always difficult to measure vibrational spectra with enough accuracy for this calculation. Further experimental and theoretical studies are required to connect EXAFS  $\sigma$  and vibrational spectra more conveniently.

### 5.3.6 Absorption edge shifts

The absorption edge shifts  $\Delta E_0$  of EXAFS curve-fitting are summarized in Table 5.9. In Table 5.9 some trends can be pointed out with the variation of ligands but not with that of metal ions because the absorption edges have much different energies from each other. Then,  $\Delta E_0$  are discussed using these values versus the  $1s \rightarrow 3d$  transition peak position that appears in each pre-edge region except for Zn. If both two 3d levels of the central metal,  $e$  and  $t_2$ , are not fully occupied, two pre-edge peaks due to  $1s \rightarrow e$  and  $1s \rightarrow t_2$  transitions are observed. For the complexes in Table 5.9 six-coordinate complexes of Ti(III), V(III), Cr(II), Cr(III), high-spin Fe(II), and Fe(III) exhibit these two peaks, whereas Mn(II), Co(II), and four-coordinate complexes show only one peak

Table 5.9 (a). Edge Shift  $\Delta E_b$ /eV of EXAFS Curve-fitting for Six-coordinate Samples.

Metal	H <sub>2</sub> O and SO <sub>4</sub> <sup>2-</sup> (s)		Ligand and State					
	H <sub>2</sub> O(s)	SO <sub>4</sub> <sup>2-</sup> (s)	H <sub>2</sub> O(aq)	NH <sub>3</sub> (s)	NH <sub>3</sub> (aq)	NCS <sup>-</sup> (s)	NO <sub>2</sub> <sup>-</sup> (s)	CN <sup>-</sup> (s)
Cr(II)		9.2	7.8					
Mn(II)	3.9	4.2	3.7		4.4	3.5		
Fe(II)	2.4 <sup>S</sup> , 4.0 <sup>P</sup>		3.5		3.7			6.2
Co(II)	3.5 <sup>S</sup> , 3.1 <sup>N</sup> 3.9 <sup>P</sup>		3.1	4.9				
Ni(II)	2.1 <sup>S</sup> , 2.9 <sup>N</sup>		3.4	3.5	3.7		8.9	
Cu(II)	6.9	8.3	5.4	5.9			7.5	
Zn(II)	5.3 <sup>S</sup> , 4.5 <sup>N</sup> 4.8 <sup>P</sup>		5.0					
Ti(III)		9.2	9.6					
V(III)			6.5			6.9		
Cr(III)	5.4 <sup>P</sup> , 5.4 <sup>S</sup>		5.5	5.9	6.2	6.2		
Fe(III)	4.7		4.7			5.9		6.1
Co(III)				4.4	4.3		8.5	5.3

S) Sulfate, N) Nitrate, P) Perchlorate  
(s): solid, (aq): aqueous solution

Table 5.9 (b). Edge Shifts  $\Delta E_0$ /eV of EXAFS Curve-fitting for Four-coordinate Samples.

Metal	Ligand			
	Cl <sup>-</sup>	Br <sup>-</sup>	I <sup>-</sup>	Br <sup>-</sup> (Br edge)
Mn(II)	5.2	3.4	2.8	4.2
Fe(II)	4.9	3.3		4.9
Co(II)	4.7	2.1	1.4	4.5
Ni(II)	5.0	4.1		4.5
Cu(II)	5.1	4.0		6.7
Zn(II)	5.7	2.6	2.6	3.0
Fe(III)	6.0			

Table 5.10 (a). Edge Shift  $\Delta E_{0,p}/eV$ ,  $\Delta E_0$  vs.  $1s \rightarrow 3d$  Peak Position, of EXAFS Curve-fitting for Six-coordinate Samples.

Metal	H <sub>2</sub> O(s)	H <sub>2</sub> O and SO <sub>4</sub> <sup>2-</sup> (s)	H <sub>2</sub> O(aq)	Ligand and State					
				NH <sub>3</sub> (s)	NH <sub>3</sub> (aq)	NCS <sup>-</sup> (s)	NO <sub>2</sub> <sup>-</sup> (s)	CN <sup>-</sup> (s)	
Cr(II)		14.8	13.5						
Mn(II)	10.1	10.4	10.1	10.4	11.6				
Fe(II)	8.7 <sup>S</sup> , 10.8 <sup>P</sup>		10.2	10.3					18.1
Co(II)	12.3 <sup>S</sup> , 12.5 <sup>N</sup> , 13.2 <sup>P</sup>		12.5	13.8					
Ni(II)	12.6 <sup>S</sup> , 13.1 <sup>N</sup>		13.3	13.7	13.8		18.0		
Cu(II)	17.9	19.1	16.4	15.6			17.1		
Ti(III)		17.4	18.5						
V(III)			16.3			20.7			
Cr(III)	16.9 <sup>P</sup> , 16.8 <sup>S</sup>		16.6	16.1	16.4	18.9			
Fe(III)	15.7		15.7			14.6		21.6	
Co(III)				16.1	16.2		17.8	17.9	

S) Sulfate, N) Nitrate, P) Perchlorate  
(s): solid, (aq): aqueous solution

Table 5.10 (b). Edge Shifts  $\Delta E_{0,p}/\text{eV}$ ,  $\Delta E_0$  vs.  $1s \rightarrow 3d$   
 Pre-edge Peak Position, of EXAFS Curve-fitting  
 for Four-coordinate Samples.

Metal	Ligand		
	Cl <sup>-</sup>	Br <sup>-</sup>	I <sup>-</sup>
Mn(II)	10.1	8.9	7.1
Fe(II)	11.5	10.9	
Co(II)	11.7	11.0	7.3
Ni(II)	13.1	12.1	
Cu(II)	13.9	14.1	
Fe(III)	13.5		

because the splitting between  $e$  and  $t_2$  is not satisfactorily wide compared to the energy resolution. Table 5.10 lists  $\Delta E_0$  vs. to  $1s \rightarrow 3d$  peak position (hereafter note as  $\Delta E_{0,p}$ ). The peak adopted as the origin is  $1s \rightarrow t_{2g}(O_h)$  for six-coordinate Ti(III), V(III), and Cr(III),  $1s \rightarrow e_g(O_h)$  for six-coordinate Cr(II), Fe(II), Fe(III), Co(III), Ni(II), and Cu(II), or convoluted peak for the others. In this reference,  $\Delta E_{0,p}$  correspond to the minimum energy required to free a highest occupied 3d electron except for Co(III) and  $Fe^{II}(CN)_6$  (low-spin  $d^6$ , full  $t_{2g}$ ).

It is clear in Table 5.10 that  $\Delta E_{0,p}$  for trivalent ions are larger than that for divalent ones. This can be naturally interpreted as the increasing of positive charge on an ion causes increase in energy required to separate an electron from it. The upward trend from Fe(II) to Cu(II) is reasonable since the ionization potentials for these ions increase in the same order if no other factors are considered. Other trends between the metal ions can be hardly explained. It seems that the orders of  $Cl > Br > I$  for four-coordinate complexes reflect the difference in the charge on the ions due to the electronegativity of the ligand. The values for  $NCS^-$ ,  $NO_2^-$ , and  $CN^-$  complexes indicate the relatively large charge on the metal ions because the central metals have back-donation to the ligands.

### 5.3.7 Comparison of metal edge and Br edge of bromo complexes

In principle, EXAFS analysis for the absorption edge of any side of an absorber-scatterer pair will give the same  $r$  and  $\sigma$  value.  $r$  and  $\sigma$  for metal K-edge (abscissa) and Br K-edge (ordinate) of bromo complexes are plotted in Fig. 5.9. The

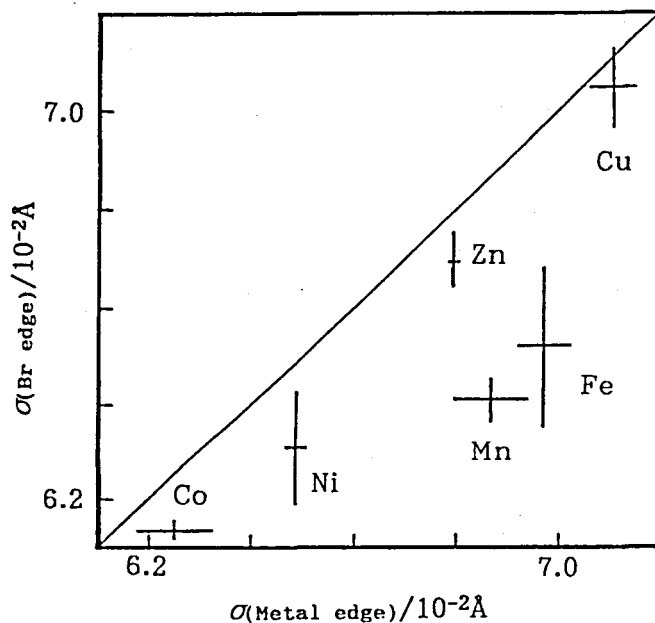
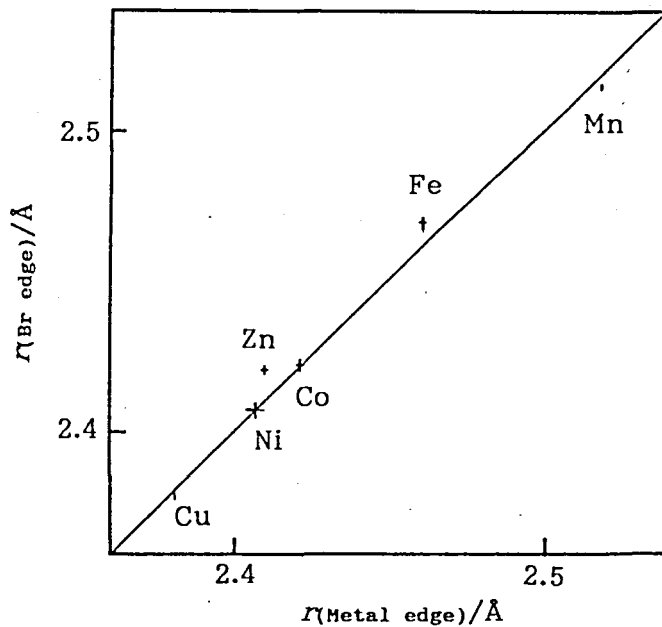


Figure 5.9. Comparison of interatomic distances  $r$  and Debye-Waller factors  $\sigma$  of  $[(\text{C}_2\text{H}_5)_4\text{N}]_2[\text{MBr}_4]$  between metal K-edge and Br K-edge.

interatomic distances  $r$  of both edges show a good agreement with each other. On the other hand, the Debye-Waller factors  $\sigma$  show discrepancies at Mn and Fe. These results mean that the phase shifts are corrected enough exactly but the back-scattering amplitudes are not.

### 5.3.8 Calculation of characteristic value of EXAFS parameters

The predictions of the (intrinsic) characteristic EXAFS parameter values of each metal ion and its variation with ligands would be useful in analyzing EXAFS spectra of metal complexes. Scale factor  $S$  and Debye-Waller factor  $\sigma$  for aqua and ammine or chloro, bromo, and iodo complexes may have multiplicative property because of these contribution to the Fourier transform intensity (Eq. (5.1)) and the correlation as shown in Figs. 5.5 and 5.6 (intercepts of regressive lines in the figures are ignored). Therefore, their characteristic values can be calculated so as to be used in the next form;

$$S = S^0 \cdot S^c(\text{metal-ion}) \cdot S^c(\text{ligand-and-state}) \quad (5.2)$$

$$\sigma = \sigma^0 \cdot \sigma^c(\text{metal-ion}) \cdot \sigma^c(\text{ligand-and-state}). \quad (5.3)$$

$S^0$  and  $\sigma^0$  have a constant value irrespective to the kind of central metal ion, ligand, and state.  $S^c$  and  $\sigma^c$  are the characteristic value of the parameters. On the other hand, for trial, additivity of  $\Delta E_{0,p}$  is assumed.

$$\Delta E_{0,p} = \Delta E_{0,p}^c(\text{metal-ion}) + \Delta E_{0,p}^c(\text{ligand-and-state}) + \Delta E_{0,p}^0. \quad (5.4)$$

Table 5.11. Characteristic Values of  $S$ ,  $\sigma$ , and  $\Delta E_{0,p}$  for Aqua, Ammine, Chloro, Bromo, and Iodo Complexes.

(a) central metal ion

Metal	for six-coordinate			for four-coordinate		
	$S^c$	$\sigma^c$	$\Delta E_{0,p}^c/\text{eV}$	$S^c$	$\sigma^c$	$\Delta E_{0,p}^c/\text{eV}$
Mn(II)	0.94	1.16	-2.5	1.00	1.00	0.0
Fe(II)	0.94	1.18	-2.6	0.98	1.01	1.7
Co(II)	0.95	1.12	-0.3	1.02	0.95	1.3
Ni(II)	1.00	1.00	0.0	0.98	0.96	3.1
Cu(II)	0.95	0.81	2.1	0.93	1.08	4.5
Zn(II)	0.99	1.33	-	1.07	1.05	-
Cr(III)	0.97	0.47	3.1	—	—	—
Fe(III)	0.98	0.68	2.6	—	—	—
Co(III)	0.97	0.33	2.4	—	—	—

(b) ligand and state

Ligand	in solids			in aqueous solutions		
	$S^c$	$\sigma^c$	$\Delta E_{0,p}^c/\text{eV}$	$S^c$	$\sigma^c$	$\Delta E_{0,p}^c/\text{eV}$
H <sub>2</sub> O	0.91	0.96	0.2	1.00	1.00	0.0
H <sub>2</sub> O and SO <sub>4</sub> <sup>2-</sup>	0.90	0.82	0.8	—	—	—
NH <sub>3</sub>	0.85	0.96	0.1	0.89	0.99	0.2
Cl	1.00	1.00	0.0	—	—	—
Br	1.02	1.05	-0.7	—	—	—
I	0.83	1.08	-3.7	—	—	—

Constant values.

$S^0 = 0.46$ , for six-coordinate

0.53, for four-coordinate

$\sigma^0 = 0.064 \text{ \AA}$ , for six-coordinate

0.063  $\text{\AA}$ , for four-coordinate

$\Delta E_{0,p}^0 = 13.5 \text{ eV}$ , for six-coordinate

10.0 eV, for four-coordinate

Table 5.12. Analysis Test Using Characterized EXAFS Parameter Values.

(a) solids

Compound	$r/\text{\AA}$	$N$
$[\text{Cr}(\text{NH}_3)_6]\text{Cl}_3$	2.091	5.3
$\text{MnSO}_4 \cdot 5\text{H}_2\text{O}$	2.176	5.2
$\text{FeSO}_4 \cdot 7\text{H}_2\text{O}$	2.112	5.0
$\text{Fe}(\text{ClO}_4)_2 \cdot 6\text{H}_2\text{O}$	2.116	6.1
$[\text{Co}(\text{NH}_3)_6]\text{Cl}_2$	2.170	5.6
$[\text{Co}(\text{NH}_3)_6]\text{Cl}_3$	1.967	5.7
$\text{NiSO}_4 \cdot 6\text{H}_2\text{O}$	2.044	6.0
$\text{Ni}(\text{NO}_3)_2 \cdot 6\text{H}_2\text{O}$	2.050	6.0
$[(\text{C}_2\text{H}_5)_4\text{N}]_2[\text{NiCl}_4]$	2.265	4.0
$\text{CuSO}_4 \cdot 5\text{H}_2\text{O}$	1.955	3.7
$[\text{Cu}(\text{NH}_3)_6]\text{Cl}_2$	2.033	3.9

(b) aqueous solution of aqua complexes

Metal	$r/\text{\AA}$	$N$
Cr(III)	1.980	5.7
Mn(II)	2.178	5.9
Fe(II)	2.119	5.9
Fe(III)	2.008	5.7
Co(II)	2.088	5.9
Ni(II)	2.052	5.8
Cu(II)	1.960	3.6

$\Delta E_{0,p}^0$  is the constant term irrespective of the same as  $S^0$ .  $\Delta E_{0,p}^c$  are the characteristic value of  $\Delta E_{0,p}$ . Table 5.11 lists these characteristic values of EXAFS parameters. In deriving  $\sigma^c$  for four-coordinate complexes the average values of metal K-edge and Br K-edge EXAFS  $\sigma$  of bromo complexes are used as the  $\sigma$  value for bromo complexes.

Reproductions of these parameter values by Eqs. (5.2-4) and Table 5.11 gives the following maximum deviations from the observed values; 0.06 and 0.03 of  $S$ , 0.008 Å and 0.002 Å of  $\sigma$ , and 2.7 eV and 1.0 eV of  $\Delta E_{0,p}$  for six- and four-coordinate complexes, respectively. These deviations seem to be within the measurement and analytical errors. Results of analysis test for some samples using the characterized parameter values are listed in Table 5.12. Most of interatomic distances become closer to those obtained by X-ray diffraction, which are shown in Table 5.4 (a). For the solution samples shown in Table 5.12 (b), the differences of  $r$  between EXAFS and X-ray diffraction are less than or equal to 0.02 Å. The coordination number  $N$  for solids of Co, Ni, and Cu salts and aqueous solutions can be given within the error of 10% but large errors are shown for solids of Cr, Mn, and Fe salts.

Characterization of these parameters can clarify trends of variations depending on the kind of the central metal ion and the ligand. The difference of  $S$  between aqua and ammine complexes is partially due to their interatomic distances.  $\sigma$  of divalent ions are  $\text{Co} \approx \text{Ni} < \text{Mn} \approx \text{Fe} < \text{Zn}$  and trivalent ions have much smaller  $\sigma$  than divalent ones.  $\sigma$  of halogeno complexes are varied in the order of  $\text{Cl} < \text{Br} < \text{I}$ .  $\Delta E_{0,p}$  shows almost inverse such trend of  $\sigma$  variations. These orders somewhat coincide with the difference of

ligand-field stabilization energy. However,  $\sigma$  and  $\Delta E_{0,p}$  of aqua and ammine complexes show very similar values.

#### 5.4. References

1. T. K. Sham, *Acc. Chem. Res.*, 19, 99 (1986).
2. T. Miyanaga, I. Watanabe, and S. Ikeda, *Chem. Lett.*, 1073 (1988).
3. C. Brattås, S. Jagner, and E. Ljungström, *Acta Crystallogr., Sect. B*, 34, 3073 (1978).
4. "Shin-Jikken Kagaku Koza," ed by M. Nakahara and M. Shibata, Maruzen, Tokyo, 1977, Vol. 8, part II & III; and references therein.
5. T. Distler and P. A. Vaughan, *Inorg. Chem.*, 6, 126 (1967).
6. S. Takagi, P. G. Lenhert, and M. D. Joesten, *J. Am. Chem. Soc.*, 96, 6606 (1974).
7. R. J. H. Clark and A. D. J. Goodwin, *Spectrochim. Acta*, 26A, 323 (1970).
8. T. Miyanaga, I. Watanabe, S. Ikeda, K. Tashiro, and T. Fujikawa, *Bull. Chem. Soc. Jpn.*, 61, 3199 (1988).
9. R. A. Bair and W. A. Goddard III, *Phys. Rev. B*, 22, 2767 (1980).
10. N. Kosugi, T. Yokoyama, K. Asakura, and H. Kuroda, *Chem. Phys.*, 91, 249 (1984); T. Yokoyama, N. Kosugi, and H. Kuroda, *ibid.*, 103, 101 (1986).
11. J. Kawai, Y. Gohshi, and Y. Nihei, *Adv. X-Ray Chem. Anal. Jpn.*, 19, 1 (1988).
12. B. Hedman, K. O. Hodgson, and E. I. Solomon, *J. Am. Chem. Soc.*, 112, 1643 (1990).
13. B. K. Teo, "EXAFS: Basic Principles and Data Analysis," Springer-Verlag, Berlin, 1985.
14. P. A. Lee and J. B. Pendry, *Phys. Rev. B*, 11, 2795 (1975);

- C. A. Ashley and S. Doniach, *ibid.*, 11, 1279 (1975).
15. N. Binsted, J. Evans, G. N. Greaves, and R. J. Price, *J. Chem. Soc., Chem. Commun.*, 1330 (1987); N. Binsted, S. L. Cook, J. Evans, G. N. Greaves, and R. J. Price, *J. Am. Chem. Soc.*, 109, 3669 (1987); F. B. M. Van Zon, P. S. Kirlin, B. C. Gates, and D. C. Koningsberger, *J. Phys. Chem.*, 93, 2218 (1989).
  16. H. Sakane, I. Watanabe, and S. Ikeda, *Bull. Chem. Soc. Jpn.*, 62, 1513 (1989).
  17. T. P. Vaalsta and E. N. Maslen, *Acta Crystallogr., Sect. B*, 43, 448 (1987).
  18. H. Ito, Y. Ito, F. Kanamaru, K. Koto, N. Matsubayashi, I. Watanabe, and S. Ikeda, *Z. Kristallogr.*, 181, 99 (1987).
  19. M. A. Hitchman, M. Lichon, R. G. McDonald, P. W. Smith, R. Stranger, B. W. Skelton, and A. H. White, *J. Chem. Soc., Dalton Trans.*, 1817 (1987).
  20. R. Caminiti, G. Marongiu, and G. Paschina, *Z. Naturforsch.*, 37a, 581 (1982).
  21. J. N. Varghese and E. N. Maslen, *Acta Crystallogr., Sect. B*, 41, 184 (1985).
  22. W. H. Baur, *Naturwissenschaften*, 49, 464 (1962).
  23. W. H. Baur, *Acta Crystallogr.*, 17, 1167 (1964).
  24. R. E. Gerkin and W. J. Reppart, *Acta Crystallogr., Sect. C*, 44, 1486 (1988).
  25. R. J. Angel and L. W. Finger, *Acta Crystallogr., Sect. C*, 44, 1869 (1988).
  26. M. Giménez-Huguet, *Diss. Abs.*, 22, 2209 (1962).
  27. M. Ghosh and S. Ray, *Z. Kristallogr.*, 155, 129 (1981).
  28. B. N. Figgis, B. W. Skelton, and A. H. White, *Aust. J. Chem.*, 31, 1195

- (1978).
29. Y. Morioka, K. Toriumi, T. Ito, A. Saito, and I. Nakagawa, *J. Phys. Soc. Jpn.*, 54, 2184 (1985).
  30. M. T. Barnet, B. M. Craven, and H. C. Freeman, *J. Chem. Soc., Chem. Commun.*, 307 (1966).
  31. G. J. Kruger and E. C. Reynhardt, *Acta Crystallogr., Sect. B*, 34, 915 (1978).
  32. Y. Okaya, R. Pepinsky, Y. Takeuchi, H. Kuroya, A. Shimada, P. Gallitelli, N. Stemple, and A. Beevers, *Acta Crystallogr.*, 10, 798 (1957).
  33. F. Bigoli, A. Braibanti, A. Tiripicchio, and M. Tiripicchio Camellini, *Acta Crystallogr., Sect. B*, 27, 1427 (1971).
  34. S. Takagi, M. D. Joesten, and P. G. Lenhert, *Acta Crystallogr., Sect. B*, 31, 1970 (1975).
  35. G. D. Stucky, J. B. Folkers, and T. J. Kistenmacher, *Acta Crystallogr.*, 23, 1064 (1967).
  36. N. V. Mani and S. Ramaseshan, *Z. Kristallogr.*, 115, 97 (1961).
  37. A. Ferrari, A. Braibanti, A. M. Lanfredi, and A. Tiripicchio, *Acta Crystallogr.*, 22, 240 (1967).
  38. M. Ghosh and S. Ray, *Z. Kristallogr.*, 145, 146 (1977).
  39. W. Bol and T. Welzen, *Chem. Phys. Lett.*, 49, 189 (1977)
  40. H. Ohtaki, T. Yamaguchi, and M. Maeda, *Bull. Chem. Soc. Jpn.*, 49, 701 (1976).
  41. M. Magini, *J. Inorg. Nucl. Chem.*, 40, 43 (1978).
  42. N. Matsubayashi, Doctoral Thesis, Osaka University, Osaka, Japan, 1986.
  43. R. D. Shannon, *Acta Crystallogr., Sect. A*, 32, 751 (1976).
  44. J. E. Huheey, "Inorganic Chemistry," Third ed, Harper & Row,

New York, 1983, p.258.

45. K. Nakamoto, "Infrared and Raman Spectra of Inorganic and Coordination Compounds," Fourth ed, John Wiley & Sons, New York, 1986.
46. P. P. Lottici, *Phys. Rev. B*, 35, 1236 (1987).

## Chapter 6. Solvent effect and counterion effect on XAFS of carboxylato chelate complexes

### 6.1 Introduction

The structures of metal-EDTA (ethylenediamine- $N,N,N',N'$ -tetraacetic acid) complexes are not necessarily the same. They are known to take various coordination structures.<sup>1)</sup> The structures can also vary with the environments, *i.e.* crystals<sup>2)</sup> or solutions.<sup>3,4)</sup> The XAFS techniques appear to be suitable for the structural studies of such complexes since these spectroscopic techniques extract the information regarding the local structure around the central metal irrespective of the environments. One of the complex treated in this chapter is  $[\text{Co}(\text{edta})]^-$  which is considered to be so stable that no structural change in its inner sphere would occur with the variation of the environments. In spite of the expected rigidity of the complex, it was found that its EXAFS and XANES spectra are highly sensitive to the environments. For more detailed study on the phenomena of XAFS of the solution samples, XAFS of some bidentate carboxylato complexes are measured and analyzed. This chapter describes the X-ray absorption spectra of the complexes in various environments and the possible effects of hydrogen bonding on XAFS.

### 6.2 Experimental

Sample preparations.  $\text{Li}[\text{Co}^{\text{III}}(\text{edta})]\cdot 3\text{H}_2\text{O}$  and  $\text{Na}[\text{Co}^{\text{III}}(\text{edta})]\cdot 4\text{H}_2\text{O}$  were prepared according to the literatures.<sup>5,6)</sup>  $\text{Rb}[\text{Co}^{\text{III}}(\text{edta})]\cdot 2\text{H}_2\text{O}$

was synthesized in the following way;  $\text{Rb}_2\text{CO}_3$  was added to a warm slurry solution containing  $\text{RbCl}$ ,  $(\text{CH}_3\text{COO})_2\text{Co}\cdot 4\text{H}_2\text{O}$ , and  $\text{H}_4\text{edta}$  until the pH of the solution became 4. The  $[\text{Co}^{\text{II}}(\text{edta})]^{2-}$  ion was oxidized by adding 3%  $\text{H}_2\text{O}_2$  aqueous solution. After filtration, this solution was concentrated and cooled, and ethanol was added to crystallize  $\text{Rb}[\text{Co}(\text{edta})]\cdot 2\text{H}_2\text{O}$ .  $\text{NH}_4[\text{Co}^{\text{III}}(\text{edta})]\cdot 2\text{H}_2\text{O}$  was synthesized using a similar method from  $\text{Co}(\text{NO}_3)_2\cdot 6\text{H}_2\text{O}$ ,  $\text{H}_4\text{edta}$ , and  $\text{NH}_4\text{OH}$ . All the solid samples were recrystallized twice or more from water and ethanol. Elemental analysis:  $\text{Li}[\text{Co}(\text{edta})]\cdot 3\text{H}_2\text{O}$  Found: C, 29.32; H, 4.55; N, 6.85%. Calcd for  $\text{C}_{10}\text{H}_{18}\text{O}_{13}\text{N}_2\text{CoLi}$ : C, 29.43; H, 4.45; N, 6.86%.  $\text{Na}[\text{Co}(\text{edta})]\cdot 4\text{H}_2\text{O}$  Found: C, 26.56; H, 4.26; N, 6.19%. Calcd for  $\text{C}_{10}\text{H}_{20}\text{O}_{14}\text{N}_2\text{CoNa}$ : C, 27.16, H, 4.56, N, 6.34%.  $\text{Rb}[\text{Co}(\text{edta})]\cdot 2\text{H}_2\text{O}$  Found: C, 24.21; H, 3.49; N, 5.65%. Calcd for  $\text{C}_{10}\text{H}_{16}\text{O}_{10}\text{N}_2\text{CoRb}$ : C, 25.63, H, 3.44, N, 5.98%.  $\text{NH}_4[\text{Co}(\text{edta})]\cdot 2\text{H}_2\text{O}$  Found: C, 29.63; H, 5.06; N, 10.41%. Calcd for  $\text{C}_{10}\text{H}_{20}\text{O}_{10}\text{N}_3\text{Co}$ : C, 29.94, H, 5.02, N, 10.47%.

Aqueous solutions of  $[\text{Co}(\text{edta})]^-$  ( $0.1 \text{ mol dm}^{-3}$ ) were prepared from the sodium salt.  $\text{HNO}_3$  or  $\text{NaOH}$  were used to adjust their pH to 3.0, 5.0, 7.0, and 9.0. The solutions of pH 7.0 and 9.0 turned to be pH 6.9 and 8.1, respectively, after the X-ray absorption measurements. DMF (*N,N*-dimethylformamide) solution was prepared from  $\text{K}[\text{Co}(\text{edta})]\cdot 2\text{H}_2\text{O}$  which was synthesized by the conventional method.<sup>6)</sup> An excess amount of 18-crown-6 ether was added to raise the solubility of the complex.

$\text{K}_3[\text{Co}^{\text{III}}(\text{ox})_3]\cdot 3\text{H}_2\text{O}$ ,  $\text{K}[\text{Co}^{\text{III}}(\text{ox})_2\text{en}]\cdot 1.5\text{H}_2\text{O}$ ,  $\text{K}[\text{Co}^{\text{III}}(\text{mal})_2\text{en}]\cdot \text{H}_2\text{O}$ , and  $\text{K}_3[\text{Cr}^{\text{III}}(\text{ox})_3]\cdot 3\text{H}_2\text{O}$  ( $\text{ox}^{2-}$  = oxalate ion,  $\text{mal}^{2-}$  = malonate ion, en = ethylenediamine) were kindly supplied by Dr. Toshiaki Taura from University of Aichi Prefecture. Solution samples of  $0.1 \text{ mol dm}^{-3}$  of

these complexes were prepared by the addition of Cryptand 222 that solubilize the complexes in organic solvents. The solvents used were water, methanol, ethanol, 2-propanol, acetonitrile, and DMF.

**Measurements and Calculations.** Co and Cr K-edge X-ray absorption spectra were obtained at BL-7C and BL-6B of Photon Factory in the National Laboratory for High Energy Physics. Fourier transform calculations of EXAFS for  $[\text{Co}(\text{edta})]^-$ ,  $[\text{Co}(\text{ox})_3]^{3-}$ ,  $[\text{Co}(\text{ox})_2\text{en}]^-$ ,  $[\text{Co}(\text{mal})_2\text{en}]^-$ , and  $[\text{Cr}(\text{ox})_3]^{3-}$  were performed over the  $k$  ranges of 2.9–16.75, 2.9–18.4, 2.8–18.45, 2.8–18.45, and 2.8–12.0  $\text{\AA}^{-1}$ , respectively. Transformations for  $[\text{Co}(\text{edta})]^-$  were performed by using the phase shift and the back-scattering amplitude tabulated by Teo and Lee.<sup>7)</sup> Curve-fitting calculations for  $[\text{Co}(\text{ox})_3]^{3-}$  were carried out in the  $k$  range of 4.35–15.15  $\text{\AA}$ .

## 6.3 Results and discussion

### 6.3.1 Co(III) EDTA complexes

Aqueous solutions. Figure 6.1 shows XANES spectra and Fourier transforms of EXAFS for aqueous solutions. Both spectra show no dependence on pH. Their Raman scattering and UV-Visible absorption spectra were also measured and showed no dependence on pH. According to Higginson *et al.*,<sup>4)</sup> Co(III)-EDTA takes one  $[\text{Co}(\text{Hedta})\text{H}_2\text{O}]$ ,  $[\text{Co}(\text{edta})\text{H}_2\text{O}]^-$ ,  $[\text{Co}(\text{edta})]^-$ , or  $[\text{Co}(\text{edta})\text{OH}]^{2-}$  depending on pH of the solution. In the pH range of 3.0 to 8.1, most of the complex has been known to form  $[\text{Co}(\text{edta})]^-$ . The present results indicate that the structure of  $[\text{Co}(\text{edta})]^-$  in

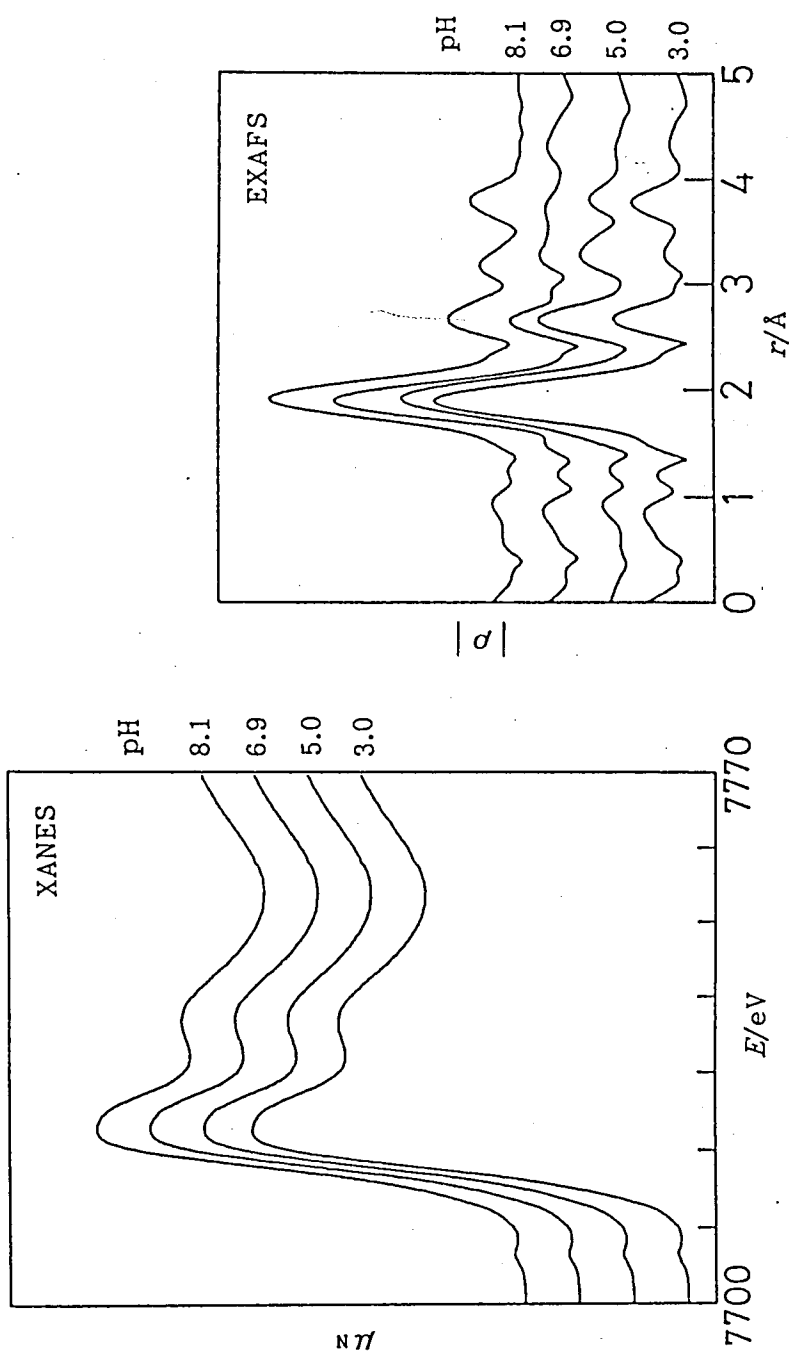


Figure 6.1. Co K-edge XANES spectra and Fourier transforms of EXAFS for  $[\text{Co}(\text{edta})]^-$  in different pH aqueous solutions.

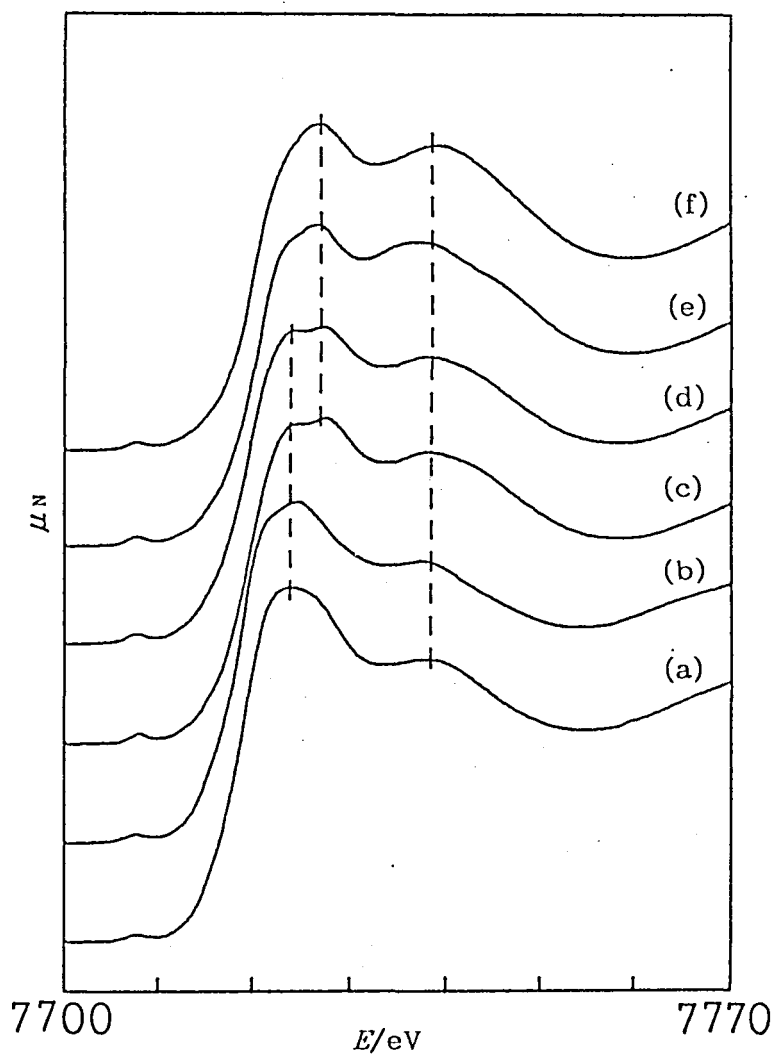


Figure 6.2. Co K-edge XANES spectra for (a) aqueous solution, (b)  $\text{Na}[\text{Co}(\text{edta})]\cdot 4\text{H}_2\text{O}$ , (c)  $\text{NH}_4[\text{Co}(\text{edta})]\cdot 2\text{H}_2\text{O}$ , (d)  $\text{Rb}[\text{Co}(\text{edta})]\cdot 2\text{H}_2\text{O}$ , (e)  $\text{Li}[\text{Co}(\text{edta})]\cdot 3\text{H}_2\text{O}$ , and (f) DMF solution.

aqueous solutions is very stable over this pH range.

XANES spectra. Figure 6.2 shows Co K-edge XANES spectra for (a) aqueous solution, (b)  $\text{Na}[\text{Co}(\text{edta})]\cdot 4\text{H}_2\text{O}$ , (c)  $\text{NH}_4[\text{Co}(\text{edta})]\cdot 2\text{H}_2\text{O}$ , (d)  $\text{Rb}[\text{Co}(\text{edta})]\cdot 2\text{H}_2\text{O}$ , (e)  $\text{Li}[\text{Co}(\text{edta})]\cdot 3\text{H}_2\text{O}$ , and (f) DMF solution. They can be classified into three groups; (A) aqueous solution and Na salt, (B)  $\text{NH}_4$  and Rb salts, and (C) Li salt and DMF solution. The spectra for group A have the lowest threshold energies and the lowest peak heights around 7740 eV. In contrast, group C has the highest threshold energies and the highest peak heights at 7740 eV. Group B is intermediate between A and C. The highest peaks, so called white line, in A or C are composed of a single peak, possibly accompanied by a shoulder, while those of B are composed of double peaks and the position of its higher energy component agrees with the position of the peak in C.

There are two possibilities which may contribute to the differences in the XANES spectra of three groups. One is the photoelectron scattering by the counter cations or solvent molecules. The other is the indirect effects of the cations or the solvents on the electronic and/or structural conditions of the complex anion,  $[\text{Co}(\text{edta})]^-$ . There is a reason for rejecting the former possibility, *i.e.* although the N in  $\text{NH}_3$  and the Rb are quite different photoelectron scatterers in respect to the amplitude and phase shift (the distances of Co-N and Co-Rb are 5.68 and 5.81 Å, respectively<sup>5</sup>), the XANES spectra of the samples having these atoms as counter cations are almost the same. In addition to this, there seems to be no systematic correlation between the XANES spectrum and the kind of counter cation. Therefore, it is almost impossible to consider that the variety of XANES spectra is caused

by the direct photoelectron scattering by the counter cation. Counterion effect on XANES are also observed in  $[\text{Co}(\text{NH}_3)_6]^{3+}$  salt.<sup>8)</sup> For  $[\text{Co}(\text{NH}_3)_6]^{3+}$  salt, the counterion effect takes place in the higher energy side of the threshold in their XANES spectra and is a somewhat different feature from this case.

EXAFS. Fourier transforms of EXAFS for  $[\text{Co}(\text{edta})]^-$  in various environments are shown in Fig. 6.3. One easily finds three peaks in each of the Fourier transforms. By referring to the crystallographic data for  $\text{NH}_4$  salt,<sup>5)</sup> these peaks are assigned to the bond distances between Co and the scatterers; the most intense peaks around 1.9 Å correspond to four oxygens ( $\text{O}_1$  in Fig. 6.4) and two nitrogens, the second peaks around 2.7 Å to ten carbons, and the third peaks around 3.8 Å to four oxygens ( $\text{O}_2$ ) uncoordinating to Co. In spite of its long distance, the third peaks due to  $\text{O}_2$  appear with an unusual intensity, particularly for the samples of groups B and C. Binsted *et al.*<sup>9)</sup> studied EXAFS of cobalt carbonyls such as  $[\text{Co}(\text{CO})_4]^-$  and found that the linear configuration of Co-C-O atoms enhances the peak corresponding to Co-O bond because of the multiple scattering effect. In the present case, it is plausible that the intensity of the third peak results from the same multiple scattering effect because the angles of Co-C<sub>1</sub>-O<sub>2</sub> are known to be about 160° and those of Co-O<sub>2</sub>-C<sub>1</sub> about 14° from the crystallographic data for  $\text{NH}_4$  salt.<sup>5)</sup>

Table 6.1 lists the peak positions in each Fourier transform and the mean distances of the corresponding bonds which are taken from the crystallographic data.<sup>5,10)</sup> The third peaks are not clear for some samples of aqueous solutions.

There are large differences in the amplitude of EXAFS

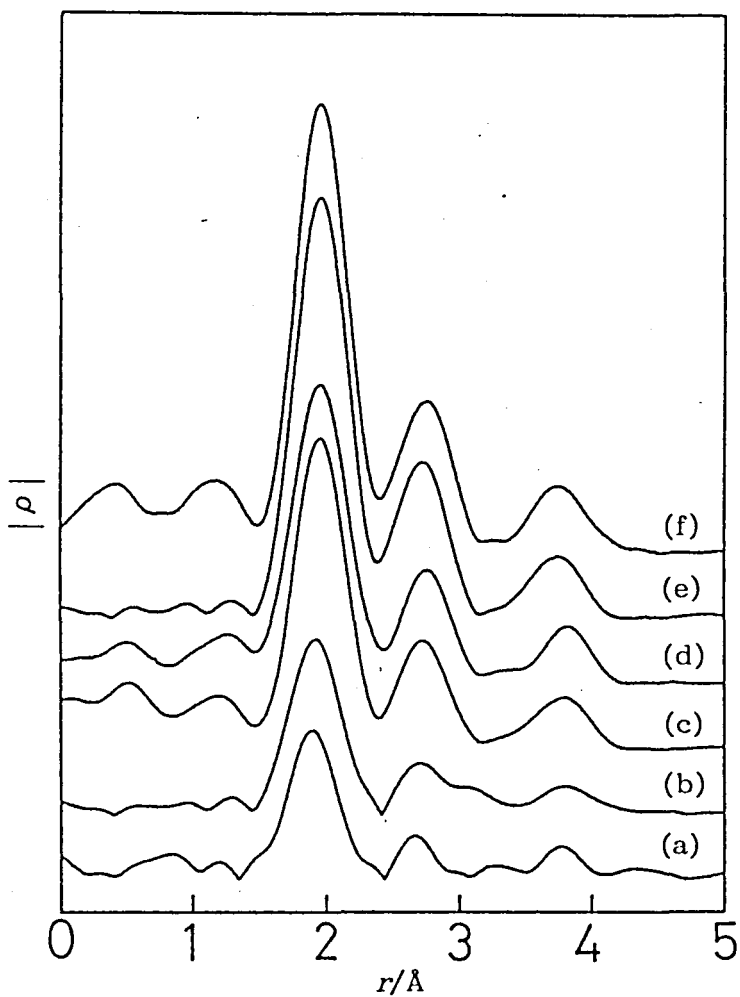


Figure 6.3. Fourier transforms of Co K-edge EXAFS for (a) aqueous solution, (b)  $\text{Na}[\text{Co}(\text{edta})]\cdot 4\text{H}_2\text{O}$ , (c)  $\text{NH}_4[\text{Co}(\text{edta})]\cdot 2\text{H}_2\text{O}$ , (d)  $\text{Rb}[\text{Co}(\text{edta})]\cdot 2\text{H}_2\text{O}$ , (e)  $\text{Li}[\text{Co}(\text{edta})]\cdot 3\text{H}_2\text{O}$ , and (f) DMF solution.

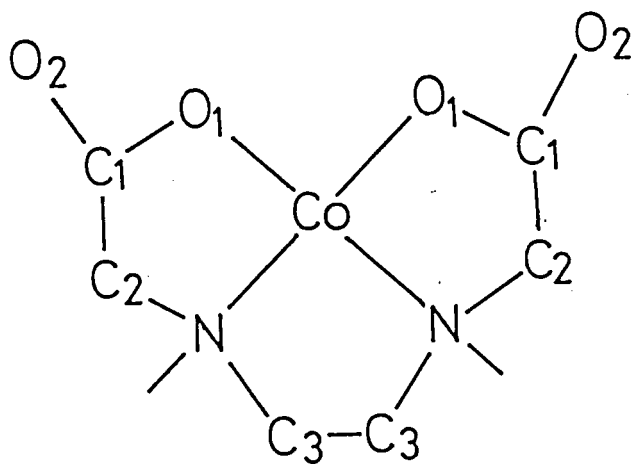


Figure 6.4. Numbering on some atoms in [Co(edta)]<sup>-</sup> complex.

Table 6.1. Peak Positions and Their Heights in Fourier Transforms of Co K-edge EXAFS for [Co(edta)]<sup>-</sup> Complexes.

sample	peak position/Å			peak height <sup>a)</sup>		
	1st	2nd	3rd	1st	2nd	3rd
(a) average of aqueous solution	1.92	2.69	-	0.5	0.4	-
(b) Na[Co(edta)]·4H <sub>2</sub> O	1.92	2.75	3.80	0.5	0.5	0.5
(c) NH <sub>4</sub> [Co(edta)]·2H <sub>2</sub> O	1.96	2.76	3.79	1.0	1.0	1.0
(d) Rb[Co(edta)]·2H <sub>2</sub> O	1.95	2.76	3.83	1.0	1.1	1.1
(e) Li[Co(edta)]·3H <sub>2</sub> O	1.97	2.75	3.77	1.4	1.4	1.1
(f) DMF solution	1.97	2.78	3.75	1.5	1.3	1.2
NH <sub>4</sub> [Co(edta)]·2H <sub>2</sub> O	1.91 <sup>b)</sup>	2.73 <sup>b)</sup>	3.85 <sup>b)</sup>	-	-	-
[Co(sarmp)(NH <sub>3</sub> ) <sub>3</sub> ][Co(edta)] H <sub>2</sub> O	1.92 <sup>c)</sup>	2.74 <sup>c)</sup>	3.89 <sup>c)</sup>	-	-	-

a) Relative intensity.

b) and c) The average of the distances of corresponding bonds for [Co(edta)]<sup>-</sup> from crystallographic data of Refs. 5 and 9, respectively.

sarmp<sup>2-</sup> = sarcosinate-*N*-propionate.

oscillation. The heights of the first peaks in Fourier transforms is roughly 1:2:3 for groups A, B, and C, respectively. Since the coordination numbers of Co in all the samples are constantly six, the large differences in peak heights must result from the differences in the root-mean-square displacement of Debye-Waller factor. The Debye-Waller factor of a peak originates from two contributions, static bond length distribution and dynamic or thermal disorder. In order to examine the contribution of static distribution, some simulation calculations were performed. The simulated EXAFS spectra were obtained by using a constant value of Debye-Waller factor for each kind of bonds and distributed bond lengths limited within reasonable ranges. However, the spectra could not give such large differences in peak heights in Fourier transforms as shown in experimental spectra. Therefore there must be some large differences in thermal disorder among the samples of group A, B, and C.

One of the origins for the solvent effect and counterion effect in thermal disorder may be the presence of hydrogen bonding which donates charge from carboxylate group to water molecule. A water molecule can approach to O<sub>2</sub> and even to O<sub>1</sub> to form hydrogen bonding. This effect appears also in other kinds of spectra, *e.g.* UV-Visible absorption spectra<sup>11)</sup> and <sup>13</sup>C NMR spectra.<sup>12)</sup> The presence of such hydrogen bonding has also been known in the [Co(edta)]<sup>-</sup> crystals<sup>10)</sup> and in an analogous complex, [Co<sup>III</sup>(trdta)]<sup>-</sup> (trdta<sup>4-</sup> = trimethylenediamine-*N,N,N',N'*-tetraacetate) crystal.<sup>13)</sup> NH<sub>4</sub>[Co(edta)]·2H<sub>2</sub>O crystals must have such hydrogen bonding, since some distances between O in water molecule and O<sub>2</sub> or O<sub>1</sub> are less than 3.0 Å. More hydrogen

bondings may exist in Na salt than in  $\text{NH}_4$  salt, because the volume of a unit cell of Na salt is only about 10% larger than that of  $\text{NH}_4$  salt and the number of waters of crystallization are twice as much. The fact that the spectrum for DMF solution sample is most intense should be due to the absence of the hydrogen bonding.

It is quite interesting to note that the weaker the peak in the Fourier transform, the shorter the bond length estimated from the first peak position. This may be due to that the Debye-Waller factors for Co-O bonds of longer lengths increase more than those for the shorter ones upon the hydrogen bonding formation (cf. the bond lengths are 1.870, 1.896, 1.913, 1.922 Å for Co-O and 1.921 and 1.925 Å for Co-N in  $\text{NH}_4$  salt<sup>5)</sup>)

### 6.3.2 Oxalato and malonato complexes

XANES spectra. Figure 6.5 shows the XANES spectra for  $\text{K}_3[\text{Co}(\text{ox})_3] \cdot 3\text{H}_2\text{O}$ ,  $\text{K}[\text{Co}(\text{ox})_2\text{en}] \cdot 1.5\text{H}_2\text{O}$ ,  $\text{K}[\text{Co}(\text{mal})_2\text{en}] \cdot \text{H}_2\text{O}$ ,  $\text{K}_3[\text{Cr}(\text{ox})_3] \cdot 3\text{H}_2\text{O}$ , and solutions of these complexes. There are small differences between XANES of solid samples and that of solution samples due to the little distortion of the complexes and/or the scattering by the counter cations and the water of crystallization. It is quite interesting that  $[\text{Co}(\text{ox})_3]^{3-}$  and  $[\text{Cr}(\text{ox})_3]^{3-}$  show very similar XANES spectra. Although XANES of solutions of the complexes containing ethylenediamine are quite identical with each other, the solutions of trisoxalato complexes exhibit slight differences on XANES spectra for their solution samples between the variations of the solvents. To emphasize these little differences, the differential XANES spectra for some of

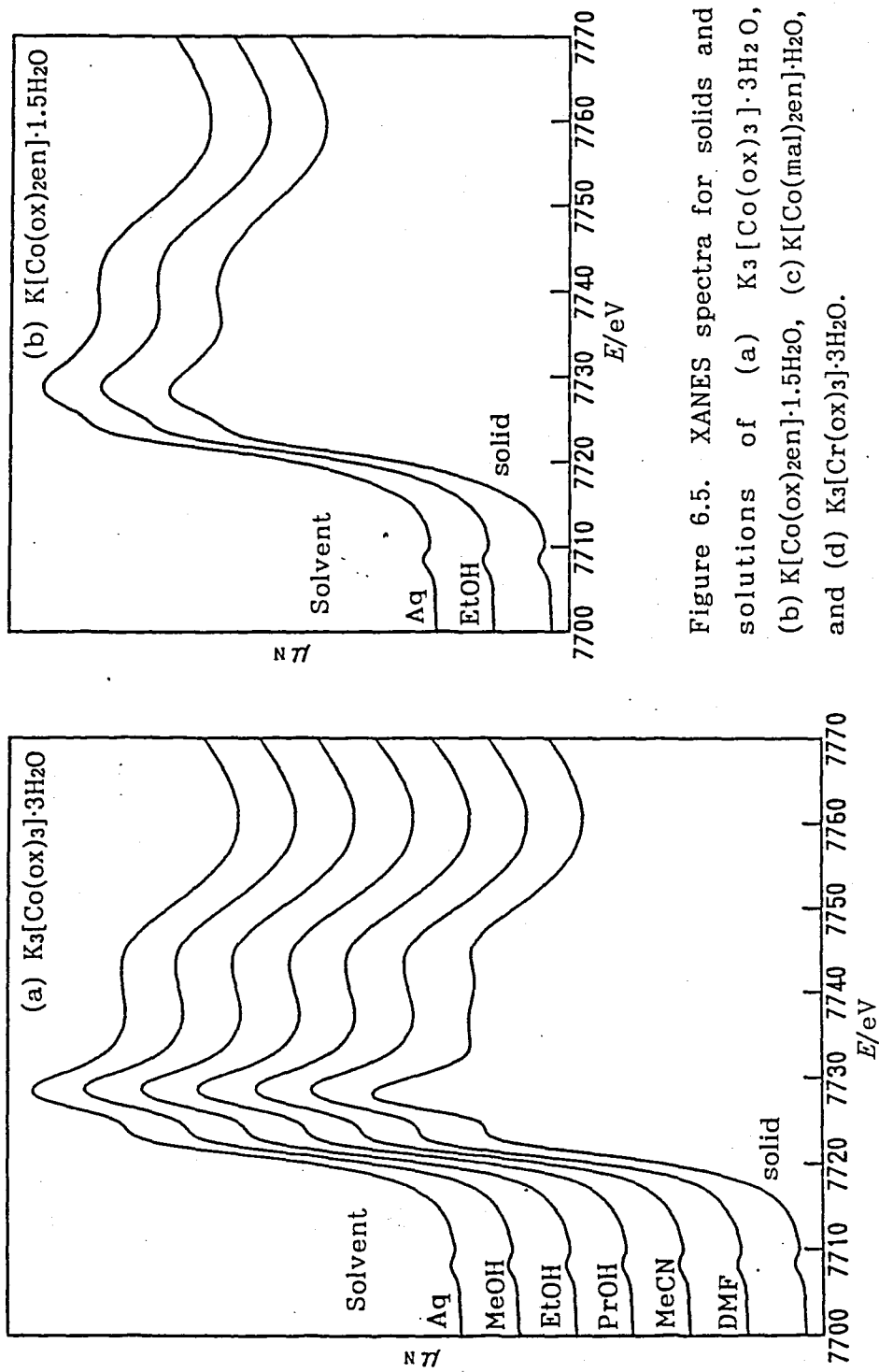


Figure 6.5. XANES spectra for solids and solutions of (a)  $K_3[Co(ox)_3] \cdot 3H_2O$ , (b)  $K[Co(ox)_2en] \cdot 1.5H_2O$ , (c)  $K[Co(mal)_2en] \cdot H_2O$ , and (d)  $K_3[Cr(ox)_3] \cdot 3H_2O$ .

Solvents of solutions are Aq: aqueous, MeOH: methanol, EtOH: ethanol, PrOH: 2-propanol, MeCN: acetonitrile, and DMF: dimethylformamide.

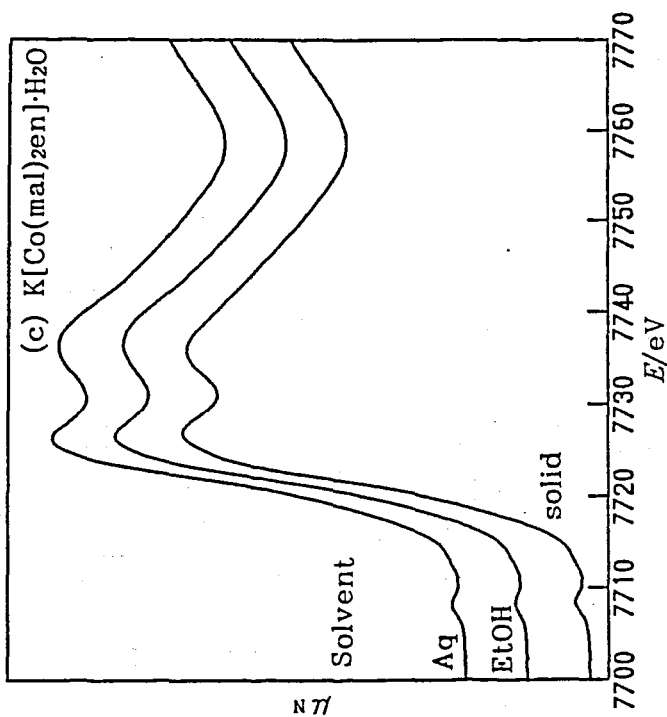
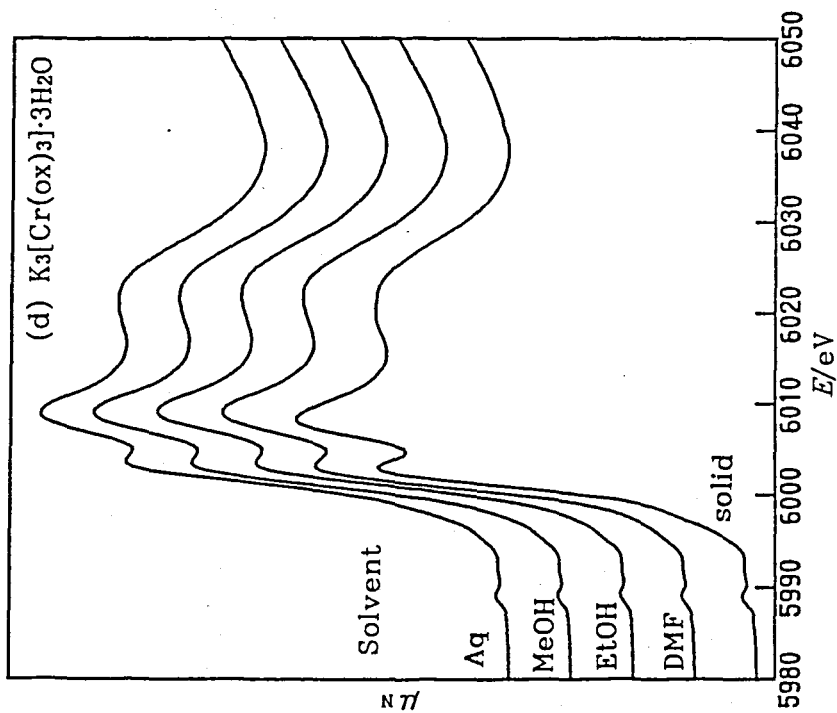


Figure 6.5. XANES spectra for solids and solutions of (a)  $K_3[Co(ox)_3] \cdot 3H_2O$ , (b)  $K[Co(ox)_2en] \cdot 1.5H_2O$ , (c)  $K[Co(mal)_2en] \cdot H_2O$ , and (d)  $K_3[Cr(ox)_3] \cdot 3H_2O$ . (continued)

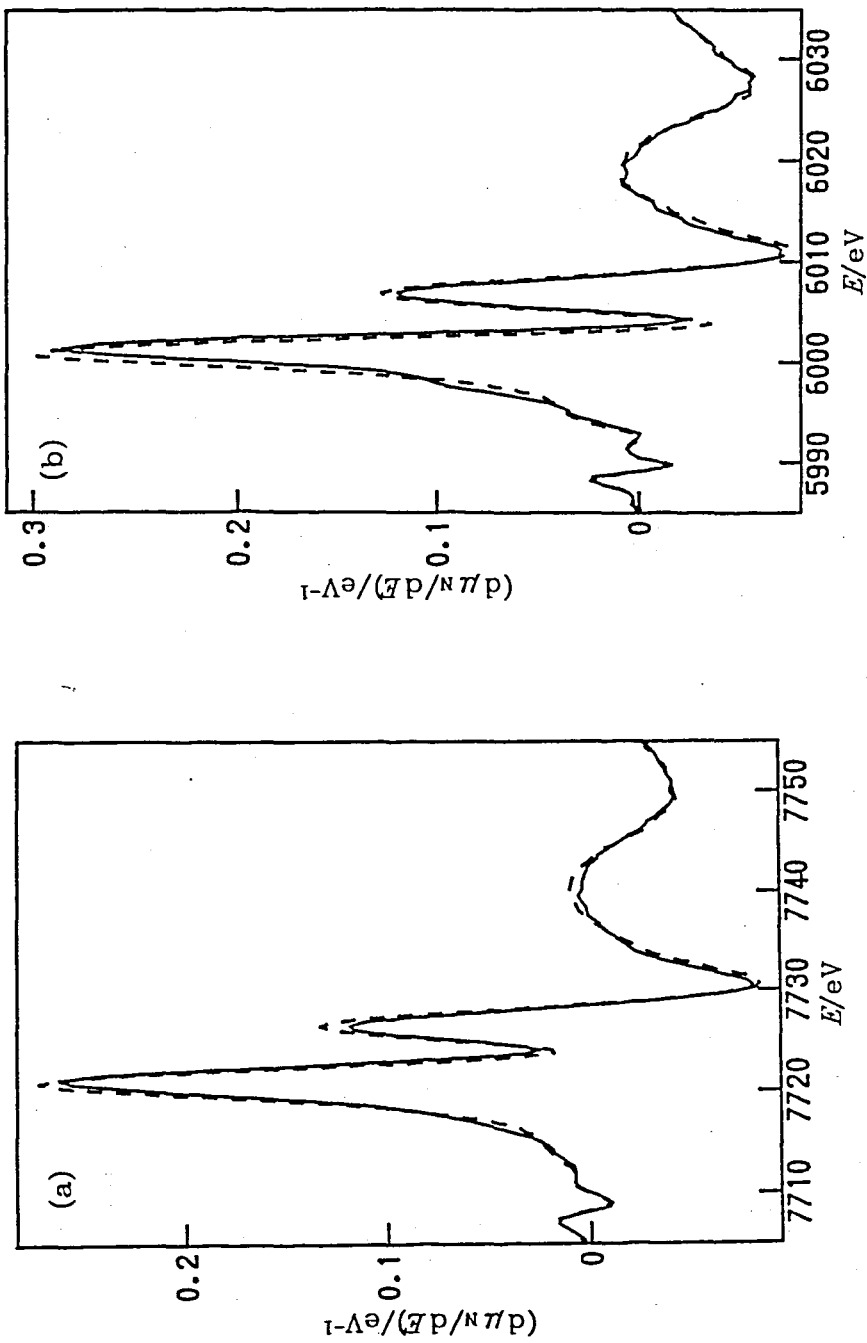


Figure 6.6. Differential XANES spectra for aqueous (solid lines) and DMF (broken lines) solutions of (a)  $[\text{Co}(\text{ox})_3]^{3-}$  and (b)  $[\text{Cr}(\text{ox})_3]^{3-}$ .

the solutions are shown in Fig. 6.6. It can be seen that the differential XANES spectra of DMF solutions is higher at the maxima and lower at the minima than those of aqueous solutions do. Even in the differential spectra these differences are very slight compared to  $[\text{Co}(\text{edta})]^-$ . This solvent effect should influence the XANES of  $[\text{Co}(\text{ox})_2\text{en}]^-$  and  $[\text{Co}(\text{mal})_2\text{en}]^-$  because these two complexes show the solvent effects on the other spectra such as UV-Visible absorption.<sup>14)</sup> But the effect does not appear in the XANES spectra. This may be due to the selective character of the solvent effect. The effect can act only through the carboxylato ligand and there may be no effect on the ethylenediamine. Therefore, this weak solvent effect may be screened in these ethylenediamine complexes.

EXAFS. Figure 6.7 shows EXAFS Fourier transforms for solids and aqueous solutions. Three prominent peaks are seen in all of the transforms. The first peaks around 1.9 Å are assigned to the direct coordinate atoms, *i.e.* oxygens of  $\text{ox}^{2-}$  and  $\text{mal}^{2-}$  and nitrogens of en. The second at 2.6–2.7 Å are correspond to carbons of the ligands. The third peaks are due to oxygens of  $\text{ox}^{2-}$  or  $\text{mal}^{2-}$  at the outside of the complexes and enhanced by the multiple scattering effect as shown in EDTA complexes.

Since  $[\text{Co}(\text{ox})_3]^{3-}$  has a simplest first coordination sphere among the complexes and the three peaks are well resolved in the Fourier transforms, curve-fitting analysis are performed for  $[\text{Co}(\text{ox})_3]^{3-}$  samples. The results for the model compound,  $\text{K}_3[\text{Co}(\text{ox})_3]\cdot 3\text{H}_2\text{O}$ , are listed in Table 6.2. The distances to the first and second shell are refined loosely bound with a standard deviation 0.0064 Å and 0.0026 Å around these initial values, 1.902 Å

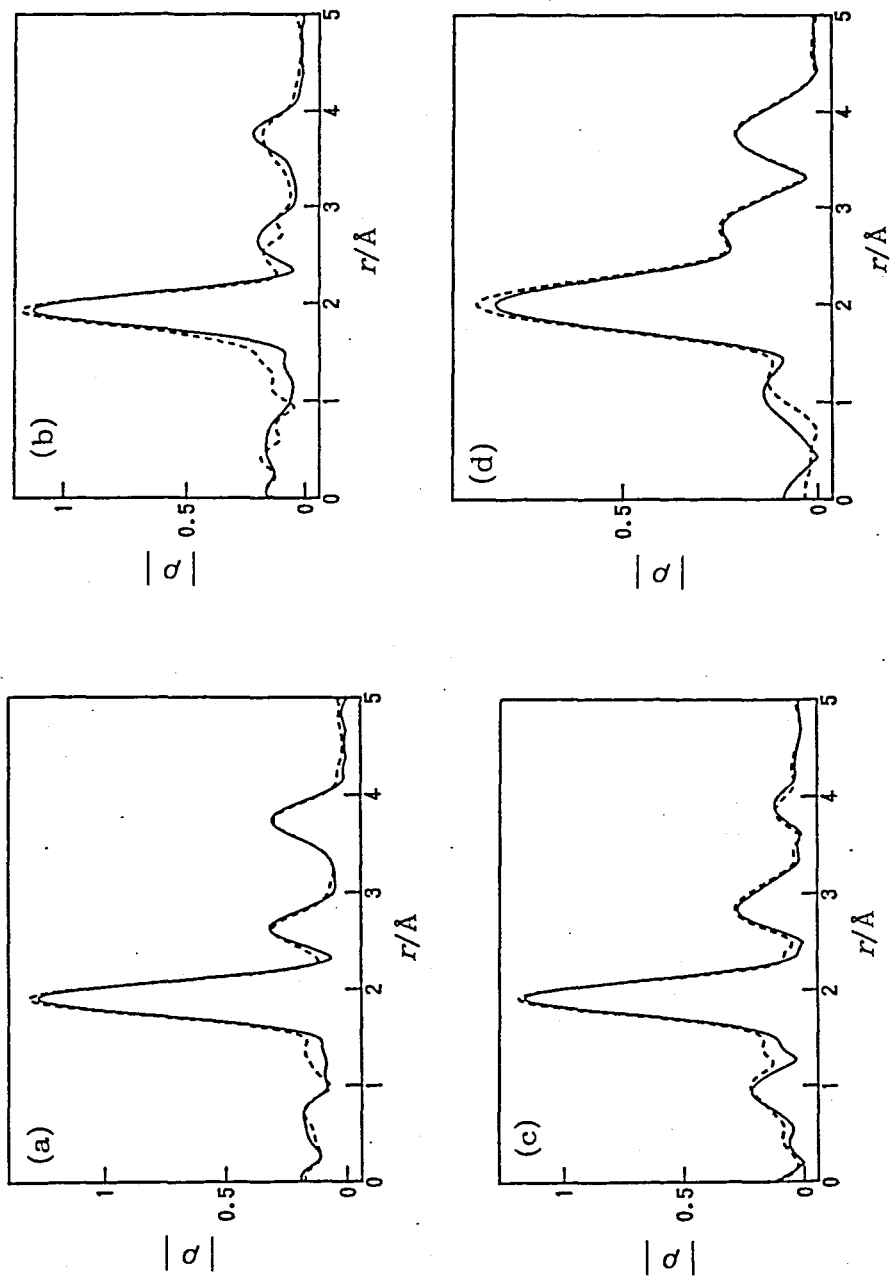


Figure 6.7. EXAFS Fourier transforms for solids (solid lines) and aqueous solutions (broken lines) of (a)  $K_3[Co(ox)_3] \cdot 3H_2O$ , (b)  $K[Co(ox)_2en] \cdot 1.5H_2O$ , (c)  $K[Co(mal)_2en] \cdot H_2O$ , and (d)  $K_3[Cr(ox)_3] \cdot 3H_2O$ .

Table 6.2. Curve-fitting Results for  $K_3[Co(ox)_3] \cdot 3H_2O$  Powder  
as Model Compound.

shell	$r/\text{\AA}$	$B$	$\sigma/10^{-2}\text{\AA}$	$\Delta E_b/eV$	$\phi_0/\text{rad}$
1	1.907(1) <sup>a)</sup>	2.948(0)	4.136(8)	-0.5(1)	-0.44(1)
2	2.671(0) <sup>b)</sup>	3.14(2)	5.77(8)	-7.1(1)	-0.20(2)
3 <sup>c)</sup>	3.829(4)	4.54(4)	5.50(5)	-18.7(3)	1.6(1)

Average of two data.

Differences of each data from the average on the last significant digits are given in parentheses.

a) and b) are loosely bound to 1.902  $\text{\AA}$  and 2.671  $\text{\AA}$  with a

standard deviation 0.0064  $\text{\AA}$  and 0.0026  $\text{\AA}$ , respectively.

c) Values for the third shell are not correct because of the multiple scattering effect.

Table 6.3. Curve-fitting Results of  $[\text{Co}(\text{ox})_3]^{3-}$  in Solutions.

Solvent	shell=	$r/\text{\AA}$			$\sigma/10^{-2}\text{\AA}$			$AN$
		1	2	3 <sup>a)</sup>	1	2	3 <sup>a)</sup>	
H <sub>2</sub> O <sup>b)</sup>		1.907	2.667	3.828	4.00	6.09	5.57	54.8
methanol		1.909	2.666	3.830	4.05	6.02	5.56	41.3
ethanol <sup>b)</sup>		1.909	2.665	3.833	3.99	6.05	5.40	37.1
2-propanol		1.910	2.670	3.833	4.03	5.94	5.45	33.5
acetonitrile <sup>b)</sup>		1.910	2.672	3.834	4.07	6.06	5.70	18.9
DMF <sup>b)</sup>		1.911	2.675	3.838	4.03	6.10	5.72	16.0

$B$ ,  $\Delta E_0$ , and  $\phi_0$  are fixed to the values specified in Table 6.2.

a) Values for the third shell are not correct because of the multiple scattering effect, but may be used as relative ones.

b) Average of two data.

and 2.671 Å. The initial values are average of the Co-O or Co-C distances calculated from crystallographic data.<sup>15)</sup> For the third shell all of the parameters are refined in the calculations because the phase shifts and the back-scattering amplitudes may be corrected insufficiently due to the multiple scattering effect. Therefore the results of the third peaks are not correct, but they may be used as relative values. Table 6.3 lists the curve-fitting results of  $[\text{Co}(\text{ox})_3]^{3-}$  in various solvents. Though the Debye-Waller factors  $\sigma$  do not show any apparent trends in the solvents, the interatomic distances  $r$  have systematic variations. In Fig. 6.8  $r$  are plotted against the acceptor number  $AN$  of the solvents. This figure indicates that the plots of  $r$  give straight lines. It is surprising that the larger  $AN$  corresponds to the shorter distances. But this trend coincides with that of the peak position in their UV-Visible absorption spectra.<sup>14)</sup> The change of crystal field splitting parameter ( $10Dq$ ) due to the change of Co-O bond lengths between aqueous and DMF solutions can be estimated to be ca. 1% from the relation:  $10Dq \propto r^{-5}$ .<sup>16)</sup> This estimation shows a good agreement with the change of the first absorption band in the UV-Visible absorption spectra, 0.8%.<sup>14)</sup>

The interatomic distance of  $[\text{Co}(\text{ox})_3]^{3-}$  in a solution can be approximately estimated by the acceptor number of the solvent. The correlation between the  $r_j$  values ( $j$  denotes the peak number, 1, 2, or 3) and  $AN$  can be expressed by the following equations;

$$\begin{aligned}
 r_1/\text{\AA} &= -0.00009AN + 1.912 \\
 r_2/\text{\AA} &= -0.00022AN + 2.677 \\
 r_3/\text{\AA} &= -0.00021AN + 3.840.
 \end{aligned}
 \tag{6.1}$$

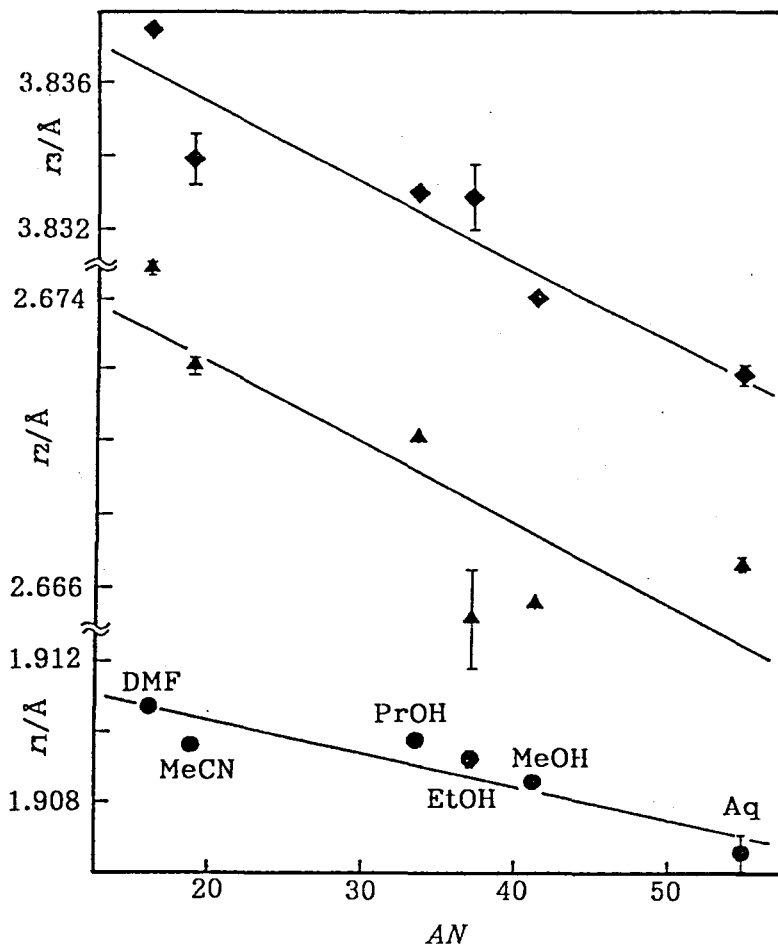


Figure 6.8. Correlation between interatomic distances  $r$  and acceptor number  $AN$  of the solvents on  $[\text{Co}(\text{ox})_3]^{3-}$  solutions. Solvents are Aq: aqueous, MeOH: methanol, EtOH: ethanol, PrOH: 2-propanol, MeCN: acetonitrile, and DMF: dimethylformamide.

It is noted that the magnitude of the slopes of the equations for the second and third peaks is larger than that for the first peak. This suggests that the C-(O of the first peak) bond lengths and/or (O of the first peak)-C-C angles in the oxalate ion are also affected by the influence of electrophilic effect which is implied as  $AN$ .

From Eq. (6.1) one may imagine an "acceptor number in a solid state". The interatomic distances for  $K_3[Co(ox)_3] \cdot 3H_2O$  are obtained as  $r_1=1.907 \text{ \AA}$ ,  $r_2=2.671 \text{ \AA}$ , and  $r_3=3.829 \text{ \AA}$  by the same method as that for Table 6.3, then the imaginary  $AN$  for  $K_3[Co(ox)_3] \cdot 3H_2O$  can be estimated to be 58, 23, or 50 by Eq. (6.1). Since the surroundings of  $[Co(ox)_3]^{3-}$  is not equivalent to the solutions in the solid state, the  $AN$  can not be comparable with that of solutions. But the imaginary  $AN$  can not be zero and this electrophilic effect may originate from hydrogen bonds with the water of crystallization.

## 6.4 References

1. S. Harada, Y. Funaki, and T. Yasunaga, *J. Am. Chem. Soc.*, 102, 136 (1980); S. Kaizaki and H. Mizu-uchi, *Inorg. Chem.*, 25, 2732 (1986); W. C. E. Higginson and B. Samuel, *J. Chem. Soc. (A)*, 1579 (1970); J. Oakes and E. G. Smith, *J. Chem. Soc., Faraday Trans. 1*, 79, 543 (1983); S. Richards, B. Pedersen, J. V. Silverton, and J. L. Hoard, *Inorg. Chem.*, 3, 27 (1964).
2. C. H. L. Kennard, *Inorg. Chim. Acta*, 1, 347 (1967); M. D. Lind and J. L. Hoard, *Inorg. Chem.*, 3, 34 (1964); M. J. Hamor, T. A. Hamor, and J. L. Hoard, *ibid.*, 3, 34 (1964); X. Solans, M. Font-Altaba, and J. Garcia-Oricain, *Acta Crystallogr., Sect. C*, 40, 635 (1984); N. V. Novozhilova, T. N. Polynova, and M. A. Porai-Koshits, *Zh. Struct. Khim.*, 16, 865 (1975).
3. W. D. Wheeler and J. I. Legg, *Inorg. Chem.*, 23, 3798 (1984); K. Kanamori and K. Kawai, *ibid.*, 25, 3711 (1986).
4. I. A. W. Shimi and W. C. E. Higginson, *J. Chem. Soc.*, 260 (1958); R. Dyke and W. C. E. Higginson, *ibid.*, 1998 (1960).
5. H. A. Weakliem and J. L. Hoard, *J. Am. Chem. Soc.*, 81, 549 (1959).
6. F. P. Dwyer, E. C. Gyarfas, and D. P. Mellor, *J. Phys. Chem.*, 59, 296 (1955); S. Kirschner and E. C. Gyarfas, *Inorg. Synth.*, V, 186 (1957).
7. B. K. Teo and P. A. Lee, *J. Am. Chem. Soc.*, 101, 2815 (1979).
8. M. Sano, *Inorg. Chem.*, 27, 4249 (1988).
9. N. Binsted, S. L. Cook, J. Evans, R. J. Price, and G. N. Greaves, *J. Phys. (Paris), Colloq.*, 47, C8-589 (1986); N. Binsted, S. L. Cook, J. Evans, G. N. Greaves, and R. J. Price, *J. Am. Chem. Soc.*, 109,

- 3669 (1987).
10. K. Okamoto, T. Tsukihara, J. Hidaka, and Y. Shimura, *Bull. Chem. Soc. Jpn.*, 51, 3534 (1978).
  11. T. Taura, *Chem. Lett.*, 2011 (1984).
  12. T. Taura, *Inorg. Chem.*, 27, 2845 (1988).
  13. R. Nagao, F. Marumo, and Y. Saito, *Acta Crystallogr., Sect. B*, 28, 1852 (1972).
  14. T. Taura, *37th Symposium on Coordination Chemistry*, Tokyo, Japan, 1987, Abstr. 3B08; T. Taura, personal communication.
  15. H. Okazaki, Y. Kushi, and H. Yoneda, *J. Am. Chem. Soc.*, 107, 4183 (1985).
  16. E. König and K. J. Watson, *Chem. Phys. Lett.*, 6, 457 (1970).

## Chapter 7. Structures of Fe(III) complexes with EDTA and analogous ligands in aqueous solutions revealed by XAFS

### 7.1 Introduction

It is known that Fe(III)-EDTA (EDTA = ethylenediamine-*N,N,N',N'*-tetraacetic acid) takes either six-<sup>1)</sup> or seven-coordinate<sup>2)</sup> structure when it crystallizes from neutral or weakly acidic solution: Li, Na, K, Ag, and Tl salts are of sexidentate seven-coordinate geometry, some of Li salt has sexidentate six-coordinate one, and the quinquedentate six-coordinate monoqua complex has been found in acidic salt.<sup>3)</sup> The seven-coordinate structure is similar to that of the Mn(II)-EDTA complex in  $Mn_3(Hedta)_2 \cdot 10H_2O$ ,<sup>4)</sup> in which the complexes have a distorted pentagonal bipyramidal geometry with two amino nitrogens, two carboxylato oxygens, and a water molecule at the apices of the pentagon, while the axial positions are occupied by the remaining two carboxylato oxygens. While the structure of Fe(III)-EDTA in the crystal phase has been established by reliable diffraction techniques, little is known about the structure in the solution phase due to the lack of adequate analytical techniques. It is also due to the fact that the Fe(III)-EDTA complex undergoes a rapid ligand substitution reaction in aqueous solution.<sup>5)</sup> In order to study the structure of the complex in solution, or its coordination number, its XAFS spectra will be reported in this chapter. The spectra of crystalline samples with known structures have been also measured as the reference materials. The spectra of Fe(III) complexes with EDDDA

(ethylenediamine-*N,N'*-diacetate-*N,N'*-dipropionate) were also measured. The XAFS techniques are suitable for determining the coordination numbers of such complexes since these techniques extract the information regarding the local structure around the central metal irrespective of the environments.

## 7.2 Experimental

**Sample preparations.** The samples of Fe(III) complexes studied in this work are, (a) Na[Fe(edta)H<sub>2</sub>O]·2H<sub>2</sub>O, (b) Li[Fe(edta)H<sub>2</sub>O]·2H<sub>2</sub>O, (c) Li[Fe(edta)], (d) [Fe(Hedta)H<sub>2</sub>O]·2H<sub>2</sub>O, (e) Li[Fe(eddda)]·2H<sub>2</sub>O, (f1) Fe(III)-EDTA aqueous solution at pH 1, (f2) Fe(III)-EDTA aqueous solution at pH 3, (f3) Fe(III)-EDTA aqueous solution at pH 5, and (g) Fe(III)-EDDDA aqueous solution at pH 7. Li[Fe(edta)H<sub>2</sub>O]·2H<sub>2</sub>O,<sup>2)</sup> Na[Fe(edta)H<sub>2</sub>O]·2H<sub>2</sub>O,<sup>2)</sup> [Fe(Hedta)H<sub>2</sub>O]·2H<sub>2</sub>O,<sup>3)</sup> and Li[Fe(eddda)]·2H<sub>2</sub>O<sup>6)</sup> (bright yellow) were prepared according to the literature references with slight modifications. Elemental analyses confirmed the above compositions for the respective complexes. Li[Fe(edta)] (light yellow powder) was obtained by drying Li[Fe(edta)H<sub>2</sub>O]·2H<sub>2</sub>O (dark brown crystals) at 100–110 °C and was identified by its decrease in weight and the elemental analysis. Aqueous solutions of *ca.* 0.1 mol dm<sup>-3</sup> were prepared by dissolving each solid Fe(III) complex sample. Hydrochloric acid and sodium hydrogencarbonate were used to adjust pH.

**Measurements and Calculations.** Fe K-edge X-ray absorption spectra were obtained at BL-7C and BL-10B of Photon Factory in the National Laboratory for High Energy Physics. Fourier transform calculations were performed over the *k* range of 2.6–12.6 Å<sup>-1</sup> using the phase shift and the back-scattering

amplitude parameters tabulated by Teo and Lee.<sup>7)</sup> A curve-fitting procedure was also applied to the EXAFS spectra. However, it could not provide reliable results, possibly because of the presence of too many shells to be considered for the Fe-EDTA complex and large disorder among its coordination bonds.

The ordinate scales of the spectra are common among Figs. 7.1 and 7.2, 7.3 and 7.4, and 7.6 and 7.7, so that the relative magnitudes are directly compared among these figures.

### 7.3 Results and discussion

XANES spectra. Figure 7.1 shows Fe K-edge XANES spectra for solid samples. Noticeable variations are found in the region around the largest peak. There is a strong sharp peak B in the seven-coordinate complexes of (a)  $\text{Na}[\text{Fe}(\text{edta})\text{H}_2\text{O}] \cdot 2\text{H}_2\text{O}$ <sup>2)</sup> and (b)  $\text{Li}[\text{Fe}(\text{edta})\text{H}_2\text{O}] \cdot 2\text{H}_2\text{O}$ ,<sup>2)</sup> while the peak is weak or almost absent in six-coordinate complexes of (c)  $\text{Li}[\text{Fe}(\text{edta})]$ , (d)  $[\text{Fe}(\text{Hedta})\text{H}_2\text{O}] \cdot 2\text{H}_2\text{O}$ ,<sup>3)</sup> and (e)  $\text{Li}[\text{Fe}(\text{eddda})] \cdot 2\text{H}_2\text{O}$ .

The six-coordinate structure of (c) was confirmed by diffuse reflectance spectroscopy. The diffuse reflectance spectra of (b) and (c) were obtained and compared with the results of Garbett et al.<sup>8)</sup> The color of (b) (dark brown) and (c) (bright yellow) indicates that the former complex is seven-coordinate and the latter six-coordinate. For the Fe(III)-EDDDA complexes,<sup>6)</sup> it has been reported that only the *trans*(O<sub>5</sub>) six-coordinate isomer with two oxygens (O<sub>5</sub>) of five membered N-O rings at the trans position was isolated and there is little room for a seventh coordination site in the *trans*(O<sub>5</sub>) isomer.

Now one can compare XANES spectra for solid samples in

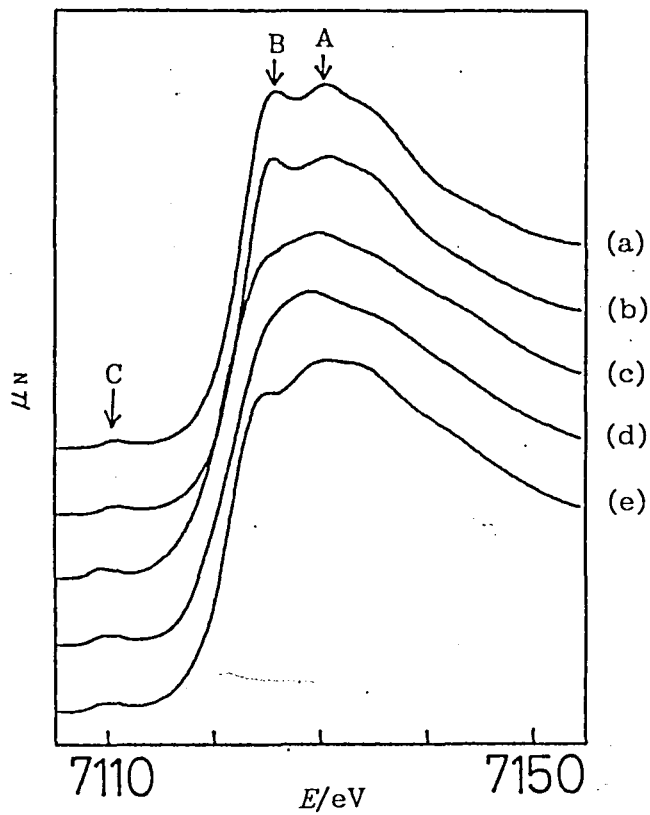


Figure 7.1. Fe K-edge XANES spectra for (a)  $\text{Na}[\text{Fe}(\text{edta})\text{H}_2\text{O}] \cdot 2\text{H}_2\text{O}$ , (b)  $\text{Li}[\text{Fe}(\text{edta})\text{H}_2\text{O}] \cdot 2\text{H}_2\text{O}$ , (c)  $\text{Li}[\text{Fe}(\text{edta})]$ , (d)  $[\text{Fe}(\text{Hedta})\text{H}_2\text{O}] \cdot 2\text{H}_2\text{O}$ , and (e)  $\text{Li}[\text{Fe}(\text{eddda})] \cdot 2\text{H}_2\text{O}$ .

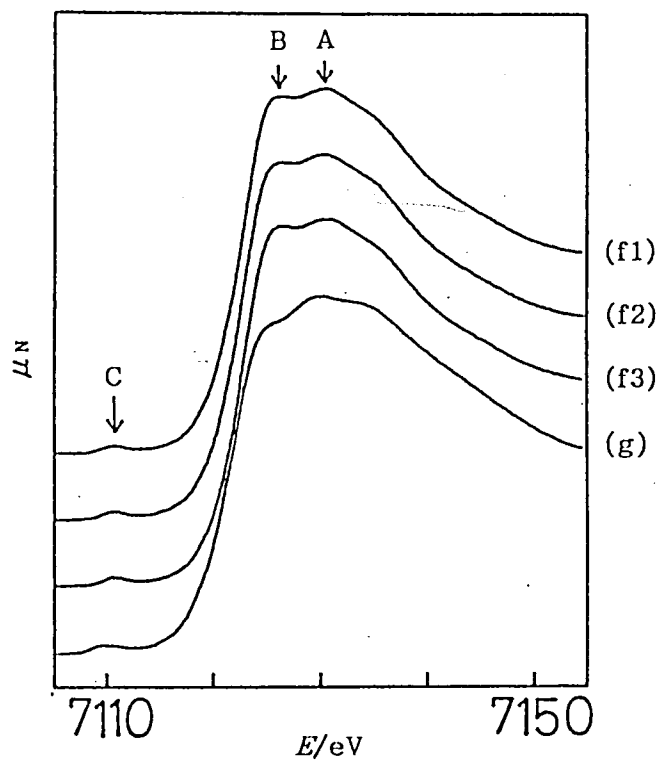


Figure 7.2. Fe K-edge XANES spectra for Fe(III)-EDTA in aqueous solution at pH of 1 (f1), 3 (f2), and 5 (f3), and (g) Fe(III)-EDDDA at pH 7.

Fig. 7.1 with those for aqueous solutions of Fe(III)-EDTA, (f1-f3) in Fig. 7.2. It is quite obvious that the spectral features for solution do not depend on its pH value, and that they are the same as those for solid samples (a) and (b). Therefore, one can conclude that the coordination number of the complex in aqueous solution is seven. Since the spectrum of EDDDA complex in solution (g) is similar to that in the solid state, (e), and does not contain the peak B, this complex in solution must be of a six-coordinate structure.

Pre-edge peaks. One can also use the shape of peak C (indicated in Figs. 7.1 and 7.2) to determine the symmetries of the complexes. The expanded spectra for the peak C are shown in Figs. 7.3 and 7.4. Since the spectra were collected on different occasions, the calibration error in photon energy for these spectra may amount to a few tenths of an eV. Therefore we do not use the absolute photon energy scale here. Careful inspection of Fig. 7.3 leads to the fact that the peak of the six-coordinate complexes (c, d, and e) is unsymmetrical while the seven-coordinate ones (a and b) show a smooth peak with Gaussian shape. The peak C is due to  $1s \rightarrow 3d$  transition<sup>9)</sup> with two components,  $1s \rightarrow t_2$  and  $1s \rightarrow e$ . For example, Fe(III) hexaaqua complex in acidic aqueous solution shows a convoluted two pre-edge peak as shown in Fig. 7.5. The splitting of this peak is 1.5 eV which agrees with the known crystal field splitting value, 1.7 eV. The two components are resolved indistinctly in the spectra for the six-coordinate complexes with almost octahedral symmetry, but they are not resolved at all for the seven-coordinate complexes with lower symmetry. The results for solution samples (f1), (f2), and (f3) in

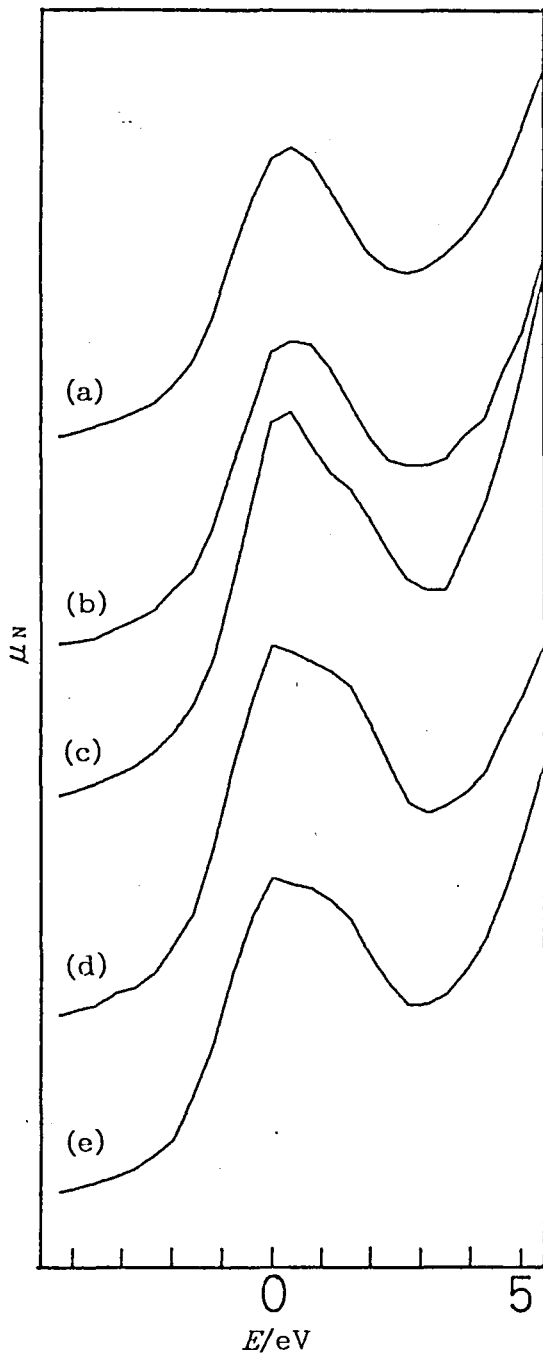


Figure 7.3. Expanded spectra for peak C. Photon energies are relative scale and may contains some uncertainty. The notations are the same as in Fig. 7.1.

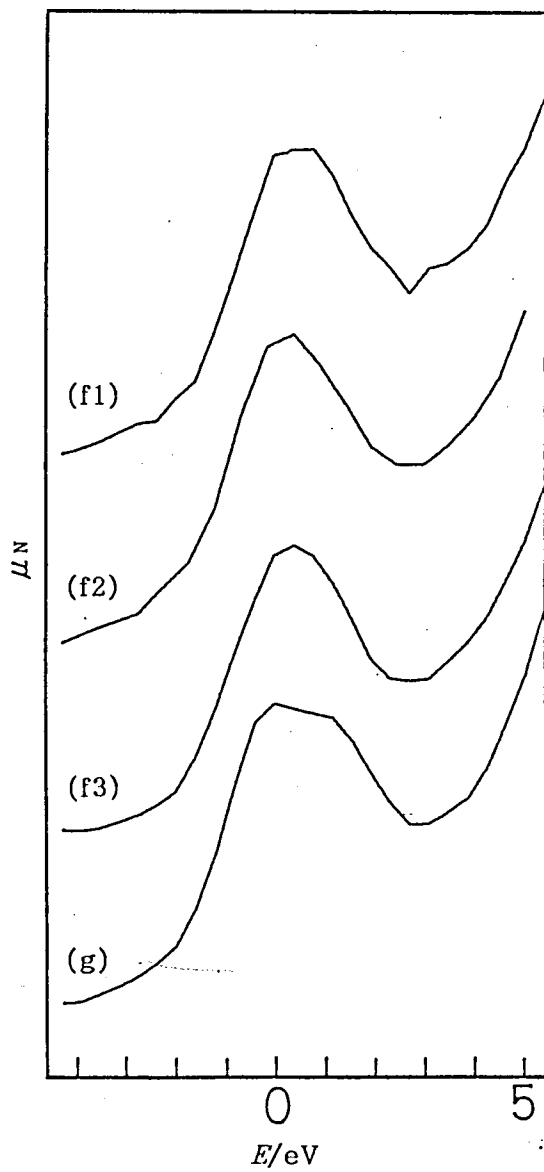


Figure 7.4. Expanded spectra for peak C. The notations are the same as in Fig. 7.2.

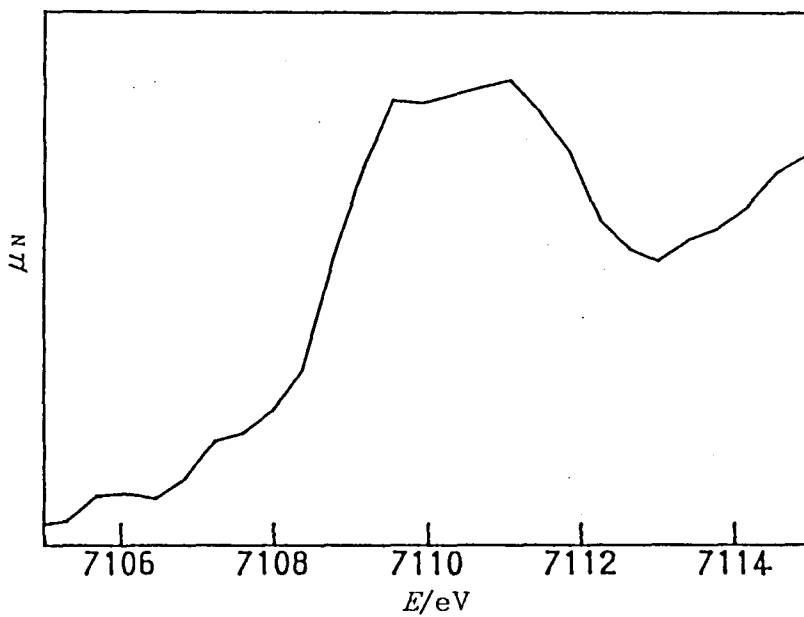


Figure 7.5. Fe K-edge XANES spectra around pre-edge peak for Fe(III) perchlorate acidic solution.

Fig. 7.4 look similar to those for (a) and (b) with seven-coordination.

EXAFS. Fourier transforms of EXAFS for the Fe(III) complexes in the solid state are shown in Fig. 7.6. By referring to the EXAFS of  $[\text{Co}(\text{edta})]^-$ <sup>10)</sup> and by consideration of the crystallographic data for Na and Li salts of  $[\text{Fe}(\text{edta})\text{H}_2\text{O}]^-$ ,<sup>2)</sup> and  $[\text{Fe}(\text{Hedta})\text{H}_2\text{O}]$ ,<sup>3)</sup> one may expect that the Fe-EDTA complexes give three peaks in their Fourier transforms; the most intense peak (the first peak) around 2.1 Å corresponding to the bonds Fe-O and Fe-N, the second peaks at 2.8–3.2 Å to Fe-C, and the third peaks at around 4 Å to Fe-O of uncoordinated oxygen atoms of carboxylato group.

For the six-coordinate Fe complexes, *i.e.* (c)  $[\text{Fe}(\text{edta})]^-$ , (d)  $[\text{Fe}(\text{Hedta})\text{H}_2\text{O}]$ , and (e)  $[\text{Fe}(\text{eddda})]^-$ , the Fourier transforms show the expected three peaks, while for the seven-coordinate complexes,  $[\text{Fe}(\text{edta})\text{H}_2\text{O}]^-$  salts, *i.e.* (a) and (b), the second peak can hardly be observed. Further, the first peaks of the seven-coordinate complexes are obviously weaker than those of six-coordinate complexes. The static disorders for the first peaks of the seven- and six-coordinate complexes are estimated to be 0.13 and 0.11–0.12 Å, respectively, from the root-mean-square standard deviation of Fe-O,N bond lengths of their crystallographic data<sup>2,3,6)</sup> by Eq. (3.30). Because the effect of the static disorder on the peak intensity is partly cancelled out by the coordination number, 6 or 7, the thermal disorder of Fe-O and/or Fe-N bond in seven-coordinate complexes must be considerably larger than that of six-coordinate ones.

Now we can study the Fourier transforms for aqueous solution samples shown in Fig. 7.7. The first and the second peaks for the

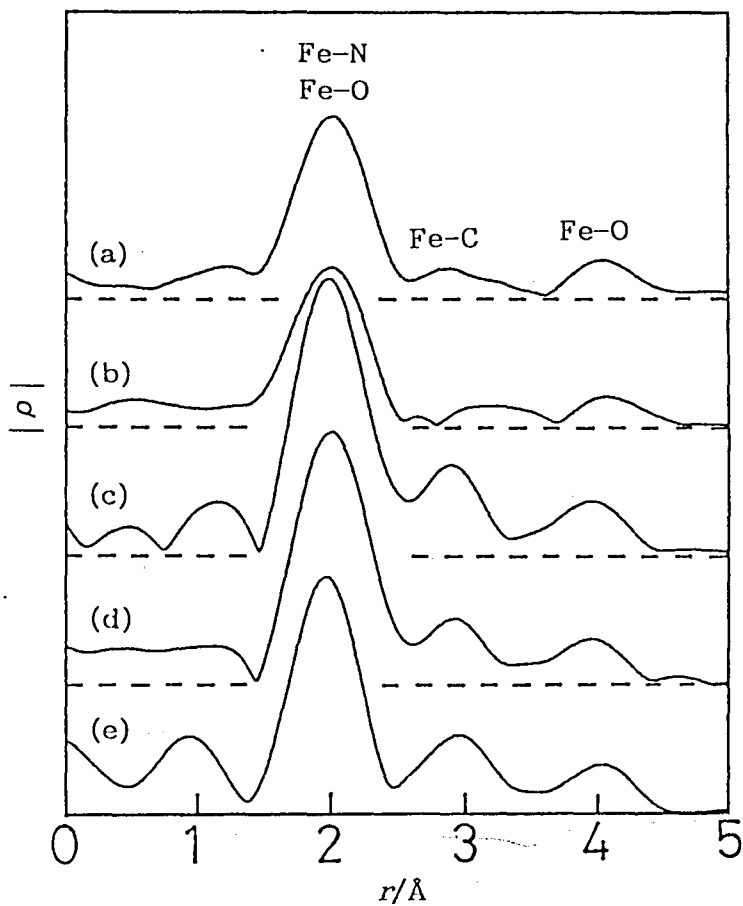


Figure 7.6. Fourier transforms of Fe K-edge EXAFS. The notations are the same as in Fig. 7.1.

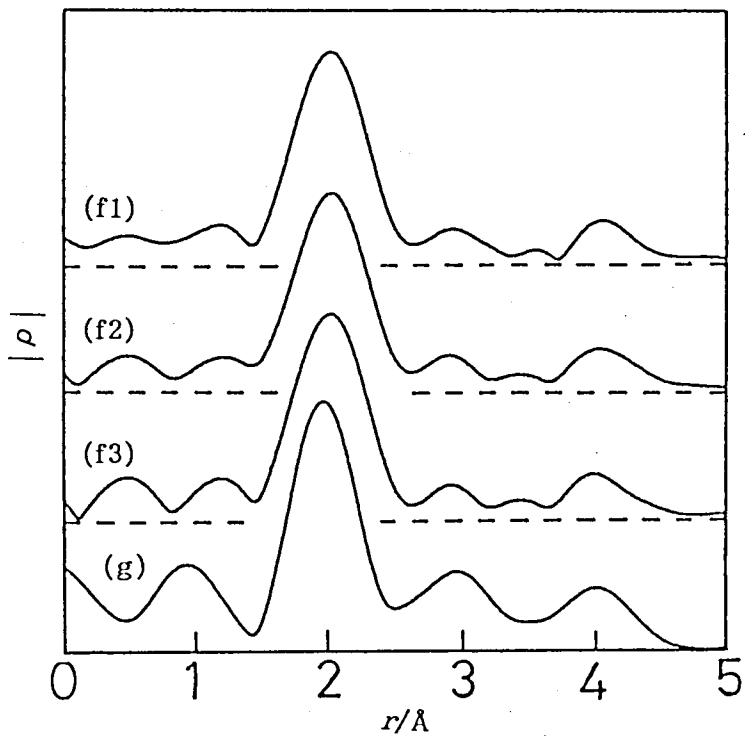


Figure 7.7. Fourier transforms of Fe K-edge EXAFS for Fe(III) complex aqueous solutions. The notations are the same as in Fig. 7.2.

EDTA complex solution are weak compared with that for the solution of the EDDDA complex and those for six-coordinate solid samples of (c), (d), and (e). This observation again suggests that the structure of Fe(III)-EDTA complex in aqueous solution is mainly seven-coordinate. The conclusion derived from the present XANES and EXAFS studies agrees with the recent Raman study.<sup>11)</sup>

The spectra for Fe(III)-EDDDA in solid and in solution are compared and both spectra are identical with respect to the XANES pre-edge peak (e) in Fig. 7.3 and (g) in Fig. 7.4, and Fourier transform (e) in Fig. 7.6 and (g) in Fig. 7.7. Thus the coordination number in solution should be six.

Strictly speaking, the EDTA or the EDDDA complex in solution should not necessarily take only the seven- or only the six-coordinate structure, respectively. They can be a mixture of six- and seven-coordinate species. But it seems that the major portion of the EDTA and the EDDDA complexes in solution take the seven- and six-coordinate structure, respectively.

## 7.4 References

1. N. V. Novozhilova, T. N. Polynova, M. A. Porai-Koshits, N. I. Pechurova, L. I. Martynenko, and A. Khadi, *Zh. Strukt. Khimi.*, 14, 745 (1973); Y. Kushi, K. Morimasa, K. Yoshitsugu, and H. Yoneda, *35th Symposium on Coordination Chemistry*, Hiroshima, Japan, 1985, Abstr. 2B01; M. A. Porai-Koshits, *Sov. Sci. Rev. B. Chem.*, 10, 91 (1987).
2. J. L. Hoard, M. Lind, and J. V. Silverton, *J. Am. Chem. Soc.*, 83, 2770 (1961); M. D. Lind and J. L. Hoard, *Inorg. Chem.*, 3, 34 (1964); M. J. Hamor, T. A. Hamor, and J. L. Hoard, *ibid.*, 3, 34 (1964); X. Solans, M. Font-Altava, and J. Garcia-Oricain, *Acta Crystallogr., Sect. C*, 40, 635 (1984); J. M. López-Alcalá, M. C. Puetra-Vizcaíno, F. González-Vílchez, E. N. Duesler, and R. E. Tapscott, *ibid.*, 40, 939 (1984).
3. C. H. L. Kennard, *Inorg. Chim. Acta*, 1, 347 (1967).
4. S. Richards, B. Pedersen, J. V. Silverton, and J. L. Hoard, *Inorg. Chem.*, 3, 27 (1964).
5. H. Ogino, M. Shimura, and N. Tanaka, *Inorg. Chem.*, 18, 2497 (1979); H. Ogino and M. Shimura, *Adv. Inorg. Bioinorg. Mech.*, 4, 107 (1986).
6. T. Yamamoto, K. Mikata, K. Miyoshi, and H. Yoneda, *Inorg. Chim. Acta*, 150, 237 (1988).
7. B. K. Teo and P. A. Lee, *J. Am. Chem. Soc.*, 101, 2815 (1979).
8. K. Garbett, G. Lang, and R. J. P. Williams, *J. Chem. Soc. (A)*, 3433 (1971).
9. B. Poumellec, F. Lagnel, J. F. Marucco, and B. Touzelin, *Phys. Status Solidi B*, 133, 371 (1986).

10. H. Sakane, I. Watanabe, and S. Ikeda, *Bull. Chem. Soc. Jpn.*, 62, 1513 (1989).
11. K. Kanamori, S. Dohniwa, and K. Kawai, *38th Symposium on Coordination Chemistry*, Tokushima, Japan, 1988, Abstr. 2BP02; K. Kanamori, H. Dohniwa, N. Ukita, I. Kanesaka, and K. Kawai, *Bull. Chem. Soc. Jpn.*, 63, 1447 (1990).

## Concluding remarks

EXAFS for a series of simple six- and four-coordinate first transition metal complexes are analyzed systematically. A qualitative agreement is shown between Debye-Waller factors,  $\sigma$ , and those calculated from vibrational frequency for six-coordinate complexes. Characterizations of scale factor,  $S$ ,  $\sigma$ , and the change of edge shift,  $\Delta E_0$ , are attempted by assuming multiplicative property of  $S$  and  $\sigma$  and additivity of  $\Delta E_0$ . The characterized parameter values reproduce their observed values within uncertainties in the present study. Calculations using the reproduced values give reasonable interatomic distance,  $r$ , and coordination number,  $N$ , in most cases without model samples. But it sometimes give large errors in  $N$  about 1.

Large solvent effect and counterion effect on X-ray absorption spectra are observed in  $[\text{Co}(\text{edta})]^-$ . Detailed study on the solvent effect is made on  $[\text{Co}(\text{ox})_3]^{3-}$  solutions and concludes that the metal-ligand interatomic distances are shortened by the electrophilic effect of the solvents. Linear relationships are shown between the distances and the acceptor number of solvents. The electrophilic effect is also shown in the solid state and it is concluded that the effect would be caused by the hydrogen bonding with the water of crystallization.

XAFS of Fe(III)-EDTA and Fe(III)-EDDDA complexes in solids and in aqueous solutions are compared. The coordination number of Fe(III) of EDTA and EDDDA complexes in aqueous solution are determined to be seven and six, respectively, by the comparison

of XAFS. However, it is difficult to presume the coordination structure of the ligands.

## Acknowledgement

The author wishes to express his greatest gratitude to Prof. Yu Yokoyama for his kind suggestion and support in coordinating this work.

The author also would like to express his sincere thanks to Dr. Iwao Watanabe for his helpful discussion and encouragement.

The author is grateful to Dr. Toshiaki Taura of University of Aichi Prefecture for his kind supply of Co and Cr complexes (Chapter 6) and guidance for the solvent effect.

The author thanks Drs. Tadashi Matsushita and Masaharu Nomura of the National Laboratory for High Energy Physics for their help and suggestion on X-ray absorption spectra measurement.

The author is also grateful to many members of Yokoyama Laboratory for their helpful advice and assistance.

Papers relevant to the present study

1. EXAFS and XANES spectra of Cobalt(III) EDTA Complexes in Solids and Solutions  
H. Sakane, I. Watanabe, and S. Ikeda  
*Bull. Chem. Soc. Jpn.*, 62, 1513 (1989).
2. EXAFS Amplitudes of Six-Coordinate Aqua and Ammine 3d Transition Metal Complexes in Solids and in Aqueous Solutions  
H. Sakane, T. Miyanaga, I. Watanabe, and Y. Yokoyama  
*Chem. Lett.*, 1623 (1990).
3. Structures of Fe(III) Complexes with EDTA and EDDDA in Aqueous Solution by EXAFS and XANES  
H. Sakane, I. Watanabe, K. Ono, S. Ikeda, S. Kaizaki, and Y. Kushi  
*Inorg. Chim. Acta*, 178, 67 (1991).
4. X-Ray Absorption Fine Structures for Simple Six- and Four-Coordinate First Transition Metal Complexes  
H. Sakane, T. Miyanaga, I. Watanabe, S. Ikeda, and Y. Yokoyama  
*Bull. Chem. Soc. Jpn.*, under preparation.
5. Solvent effects on X-Ray Absorption Fine Structure for Co(III) and Cr(III) bidentate carboxylato complexes  
H. Sakane, T. Taura, I. Watanabe, and Y. Yokoyama  
*Inorg. Chim. Acta*, under preparation.

